AN ABSTRACT OF THE THESIS OF

Nicholas T. Legg for the degree of Master of Science in Geology presented on March 15, 2013

Title: Debris Flows in Glaciated Catchments: A Case Study on Mount Rainier, Washington

Abstract approved:

____

Andrew J. Meigs

Debris flows, which occur in mountain settings worldwide, have been particularly damaging in the glaciated basins flanking the stratovolcanoes in the Cascade Range of the northwestern United States. This thesis contains two manuscripts that respectively investigate the (1) initiation processes of debris flows in these glaciated catchments, and (2) debris flow occurrence and its effect on valley bottoms over the last thousand years.

In a 2006 storm, seven debris flows initiated from proglacial gullies of separate basins on the flanks of Mount Rainier. Gully heads at glacier termini and distributed collapse of gully walls imply that clear water was transformed to debris flow through progressive addition of sediment along gully lengths. In the first study, we analyze gully changes, reconstruct runoff conditions, and assess spatial distributions of debris flows to infer the processes and conditions necessary for debris flow initiation in glaciated catchments. Gully measurements suggest that sediment bulking requires steep gradients, abundant unstable material, and sufficient gully length. Reconstruction of runoff generated during the storm suggests that glaciers are important for generating the runoff necessary for debris flow initiation, particularly because infiltration capacities on glacial till covered surfaces well exceed measured rainfall rates. Runoff generation from glaciers and abundant loose debris at their termini explain why all debris flows in the storm initiated from proglacial areas. Proglacial areas that produced debris flows have steeper drainage networks with significantly higher elevations and lower drainage areas, suggesting that debris flows are associated with high elevation glaciers with relatively steep proglacial areas. This correlation reflects positive slope-elevation trends for the Mount Rainier volcano. An indirect effect of glacier change is thus the change in the distribution of ice-free slopes, which

influence a basin's debris flow potential. These findings have implications for projections of debris flow activity in basins experiencing glacier change.

The second study uses a variety of dating techniques to reconstruct a chronology of debris flows in the Kautz Creek valley on the southwest flank of Mount Rainier (Washington). Dendrochronologic dating of growth disturbances combined with lichenometric techniques constrained five debris flow ages from 1712 to 1915 AD. We also estimated ages of three debris flows ranging in age from ca. 970 to 1661. Run-out distances served as a proxy for debris flow magnitude, and indicate that at least 11, 2, and 1 debris flow(s) have traveled at least 1, 3, and 5 km from the valley head, respectively since ca. 1650. Valley form reflects the frequency-magnitude relationship indicated by the chronology. In the upper, relatively steep valley, discrete debris flow snouts and secondary channels are abundant, suggesting a process of debris flow conveyance, channel plugging, and channel avulsion. The lower valley is characterized by relatively smooth surfaces, an absence of bouldery debris flow snouts, few secondary channels, and relatively old surface ages inferred from the presence of tephra layers. We infer that the lower valley is deposited on by relatively infrequent, large magnitude, low-yield strength debris flows like an event in 1947, which deposited wide, tabular lobes of debris outside of the main channel. Debris flows during the Little Ice Age (LIA) predominantly traveled no further than the upper valley. Stratigraphic evidence suggests that the main Kautz Creek channel was filled during the LIA, enhancing debris flow deposition on the valley surface and perhaps reducing run-out lengths. Diminished areas and gradients in front of glaciers during the LIA also likely contributed to decreased run-out lengths. These findings suggest that changes in debris flow source and depositional zones resulting from temperature and glacier cycles influence the magnitude and run-out distances of debris flows, and the dynamics of deposition in valley bottoms.

Debris Flows in Glaciated Catchments: A Case Study on Mount Rainier, Washington

by
Nicholas T. Legg

A THESIS

submitted to

Oregon State University

in partial fulfillment of
the requirements for the
degree of

Master of Science

Presented March 15, 2013
Commencement June 2013

Master of Science thesis of Nicholas T. Legg presented on March 15, 2013.

APPROVED:

____

Major Professor, representing Geology

____

Dean of the College of Earth, Ocean, and Atmospheric Sciences

____

Dean of the Graduate School

I understand that my thesis will become part of the permanent collection of Oregon State University libraries. My signature below authorizes release of my thesis to any reader upon request.

____

Nicholas T. Legg, Author

ACKNOWLEDGEMENTS

I am indebted to a number of wonderful people who have helped me complete this project. First, I would like to thank my major advisor, Andrew Meigs. He has been remarkably generous with his time and knowledge, reviewing numerous proposals and papers, discussing geomorphology with me at length, and talking through life's 'big questions'. His optimism and light-heartedness have lifted me from low points, made me laugh, and made this project a joy. I also thank one of my committee members, Gordon Grant. Gordon connected me with the 'locals', pushed me intellectually, and always helped me see the big picture. I feel incredibly fortunate to have had the opportunity to work with Andrew and Gordon together. I also appreciate assistance from committee members Stephen Lancaster, Anne Nolin, and Michael Olsen, who gave their knowledge though discussions in and out of the classroom. This project would not have been possible without Paul Kennard, who has provided logistical support, comic relief, valuable ideas, and field assistance. Thank you, Paul. Trevor Waldien and K. Sean Daniels remained positive through swarms of mosquitos, while helping in the field collecting countless tree cores and boulder measurements. I thank them for their help and companionship. A number of my fellow graduate students helped me through this process; I thank Pat Burns and Eduardo Guerrero in particular for their friendship. I learned a great deal from the weekly Geomorphology Brown Bag Meeting and thank Sarah Lewis for organizing and providing the necessary glue that keeps the group together. James Johnston and Pat Pringle lent me equipment and gave invaluable help with tree ring techniques. I also thank George Sharp for showing interest in my project. Chris Magirl provided aerial photographs and insights into debris flow processes. I thank everyone mentioned here, and many unmentioned, for the amount I learned, and the fun I had. Of the many positives of graduate school life, I will miss the people and the conversations most.

This project received generous support from the National Park Service, the Geological Society of America, the Mazamas Mountaineering Organization, National Center for Airborne Laser Mapping, the Oregon State University (OSU) College of Earth, Ocean and Atmospheric Sciences Student Advisory Committee Travel Fund, and the OSU Student Sustainability Initiative Travel Fund. George Sharp also provided generous support through a fellowship in his family's name. Thank you.

I would also like to acknowledge my family. I would not be here without the help and encouragement of my parents, Tom and Sharon. Thank you for hanging maps on the cabin wall, and for pushing me to follow my interests. Last, but not least, I thank Erin for keeping me balanced, for helping me through the tough times of graduate school, and for remaining patient with me when I was away. I love her so much.

CONTRIBUTION OF AUTHORS

First Manuscript: Dr. Andrew Meigs contributed ideas and support relating to project design, logistics, and funding procurement. He also reviewed the manuscript. Dr. Gordon Grant helped conceptualize the project and reviewed the manuscript. Paul Kennard provided “on-the-ground” knowledge of Mount Rainier geomorphology, and logistical and field support through this study.

Second Manuscript: Dr. Andrew Meigs contributed ideas and support relating to project conceptualization, design, logistics, and procurement of funding. He also assisted with data collection in the field, and reviewed the second manuscript. Dr. Gordon Grant helped conceptualize the project, provided logistical support, assisted with funding procurement, and reviewed the manuscript. Paul Kennard provided scientific, logistical, and field support through the entire project.

TABLE OF CONTENTS

Page

TABLE OF CONTENTS (Continued)

Page

LIST OF FIGURES

LIST OF FIGURES (Continued)

LIST OF TABLES

1 Introduction

Debris flows are a slurry of sediment and water that initiate on steep slopes and run-out to distances that can impact communities, cause loss of life, and damage infrastructure (Iverson, 1997). Debris flows occur in environments ranging from tectonically-active mountain ranges, basins recently burned by wildfire, and glaciated alpine settings (Stock and Dietrich, 2003; Wells, 1987; Moore et al., 2009). A devastating precipitation-induced debris flow in 1999 initiated from a tectonically-active mountain range, inundated the city of Vargas, Venezuela, and sadly killed more than 15,000 people (Larsen et al., 2001). In 2003, recently burned watersheds of the San Gabriel Mountains rimming Los Angeles, California unleashed numerous debris flows that killed 16 people (Cannon and Gartner, 2005). In the Pacific Northwest, a 2006 storm induced debris flows from glaciated catchments on multiple volcanic peaks, causing infrastructure damages in the millions of dollars (Lancaster et al., 2012). These examples of debris flow impacts demand that we understand the processes controlling their occurrence.

Steep slopes and incompetent bedrock combine to make stratovolcanoes some of the most erodible landforms on Earth. In the Cascade Range of the northwestern United States, andesitic volcanoes have large glaciers, causing rapid erosion and enormous sediment loads in rivers draining their slopes (Czuba et al., 2011; Czuba et al., 2012). This sediment poses challenges to dam operators and river managers by filling reservoirs, aggrading channels, and decreasing the flood conveyance capacity of channels (Czuba et al., 2010). Sediment transport and mass movement processes on volcanic slopes therefore link volcano erosion with management of rivers downstream. Moreover, recent debris flows have caused concern that change in climate and related factors like increasing storm intensity, retreating glaciers, and reduced snow-packs may cause more debris flows in the future, yet these interactions remain poorly understood.

How might debris flow occurrence change in glaciated catchments as climate warms? Warming climate can change seasonal precipitation patterns, snow levels, storm intensities, or cause glaciers to retreat (Mote, 2003; Mote et al., 2003; Moore et al., 2009). At first inkling, some of these changes have seemingly obvious effects on debris flow occurrence; for instance, increases in storm frequency should have corresponding increases in debris flow activity. Yet, underlying geomorphic thresholds may confound these simple predictions (Schumm, 1979). What controls a watershed's response and sensitivity to change? Bovis and Jakob (1999) showed that basins with abundant debris supply had debris flow frequencies closely coupled with storm frequencies, whereas basins with limited debris supply were insensitive to storm frequency (Figure 1-1). Their findings show that we must account for the geology and geomorphology of an area before attempting to predict responses of debris flow occurrence to climate change.

This study seeks to better constrain the geomorphic processes and conditions that lead to debris flow occurrence on Mount Rainier and on other volcanoes in the Cascade Range. Our driving questions are:

1. What factors influence the occurrence of debris flows in glaciated basins? How do these factors respond to fluctuations in climate and glaciers?
2. How has debris flow occurrence changed in response to climate and glacier fluctuations in the past? How do observed patterns inform projections of future debris flows?
3. How can concepts of debris flow processes on Mount Rainier be applied to other areas prone to debris flows?

Our ability to forecast debris flows in glaciated catchments on Mount Rainier and other volcanic peaks is limited by two major data gaps. First, the conditions and mechanisms of debris flow initiation in these catchments are poorly understood. Second, the set of recorded debris flow events is too short and incomplete to interpret debris flow occurrence with respect to climate and glacier fluctuations. The two manuscripts contained in this thesis thus address these two data gaps. In the first manuscript, we use recent debris flow initiation sites to infer processes and controls on debris flow initiation. The second study builds a debris flow chronology spanning approximately 1,000 years that is correlated with local climate and glacier records.

1.1 Figures

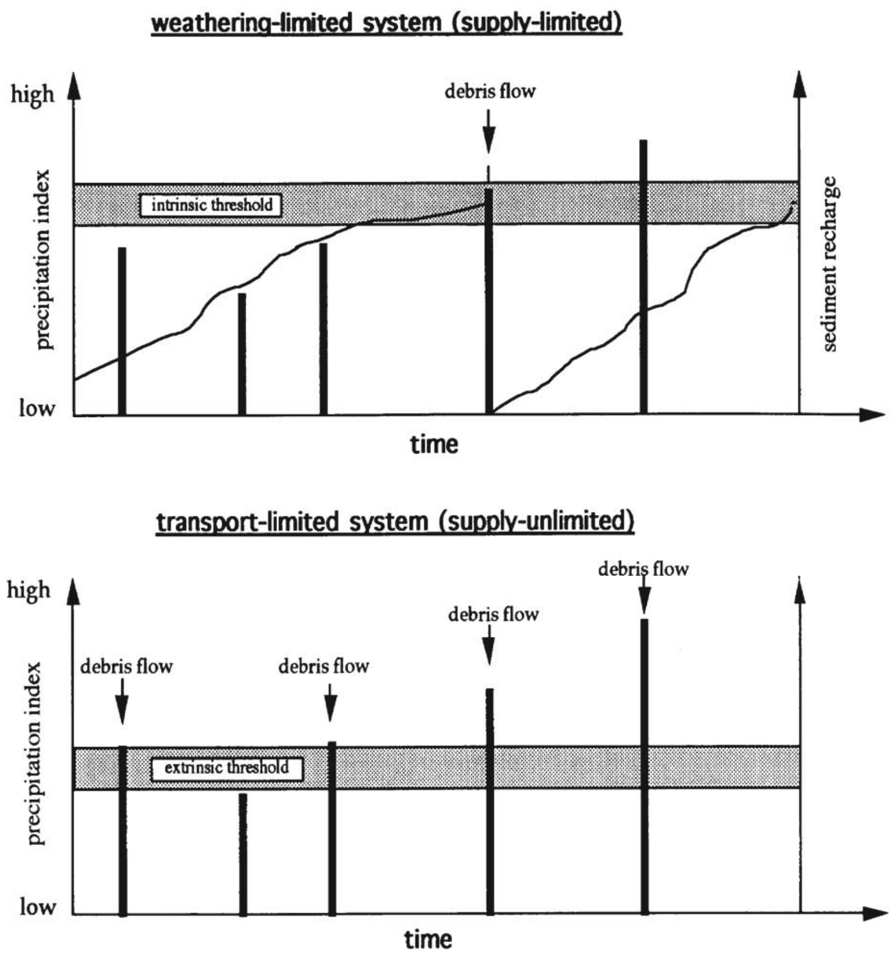

Figure 1-1 Figure by Bovis and Jakob (1999) demonstrating thresholds of debris flow initiation in weathering-limited and transport-limited systems.

2 Debris flow initiation in proglacial gullies on Mount Rainier (Washington)

Nicholas T. Legg[a], Andrew J. Meigs[a], Gordon E. Grant[b], Paul Kennard[c]

[a] Oregon State University, College of Earth, Ocean, and Atmospheric Sciences, Corvallis, OR 97331, USA

[b] USDA, Forest Service, Pacific Northwest Research Station, 3200 Jefferson Way, Corvallis, OR 97331, USA

[c] Mount Rainier National Park, 55210 238th Ave E, Ashford, WA 98304, USA

2.1 Abstract

In a 2006 storm, seven debris flows initiated from proglacial gullies of separate basins on the flanks of Mount Rainier. Gully heads at glacier termini and distributed collapse of gully walls imply that clear water was transformed to debris flow along gully lengths through progressive addition of sediment. We analyze gully changes, reconstruct runoff conditions, and assess spatial distributions of debris flows to infer the processes and conditions necessary for this type of debris flow initiation in glaciated catchments. Gully measurements suggest that this sediment bulking process requires steep gradients, abundant unstable material, and sufficient gully length. Reconstruction of runoff generation suggests that glaciers are likely important for generating the runoff necessary for debris flow initiation, particularly because infiltration capacities on glacial till covered surfaces well exceed measured rainfall rates. Runoff generation from glaciers and abundant loose debris at their termini explain why all debris flows in the storm initiated from proglacial areas. Proglacial areas that produced debris flows have steeper drainage networks with significantly higher elevations and lower drainage areas, suggesting that debris flows are associated with high elevation glaciers with relatively steep proglacial areas. This correlation reflects positive slope-elevation trends for the Mount Rainier volcano and points to a glacier's ability to influence the slope distribution of a basin, and thus potential for debris flow generation. These findings have implications for projections of debris flow activity in basins experiencing glacier change.

2.2 Introduction

Steep slopes and incompetent bedrock combine to make stratovolcanoes some of the most erodible landforms on Earth. In the Cascade Range in the northwestern United States, andesitic volcanoes stand well above the current and Quaternary average equilibrium line altitudes (ELA) of glaciers, causing rapid glacial erosion and enormous sediment loads in rivers draining their slopes (Porter, 1989; Czuba et al., 2011; Czuba et al., 2012). This sediment poses challenges to dam operators and river managers downstream by filling reservoirs, aggrading channels, and reducing the flood conveyance capacity of channels (Czuba et al., 2010). Sediment transport and mass movement processes on volcanic slopes therefore link volcano erosion with management of rivers downstream. Their destructive nature and ability to rapidly carry large volumes of sediment have notable implications for downstream areas. Moreover, recent debris flows have caused concern that climate change and related factors like increasing storm intensity, retreating glaciers, and reduced snow-packs may cause more debris flows in the future, yet these interactions remain poorly understood.

Our limited understanding of debris flow initiation processes prevents us from assessing effects of change in climate and related factors on debris flow occurrence. Recent observations of debris flows on Mount Rainier (Washington) suggest that the initiation mechanisms on volcanic flanks are unique. As opposed to the most typical initiation style where an individual mass failure liquefies and mobilizes as a debris flow, recent Mount Rainier debris flows appear to begin as clear floodwaters that entrain large amounts of sediment until they become debris flows (Iverson, 1997; Lancaster et al., 2012). The gullies where these debris flows have initiated emerge from or very near glaciers, suggesting that flows near the gully heads must have had minimal sediment concentrations. These gullies typically pass through areas dominated by loose and steep glacial till, and show evidence of wall collapse and lateral expansion along their lengths. The material derived from gully expansion therefore may represent the source material for debris flows. Despite these observations, we are still unaware of the conditions necessary for this type of debris flow initiation.

The process which floodwaters transform to debris flow by entraining sediment – referred to as bulking – has been recognized in few settings (Wells, 1987; Meyer et al., 1995; Iverson et al., 1997; Meyer and Wells, 1997; O'Connor et al., 2001). A majority of work on the bulking process focuses on catchments recently burned by wildfire (e.g. Wells, 1987; Meyer et al., 1995; Meyer and Wells, 1997; Cannon and Reneau, 2000; Gabet and Bookter, 2008). In burned areas, reduced vegetation cover and coverage of ash from burned vegetation reduce infiltration capacity, enhance runoff generation, and cause drainage networks to abruptly expand (Gabet and Bookter, 2008; Gabet and Sternberg, 2008). Burning of vegetation also releases sediment stored on hillslopes, which is delivered to existing channels by rill networks and dry ravel (Wells, 1987; Lamb et al., 2011). Floodwaters rapidly entrain material derived from rapid drainage network expansion and delivered to existing channels, and transform to debris flow. Whereas conditions leading to bulking in burned areas are well-constrained, it is unclear how these concepts can be applied to other environments where bulking occurs. Glaciated catchments represent one of these environments where debris flows generated from bulking have been documented, but the conditions and mechanisms leading to bulking remain poorly understood (O'Connor et al., 2001; Lancaster et al., 2012).

This study focuses on a November 2006 storm that initiated debris flows from proglacial areas of at least six separate catchments, causing $36 million in infrastructure damage (National Park Service, 2007). The 2006 storm was unique for the number of debris flows that initiated from separate basins, with no historical events on Mount Rainier having so many debris flows observed (Figure 2-1). Observation of initiation zones following the storm revealed expanded proglacial gullies with no single mass failures responsible for debris flow initiation (Copeland, 2009).

We analyze initiation of the 2006 debris flows at variable scales according to a conceptual model of debris flow initiation that we have proposed (Figure 2-2). This conceptual model guides our objectives by connecting basin-scale landscape and meteorological factors to conditions controlling bulking potential within an individual gully. We therefore seek to (1) characterize the nature, setting, and change of 2006 debris flow gullies in detail, (2) constrain mechanisms of runoff generation that lead to debris flow initiation, and (3) analyze basin-scale attributes that set local conditions for debris flow initiation. High-resolution airborne laser swath mapping (ALSM) topography and aerial imagery permit us to measure the morphology and change of debris flow gullies, and infer dynamics of debris flow bulking. We also reconstruct runoff conditions in a single gully for differing scenarios of runoff generation and compare flood discharges to an estimate of sediment volume in a debris flow. And finally, we compare debris flow producing basins (DFB) to non-debris flow producing basins (NDFB) in the 2006 storm to analyze basin-scale factors that set conditions for debris flow initiation. Studying debris flows within a single meteorological event with roughly similar meteorological and hydrologic conditions across basins allows us to focus on the geomorphic conditions that influence debris flow initiation.

2.3 Setting

Mount Rainier, a stratovolcano of andesite-dacite composition, is the highest peak (4,392 m asl) in the Cascade Range and supports the greatest volume of glacier ice in the lower United States (Driedger and Kennard, 1984; Hildreth, 2007). Present-day glacier extents are generally greater on the north and northeast than on the south (Figure 2-1). Mountain-wide glacier volume loss from 1970 to 2007/8 has been measured at approximately 14% (Sisson et al., 2011). With exception of a brief glacial advance in the 1960s and 1970s, these recent trends are a continuation of ice retreat that has occurred since the Little Ice Age maximum ca. 1850 (Table 2-1) (Sigafoos and Hendricks, 1972; Burbank, 1981; Heliker et al., 1984).

Both debris flows and volcanic lahars originate from Mount Rainier, but our focus here is exclusively debris flows, which can be distinguished from lahars (Scott et al., 1995; Vallance and Scott, 1997; Crandell, 1971a). Hydrologically-induced debris flows mobilize surficial debris with low clay content and corresponding low cohesiveness. Lahars are cohesive, high clay-content debris flows that often result from flank collapse of the volcanic edifice. The largest recognized lahar – the Osceola Mudflow of ~5,600 years BP – initiated from the northeastern flank of Mount Rainier and inundated portions of the Puget Sound Lowland approximately 100 km downstream (Vallance and Scott, 1997). Whereas lahars have return intervals of greater than 500 years, hydrologically-induced debris flows have been recorded numerous times in the previous century. Hydrologically-induced debris flows generally travel less than 10 km from the summit and are initiated when either runoff generated from precipitation or glacier outburst floods entrain sediment (Walder and Driedger, 1994b; Walder and Driedger, 1994a). This study focuses on precipitation-induced debris flows; however, some of the mechanisms that transform water floods to debris flows discussed here likely apply to glacier outburst floods.

2.4 2006 Storm

On November 6 and 7, 2006, an Atmospheric River storm approaching from the southwest hit Mount Rainier and dropped approximately 45 cm of rain over a 36-hour period (Neiman et al., 2008, NPS). Atmospheric River storms bring warm and moist air from tropical latitudes and drop heavy rain at high elevations, which melt antecedent snow pack (if present) (Neiman et al., 2008). During the most intense period of the storm (approximately 42 hours), the National Resource Conservation Service (NRCS) Paradise Snowpack Telemetry (SNOTEL) station (7.6 km SSE of Mount Rainier summit; 1,560 masl; 46.78^{o}, -121.75^{o}) recorded average rainfall rates of approximately 0.9 cm/hr, with a maximum of 2.0 cm/hr (Figure 2-3). For the duration of the storm, snow-water equivalent was less than 1 cm, and temperatures were above freezing. During the same period at the Morse Lake SNOTEL station (22 km ENE of Mount Rainier summit; 1,645 masl; 46.91^{o}, -121.48^{o}), rainfall intensity averaged 0.4 cm/hr and had a maximum observed intensity of 0.8 cm/hr suggesting an orographic effect. The distance of Morse Lake SNOTEL station from the summit may also exaggerate the apparent orographic effect. Both the south-draining United States Geological Survey (USGS) Nisqually River gauging station at National (USGS ID: 12085000) and north-draining Carbon River gauging station at Fairfax (USGS ID: 12094000) recorded greater than 100-year discharges and floods of record. Whereas SNOTEL data suggest an orographic effect, gauging data suggest that flooding was of similar magnitude with respect to each basin's hydrographic record. Reconnaissance by National Park Service employees and Copeland (2009) following the storm recorded evidence of debris flows from six basins, including those containing the South Tahoma, Pyramid, Kautz, Van Trump, Inter, and Curtis Ridge glaciers (Figure 2-1).

2.5 Methods

This study (1) characterizes the nature and setting of 2006 debris flow gullies in detail, (2) constrains mechanisms of runoff generation that lead to debris flow initiation, and (3) analyzes basin-scale attributes that set local conditions for debris flow initiation. We approach the first objective by measuring change of an individual 2006 debris flow gully (the Pyramid gully), and measuring slope and drainage area of all 2006 debris flow gullies to investigate whether debris flows initiate in portions of the drainage network within unique process domains. The change estimated in the Pyramid gully allowed us to approximate a sediment volume, which we compare to estimates of water discharge in the gully to constrain mechanisms of runoff generation (objective two). Finally, we used the characteristics of individual debris flow gullies to compare the characteristics of basins and explain the spatial distribution of debris flow generation in the 2006 storm.

Remotely sensed data provide a basis for much of our analysis. National Aerial Imagery Program (NAIP) aerial photography and ALSM topographic data allow us to measure gully change resulting from the 2006 storm and extract topographic and hydrologic characteristics of the landscape. One-meter spatial resolution NAIP images taken in 2006 and 2009 bracket the November 2006 storm. 2007 and 2008 images of the same resolution were not available for the study area. ALSM data were collected in September 2007 and in September and October 2008. In the sparsely vegetated areas above tree-lines where this work focuses, the ALSM survey obtained approximately 1.5-3.5 ground-classified points per square meter, data that were then processed into 1-m resolution gridded digital elevation models (DEMs).

Extraction of drainage networks from DEMs using algorithms developed by Tarboton et al. (2006) allowed us to measure drainage area at various points on the landscape. Prior to extracting drainage networks, we down-sampled the 1-m gridded ALSM DEMs to 4-m grids to lessen computing time. To minimize topographic smoothing effects introduced by grid cell assignments based on neighborhood values, grid cells within the down-sampled DEMs were assigned the mean elevation of the sixteen 1-m cells encompassed by each new cell. Extraction of drainage networks included filling pits in the DEM, creating flow direction and flow accumulation rasters, and then extracting shapes of the drainage network based on a channel head threshold of 10,000 m^2 drainage area. Our threshold choice was based on approximate rill, gully and channel head locations observed in sparsely vegetated areas. We observed appreciable scatter in drainage areas at rill, gully, and channel heads that relates to differences in local slopes and infiltration capacities of contributing areas, and chose a drainage area threshold of 10,000 m^2, which includes the observed scatter (Montgomery and Dietrich, 1989).

Since our analysis depended on identifying all debris flow initiation gullies from the 2006 storm, we used our combined air photo and ALSM time-series to confirm that the original 2006 debris flow inventory was complete. We visually scanned all basins for gullies with measurable expansion between 2006 and 2008. In basins without documented debris flows where we identified expanded proglacial gullies, we also scanned downstream areas at channel gradients typical of debris flow deposition for indications of debris flow deposits. We traveled to the same depositional areas to confirm the nature of deposits observed in aerial imagery and classified their sedimentology (debris flow versus fluvial) according to sedimentologic and geomorphic criteria outlined by *Pierson* (2005) and *Costa* (1988). In basins where debris flow evidence was observed between 2006 and 2008, we assumed the debris flow occurred in the November 2006 storm, and reclassified NDFB as DFB.

2.5.1 Gully Characterization

2.5.1.1 Pyramid Gully Change

In order to characterize geometry changes and estimate volumes of sediment entrained by debris flows, we measured plan-view changes along one debris flow gully that initiated a debris flow in November 2006 in the Pyramid Glacier proglacial area (Figure 2-1). The approximately 1.2-km long gully begins at the existing Pyramid glacier terminus with an approximate longitudinal gradient of 24^{o}, runs along a lateral moraine in an un-vegetated area covered by glacial till, and enters a bedrock channel at an approximate gradient of 10^{o}. We chose the Pyramid debris flow gully for detailed change measurement because it had the least snow coverage at the dates of the aerial image capture, which allowed us to measure width change along the debris flow gully from 2006 to 2008 (NAIP to ALSM) and 2008 to 2009 (ALSM to NAIP) (Figure 2-4). With no ALSM survey conducted prior to the November 2006 storm, we were only able to measure change in the horizontal gully extent. In addition to width change in each gully segment, we measured longitudinal gradient and hillslope contributing area.

To analyze change in the gully with respect to gully and hillslope characteristics, we digitized outlines of the debris flow gully in 2006 and 2008 and subdivided each outline into 58, 20-m gully-wise segments (Figure 2-4). For each segment, we estimated average width change (segment area change in plan-view divided by segment length). A simple model of gully geometry that required measurements of hillslope angle, gully wall angle, and gully depth then allowed us to convert width change to volume change for each segment (Figure 2-5). This model of volume change required that we assume that gully wall angles and bed elevations were unchanged by debris flow passage. Summing volume changed for all segments then yielded an estimate of total sediment volume change for the gully. Finally, we correlated changes in the gully with longitudinal slope and hillslope contributing area. Contributing area from hillslopes allowed us to analyze the effect of hillslope concavity on gully wall collapse. As opposed to measuring drainage area of the gully along its length to extract hillslope contributing area, we measured contributing area from the left hillslope only along a gully-parallel transect. This allowed us to eliminate drainage area inputs from the right hillslope where bedrock exposure prevented appreciable width change, thus isolating relationships between gully change and hillslope geometry on the left bank.

2.5.1.2 Slope and Drainage Area of Debris Flow Gullies

To characterize the energy availability in debris flow gullies, we measured slope and drainage area along their lengths. Slope and drainage area (proportional to stream discharge) relate to stream power, or the rate of energy expenditure along a channel. Slope and drainage area therefore allow us to examine the energy available for sediment transport within gullies (Whipple and Tucker, 1999; Yang, 1972). We chose each debris flow gully by identifying the gully with the greatest width change in a catchment, and assumed it to be the primary debris flow gully. We note that this differs from Lancaster et al. (2012), who identified 17 debris flow source gullies across six DFB, suggesting that multiple gullies could have contributed to an individual debris flow. Their analysis also included debris flows and associated gullies that occurred prior to 2006, which are beyond the scope of this study. We defined the endpoints of debris flow gullies by the upstream- and downstream-most points of width change and measured slope and drainage area at each point. In addition, we measured slope and drainage area at midpoints of all links between tributary junctions along the gully. Later, we refer to these three datasets as the upstream limits, downstream limits, and intermediate reaches.

2.5.2 Runoff Generation

To explore mechanisms of runoff generation, and whether total evacuated sediment volume (V_S) estimated from gully walls of Pyramid gully was sufficient to transform floodwaters to debris flow, we performed a volume flux calculation relating water discharge to sediment discharge. We first estimated water discharge at the outlet of the debris flow gully based on rainfall intensity (R), infiltration capacity (*I*), and drainage area at the debris flow gully outlet (A_{out}). We measured infiltration capacity at 19 un-vegetated locations in four proglacial areas on Mount Rainier using a *Mini Disk Infiltrometer* manufactured by *Decagon Devices.* We calculated water discharges from the gully for two end-member scenarios: (1) where bare soils infiltrate at measured rates and glacier surfaces are considered to be impervious (requiring glacier area measurement), and (2) where all soil in the contributing area is impervious (i.e. frozen). The simplifying assumption of impervious glacier surfaces is based on one study suggesting that rainfall rapidly "pushed through" englacial water storage, creating an abrupt hydrographic response (Van de Griend and Arwert, 1983). In general, our assumption tries to capture the idea that glaciers generate runoff for downstream areas at greater rates than sediment-mantled surfaces, regardless of whether rainfall sheets from the glacier surface, or rapidly replaces and forces evacuation of englacial storage. Runoff generation from rapid snowmelt is not captured explicitly by the two end-members; however, we feel the second scenario with an entirely impervious catchment area probably overestimates basin-wide runoff generation. Thus, the end members likely capture an intermediate situation where runoff is generated by a combination of sources. In addition, SNOTEL data indicate snow water equivalent (SWE) was minimal (<1 cm H_2O) during the 2006 storm, suggesting snowmelt contributed minor amounts of runoff (Figure 2-3). We calculated discharge (Q_w) using measured infiltration capacities (in cm/hr), A_{out}, and November 6-7 rainfall intensity measured at the Natural Resources Conservation Service's Paradise SNOTEL (Figure 2-3) located approximately 5 km east of the Pyramid Glacier; where Q_w is:

$$Q_w = A_{out} \cdot (R - I) \tag{1}$$

We assume that the point where floodwaters must have been converted to debris flow occurs at the downstream-most point where gully expansion was observed (where A_{out} was measured).

With a water discharge estimate, we calculated an approximate period of time *(t)* required to evacuate the estimated sediment volume as a debris flow. Neither the time nor duration of the Pyramid debris flow was recorded due to site inaccessibility, so we were unable to associate rainfall intensity with the debris flow initiation. Consequently, we perform the above calculation over a range of rainfall intensity. Assuming a volumetric sediment concentration (C_S) ranging from 0.6 to 0.8 m^3/m^3 (Pierson and Scott, 1985), we calculate a sediment discharge rate (Q_S) using:

$$Q_S = \frac{Q_W \cdot C_S}{1 - C_S} \tag{2}$$

We assumed that entrained sediment was unconsolidated and poorly sorted with a porosity (φ) of 0.20 m^3/m^3 (Fitts, 2002), that any sediment incorporated into the debris flow was completely disaggregated upon being incorporated into the flow, and that pore water volume had a negligible effect on discharge and debris flow sediment concentration. We calculated evacuation time (t) using:

$$t = \frac{V_S \cdot (1 - \varphi)}{Q_S} \tag{3}$$

We then compared sediment evacuation times to past debris flow durations observed on Mount Rainier, noting that our model estimate requires the assumption that all volume change between the 2006 image and 2008 ALSM DEM be evacuated as a debris flow.

2.5.3 Basin Scale Factors Influencing Debris Flow Generation

Our conceptual model suggesting that debris flow initiation requires both sufficient energy and debris supply guides our initial assumptions and hypotheses for basin scale analysis. Because the 2006 debris flows all initiated in proglacial areas dominated by unconsolidated glacial till, it seems reasonable that proglacial areas satisfy debris supply requirements for debris flow initiation. Yet, debris flows did not occur in all proglacial areas, and differing proglacial area morphologies suggest that proglacial areas have differences in energy availability. Proglacial areas on Mount Rainier have morphologies that vary with the catchment elevation above the ELA and the resulting glacier type. Valley glaciers tend to occur in basins that extend to the summit with large areas above the ELA. Their glaciers thus extend to lower elevations with gentler slopes. In smaller catchments that do not extend to high elevations and have correspondingly less area above equilibrium line altitudes, cirque glacier termini sit at higher elevations with greater slopes. These general groupings, however, do not explain all morphological differences in proglacial areas. Factors like aspect also influence glacier extent, the position of proglacial areas, and the characteristics of proglacial areas.

Instead of analyzing morphological differences by catchment type or glacier type, we analyzed basins grouped according to whether or not debris flows occurred in the 2006 storm, hypothesizing that the spatial patterns of 2006 debris flows reflected morphological differences in basins. As opposed to analyzing debris flow basins from a number of different storms, analysis of one storm with roughly similar meteorological (precipitation intensity, duration, and form) and hydrologic (antecedent snow) conditions allows isolation of geomorphic conditions leading to debris flow generation. According to this idea, we reason that geomorphic indices extracted from the two basin groups could explain the differences in debris flow generation. Alternatively, if morphological differences were not able to explain differences, the spatial distribution of debris flows may be a result of the stochastic nature of debris flow initiation, or from orographic gradients in precipitation that are indicated by SNOTEL data.

Because we hypothesized that geomorphic factors relating to potential energy would be best at explaining the spatial distribution of debris flows from supply-abundant proglacial areas, we extracted slope and drainage area of the drainage networks in proglacial areas as a measure of debris flow potential. Slope and drainage area (proportional to stream discharge) relate to stream power, or the rate of energy expenditure along a channel with uniform and steady flow, and thus capture energy availability in a gully or channel (Whipple and Tucker, 1999). Whereas assumptions for stream power may not hold true in steep gullies where flow may be unsteady and variable, these measurements allow us to systematically assess possible process domains of gullies (Istanbulluoglu et al., 2003) We therefore used slope-drainage area relationships observed in gullies as an rough indicator of debris flow potential in proglacial drainage networks.

In order to extract slope and drainage area in proglacial areas, we defined proglacial areas, clipped drainage networks to these outlines, and discretized the drainage network. We first defined outlines of proglacial areas in DFB and NDFB by outlining zones dominated by unconsolidated debris with sparse vegetation cover (<10% coverage), that were bounded on the up-valley end by the terminus of existing mapped glacier outlines (NPS) Figure 2-6. We omitted large areas of bedrock exposure identifiable in aerial photography. In defining these proglacial areas, we attempted to delineate areas of abundant debris supply, thereby eliminating debris supply as a factor controlling debris flow initiation. We digitized proglacial areas for all glaciers (n=22) flanking the Mount Rainier edifice with exception of the Carbon and Winthrop glaciers due to a lack of un-vegetated areas that were not low-gradient (<10^{O} (observed debris flow scour threshold by Benda and Cundy, 1990) channels. We then clipped the algorithm-derived drainage network (explained above) of the entire volcano to proglacial area shapes (Figure 2-6) (Tarboton et al., 2006). At tributary junctions, we divided the clipped drainage networks into links, and extracted longitudinal slope (elevation difference between endpoints divided by length) and drainage area (at midpoint) from each link (Figure 2-6).

In order to examine differences in slope-drainage area distributions in the two basin types, we analyzed distributions of slope-drainage area data with a series of partitions. Specifically, we aligned partitions with a power law regression of the slope and drainage area observed in debris flow gullies in order to most easily analyze slope-drainage area distributions with respect to observed values in gullies. Each partition was set parallel to the regression fit of the upstream limit of debris flow gullies in log-log space, meaning we varied the power law equation coefficient, but kept the exponent constant. For each partition, we analyzed only links of the proglacial drainage networks exceeding (greater slope and drainage area) that partition and calculated a series of simple metrics (defined below). We calculated metrics for individual proglacial areas and then averaged the two groups (DFB and NDFB). Group-averaged metrics across the set of partitions track differences between the two basin types in slope and drainage area space.

We defined two metrics that allow examination of slope and drainage area distributions in drainage networks in proglacial areas. The first metric was the sum of drainage *network length* (NL) exceeding a given partition (Figure 2-7). Across the series of partitions, the NL metric captures distributions of slope and drainage area in proglacial drainage networks. Proglacial areas more favorable for debris flow initiation would have a higher NL metrics (a greater length) coincident with the slope-drainage area trend of observed debris flow gullies. The second metric – the *length of the longest connected channel* (LCC) – is designed to incorporate observations that debris flow initiation occurs as a distributed process along a single gully or channel (Figure 2-7). To extract this metric, we programmatically searched for and measured the length of the single longest set of connected links above a given slope-drainage area partition. Whereas the NL metric captures the overall distribution of slope and drainage area contained in the drainage network, this latter metric extracts the length of the longest channel with slope-drainage areas exceeding each partition. We hypothesized that proglacial areas with a relatively high favorability for debris flow initiation would have larger LCC values in the slope-drainage area space coinciding with observed values of debris flow gullies. We expected that the overall morphology of a proglacial area (as reflected by NL) sets the conditions for long channels (as reflected by LCC) of similar slope and drainage area, but expected that the longest channel or gully with favorable conditions for debris flow initiation would best reflect the propensity of basin's proglacial area to produce debris flows. We therefore hypothesized that the LCC would show greater statistical differences between the basin groups than the NL metric. These two metrics allow connection of geomorphic conditions on broader spatial scales with local gully conditions to test differences in basin types.

This focused analysis of only proglacial areas and their drainage networks oversimplifies debris flow initiation on Mount Rainier in two ways. First, debris flows may occur in periglacial areas along the sides of glaciers, areas that fall outside of the analysis window. The 2006 debris flows identified and studied here, however, all initiated in proglacial zones. This simplification therefore should have little impact on our spatial analysis of a single storm. Secondly, our assumption that all gullies and channels in proglacial drainage networks have unlimited supply available is probably not the case. For instance, some gullies may undercut large accumulations of glacial till, whereas others may extend through areas with relatively minor accumulations of material. While we acknowledge this simplification, we also expect that the effect of variable supply will be borne out by our results. If variable debris availability is actually a limiting factor, distinctions between basins with metrics of energy supply (slope and drainage area) should be insignificant.

2.6 Results

2.6.1 Gully Characterization

2.6.1.1 Pyramid Gully Change

Estimated change in the Pyramid Gully from 2006-2008, which we assumed to be a result of the 2006 debris flow, allowed us to elucidate influences on the input of sediment into a gully, and in turn infer mechanisms of debris flow initiation. We envision two scenarios of debris flow initiation in gullies, which are not mutually exclusive, but guide our interpretation of change in the Pyramid Gully. In the first scenario, pre-conditions of the gully, such as debris supply and slope along the gully, determine whether a flood is transformed to a debris flow. In a second scenario, properties of flow relating to sediment concentration and flow rheology influence the amount of sediment entrained from gully walls, therefore, as a flows travel down a gully, changes in flow properties that occur as a result of sediment entrainment induce greater rates of sediment entrainment. This latter scenario has been suggested by Santi et al. (2008) based on threshold increases in sediment yield along gullies. We use our observations of gully change to distinguish between these two scenarios, where possible.

The Pyramid debris flow gully expanded on average 2.6 m horizontally between 2006 and 2008 along the 1.2-km reach (Figure 2-4 and Figure 2-8A). Based on this widening, we estimated that ~47,000 m^3 of sediment was evacuated from this one gully (Figure 2-8B). Gully expansion occurred in a distributed manner as a series of wall collapses along the gully length, with horizontal width change (Δw_h) exceeding zero in 51 of 57 (89%) 20-m gully segments. Minimal gully expansion occurred where bedrock exposures were visible, particularly on the right bank of the gully (Figure 2-4).

Hillslope concavities appear to influence locations of the largest gully wall collapses. Gully segments with the greatest gully expansion coincided with discrete landslide scars, which are spatially coincident with concavities in the adjacent hillslope. We used contributing area from the left hillslope as an indication of concavity (Figure 2-8C). Two un-channelized but concave locations (with contributing areas of greater than 25,000 m^2) demonstrate the nature of hillslope influences on sediment input. The uppermost location coincides with a visible landslide scar encompassing a set of 3 consecutive 20-m segments, which account for ~28% of the volume change in the Pyramid gully, whereas the second concavity has little associated gully volume change. Hillslope angles above the gully margin at these locations are 27^{O} and 16^{O} respectively, suggesting that both the presence of water (on concave hillslopes) and gradient on the hillslope influence failure of gully walls. These hillslope controls suggest that gullies must run through areas with sufficient quantities of debris that are poised for collapse in order for debris flows to initiate. Conditions that set instability in wall material include both undercutting within the gully and hillslope factors discussed here.

The volume change per unit gully length – commonly referred to as yield rate - varies across three distinct sub-reaches of the gully (labeled sub-reach 1, 2, and 3 moving downstream in Figure 2-8), which may relate to processes of sediment entrainment occurring in the gully (Hungr et al., 1984). We defined these sub-reaches by breaks in the volume changed per unit length. Volume change per unit length is modest in sub-reach 1, high in sub-reach 2 (~5 times that of sub-reach 1), and negligible in sub-reach 3. The disparity in sediment yield between sub-reaches 1 and 2 corresponds with 2.3x and 1.7x increases in average width change and gully wall height, respectively. Variation in width change induced by a flow along the gully may vary with the geometry with the gully, or with properties of the flow relate to its ability to undermine gully walls. Gully wall height relates to the thickness of glacial material adjacent to the gully. The increase in volume change per unit length (sub-reach 1 to 2) is also coincident with downstream reduction in longitudinal slope, suggesting that slope is not the main determinant of volume change per unit length. The downstream sequence of yield in the gully may suggest that feedbacks of sediment entrainment occur. Santi et al. (2008) studied a number of expanded gullies that initiated debris flows following a forest fire and consistently observed an apparent threshold increase in the volume entrained per unit length, similar to the one observed at the boundary between sub-reaches 1 and 2. They speculated that abrupt changes in yield related to transitions in flow behavior (water to hyperconcentrated flow or hyperconcentrated flow to debris flow) that made flows more erosive and thus able to entrain additional sediment at greater rates.

Regardless of whether debris flow initiation occurs as a result of pre-existing gully conditions, or as a result of changing flow properties, gully length appears to be a factor in determining whether a debris flow initiation can occur. In the former case (pre-existing gully conditions control bulking potential), the length over which material can be entrained helps determine the amount of debris available for entrainment. In the latter case, some gully length would be required for feedbacks of the bulking process to fully carry out. In either case, the portion of the gully over which length is measured is unclear, but a threshold length may relate to gully slope, flood water discharge, or debris availability along that length.

2.6.1.2 Slope and Drainage Area of Debris Flow Gullies

Because our analysis of slope and drainage area requires an account of the debris flow gullies in the 2006 storm, we note here that we identified a debris flow gully in addition to the six originally identified. Using aerial imagery, we observed a gully that expanded between 2006 and 2008 in the proglacial area of the Ohanapecosh Glacier with a downstream deposit outside of the pre-existing channel of the same age (Figure 2-1). Field reconnaissance revealed that these deposits were poorly sorted, had damaged tree trunks, and had boulder snouts, suggesting that they were debris flow in nature (Pierson, 2005; Costa, 1988). The Ohanapecosh debris flow gully increases the number of gullies measured to seven.

Slope and drainage area relate to the energy available within a gully, and also allow comparison of Mount Rainier debris flow initiation sites with slope and drainage areas of debris flow zones in other environments. Debris flow gullies of the 2006 storm are shown by three datasets in slope-drainage area space: the upstream limit (plusses in Figure 2-9, measured at upstream-most point of observed width change from 2006-2008), intermediate reaches of debris flow gullies (diamonds in Figure 2-9, extracted from reaches defined at ends by tributary junctions), and downstream limits of debris flow gullies (squares in Figure 2-9, measured at downstream-most point of width change from 2006-2008). In a downstream sense, these three datasets show the range of slope and drainage area of debris flow gullies, in which flows incised or widened gullies and bulked to debris flow.

The upstream limit data show the most significant trend of the three datasets, plotting along a low concavity (-0.107) power law trend (n =7, R^2 = 0.477). The upstream limit dataset also coincides with an outer boundary of slope and drainage area observed in drainage networks of proglacial areas (small points in Figure 2-9), adding confidence that the observed trend is significant (Figure 2-9). In general, low concavity suggests that debris flow initiation requires steep slopes, and is relatively insensitive to drainage area. The low concavity trend is similar to low concavity trends observed in longitudinal profiles in tectonically-active coastal ranges of the California and Oregon; however, the different scopes of data extraction (across multiple gullies versus longitudinal extraction along individual channels) make further comparison impossible (Stock and Dietrich, 2003).

Slope-drainage area trends of intermediate reaches and downstream gully limits are more scattered. Data points representing intermediate reaches plot along a curved trend. At drainage areas less than approximately 10^6 m^2 and above slopes of ~35 %, intermediate reaches plot along a similar trend to the upstream limit dataset. At drainage areas exceeding this break, intermediate reaches follow a higher concavity trend. Except for two outliers, downstream limits of gullies also plot along the trend of high concavity followed by intermediate reaches. The high concavity trend mimics that of equal stream power contours in slope and drainage area, suggesting that the debris flow gullies extend into portions of the drainage network that have developed longitudinal profiles from fluvial erosion controlled by stream power (Seidl and Dietrich, 1993). *Stock and Dietrich* [2003] attributed curved plots of slope and drainage area along valleys to a change in the dominant mode of erosion from debris flows (low concavities at small drainage areas) to fluvial erosion, and observed slope-area scaling breaks at drainage areas ranging from 10^4 to 10^6 m^2 and at slopes of ~0.10.

2.6.2 Runoff Generation

We used estimates of debris flow duration in the Pyramid drainage to evaluate mechanisms of runoff generation. Estimates of sediment volume and water discharge produce sediment evacuation times of approximately 1 to 10 hours (Figure 2-10), depending on rainfall rates between 0.5 and 2.5 cm per hour and the scenario of runoff generation considered. The first runoff scenario (all contributing area is impervious (i.e. frozen)) produced high estimates of water discharge (~2-10 m^3/s) and correspondingly low sediment evacuation times (~0.3-3.5 hr). Conversely, when glacier surfaces are impervious, and ice-free ground surfaces only generate runoff when infiltration capacity is exceeded, water discharge is low (~ 0.6-3 m^3/s) and evacuation times are correspondingly high (~1-10 hr). In the latter scenario, infiltration capacity values of 6.6 ± 5.1 cm/hr (1σ) generally exceeded the maximum hourly rainfall rates of ~2 cm/hr recorded during the 2006 storm. In our simple model, the high infiltration capacity forced all runoff generation to occur on the contributing area covered by glacier ice (~26% of total area), which we assumed to be impermeable. More generally, the infiltration rates that exceed rainfall rate imply that runoff during debris flow producing storms might be attributed to impermeable frozen ground, heightened discharge from glaciers, snowmelt, or a combination of these sources. During the 2006 storm, SNOTEL data indicate that little snow was present, and that atmospheric freezing levels were elevated, implying that snowmelt and frozen ground generated relatively little runoff during the 2006 storm. Process of elimination and the proximity of the Pyramid and other gullies to glaciers suggest that glaciers play an important role in generating the runoff necessary for debris flow initiation.

Estimates of debris flow duration (sediment evacuation times) were reasonable, falling within range of a the duration of a 2005 precipitation-induced debris flow that lasted approximately 1 to 3 hours from the Van Trump Glacier (observed by author Kennard). Though a rough comparison, our range of estimates for duration of the Pyramid debris flow are within an order of magnitude of the observed debris flow. These findings suggest that sediment volume contributed from gully wall collapse alone may have been sufficient to bulk floodwaters to debris flow, and imply that debris flow initiation by progressive addition of sediment from gully wall collapse is plausible.

2.6.3 Basin Scale Factors Influencing Debris Flow Generation

Comparison of debris flow and non-debris flow basins in the 2006 storm reveals that (1) spatial patterns of debris flow occurrence is reflected by the morphology (slope and drainage area) of drainage networks in proglacial areas, (2) the LCC metric, which incorporates gully length, has greater statistical significance in describing basin differences, and (3) proglacial areas, and thus glacier termini, have statistically higher elevations and lower drainage areas in debris flow basins. We used the NL and LCC metrics defined here, in addition to simple basin metrics to analyze difference in basin groups.

The NL and LCC metrics across the defined slope-drainage area partitions shown in Figure 2-11 indicate that DFB and NDFB have differing distributions of slope and drainage area in their drainage networks. On average, DFB have a greater length of their drainage network with slopes and drainage areas similar to those of measured debris flow gullies. NDFB generally have lower slopes and larger drainage areas. These patterns are shown in Figure 2-12 by divergence in the two basin groups in both NL and LCC metrics along partitions of approximately 1 and greater. We initially hypothesized that proglacial areas where debris flows initiate are supply-unlimited, meaning that slope-drainage area differences relating to energy availability would explain the contrasting occurrence of debris flows. Slope-drainage area distributions suggest that basins with energy-limited (low-gradient) proglacial areas tended not to produce debris flows, and proglacial areas with steeper slopes produced debris flows.

Statistical significance testing using p-values with assumed unequal variances indicate that the LCC metric explained differences between the two basin types better than the NL metric, supporting the idea that gully length helps determine if debris flows initiate (Figure 2-12). For the same partitions, LCC metrics consistently had greater statistical significance as indicated by lower p-values. These results align with our findings in the Pyramid Creek gully suggesting that gully length plays a role in debris flow initiation.

Simple metrics related to glacier extent show that debris flow basins tend to have smaller glaciers, and that debris flow occurrence appears unrelated to glacier retreat. Statistically significant differences ($p < 0.05$, two-tail assuming unequal variances) in mean and maximum elevation and maximum drainage area characterize proglacial areas of the two basin types, indicating that proglacial areas of DFB occur at higher elevations and smaller drainage areas than those of NDFB (Table 2-1). Because the down-valley extent of a glacier determines where a proglacial area sits, the drainage area and elevation metrics reflect glacier extent. Differences in glacier retreat between the two basins, however, are insignificant (Table 2-1). According to the paraglacial concept, glacier retreat exposes debris and increases the supply of sediment in a basin, therefore, glacier retreat can be considered a proxy for debris supply (Ballantyne, 2002). The statistically insignificant difference in glacier retreat is therefore consistent with our previous finding that debris supply is unlimited, thereby limiting the effects of increased debris supply from glacier retreat on debris flow occurrence (Bovis and Jakob, 1999).

2.7 Discussion

The 2006 storm on Mount Rainier initiated debris flows from proglacial gullies in seven basins. Material entrained from gully expansion appears to represent the sediment source for these debris flows. Gully heads at or near glacier termini suggest that clear water flows were converted to debris flow in a distributed manner over some length of each gully. This bulking process is relatively unique for glaciated catchments, yet estimates of sediment volume entrained relative to water discharge suggest that this process of debris flow initiation is plausible. Moreover, the coincidence between expanded gullies in source areas and observed debris flows in downstream areas in all DFB studied imply a linkage between the two.

Whereas we are not able to speak to the mechanics of debris flow bulking, our analysis provides insights into the necessary conditions for this type of debris flow initiation. In order for the transformation of floods to debris flows to occur, we find that gullies must be steep, sufficiently long, and have walls composed of loose, unstable and abundant material. These conditions are consistent with recently burned catchments that generate debris flows by bulking, where abrupt expansion of and sediment delivery to channel networks temporarily and abruptly increase the available debris for entrainment (Wells, 1987; Gabet and Bookter, 2008; Lamb et al., 2011). On the upper flanks of the Cascade Volcanoes, sediment supply is virtually unlimited, particularly in the fronts of glaciers. In addition, gullies and drainage networks are relatively young, having established since deglaciation of a particular area. These conditions create gullies with unstable walls of loose glacial till on steep slopes. Transformation of floodwaters to debris flow may therefore be expected in catchments dominated by loose, alluvium, or where some geomorphic disturbance abruptly makes alluvium available for entrainment.

Despite sparse monitoring data on the upper volcanic slopes, we have constrained possible mechanisms of runoff generation. Measured infiltration capacities that well exceed measured rainfall rates suggest that runoff is generated from some combination of impermeable frozen ground, heightened discharge from glaciers (either from glacier surfaces or englacial storage release), or snowmelt. SNOTEL data however suggest warm temperatures and minimal snow depths characterized the 2006 storm, implying that glaciers were a major source of runoff. Glacier runoff sources, whether from the glacier surface or englacial storage, are consistent the observation that all seven 2006 debris flow gullies were located in proglacial areas, where glacier runoff logically is most focused. The mechanisms of runoff generation and routing from glaciers are still poorly understood. Glaciers on Mount Rainier have varying surface characters and abundances of crevasses, which may influence the infiltration of rainfall. In addition, the end-of-summer timing of the 2006 storm (and other debris flow producing storms on Mount Rainier) may suggest that englacial conduits were integrated, which would have facilitated through-flow of rain water that infiltrated glacier surfaces (Anderson, 2004). The identification of runoff sources, however, does not provide insight into the amount of runoff required for debris flow initiation. Slope and drainage area of 2006 debris flow gullies indicate that debris flow initiation was relatively insensitive to drainage area, and thus the rate of discharge. This insensitivity of drainage area and discharge actually makes debris flow generation more plausible on a landscape with a relatively limited ability to generate runoff (as indicated by infiltration capacities), and is compatible with glacial sources of runoff producing just enough water for debris flow initiation.

In addition to controlling where within a basin debris flows initiate through runoff generation, glaciers also appear to indirectly control which basins produce debris flows. Spatial distributions of debris flows and volcanic shape imply an influence of glacier extent on debris flow potential within a catchment. Drainage network steepness in proglacial areas reflects the distribution of 2006 debris flows. Elevations and maximum drainage areas indicate that proglacial areas, and therefore glacier termini, in DFB are located higher on the volcano. Proglacial areas thus tend to be steeper and more favorable for debris flow initiation at higher positions on the volcano. These patterns reflect increasing slope with elevation, and concave longitudinal valley profiles on the Mount Rainier edifice (Figure 2-13). Because glacier extent controls the location of proglacial areas, proglacial areas are the most favorable zones for debris flow initiation, and slope generally increases with elevation, glacier extent therefore must have an influence on the debris flow potential for a catchment. We propose a simple model that relates glacier extent to debris flow production shown in Figure 2-14. These findings are consistent with retreat rate, a proxy for debris supply, failing to explain differences between DFB and NDFB. Instead of differences in supply, debris flow production is influenced by the slope distribution within a catchment, and in particular the slope distribution in proglacial areas where debris and water availability are greatest. Variable glacier sizes in space and time thus alter the slope distribution of sediment covered slopes in a basin, thereby changing debris flow potential. These findings differ from other studies that suggest that increased sediment availability from glacier retreat is a major driver of increased debris flow occurrence (Chiarle et al., 2007).

2.8 Conclusions

In this study, we analyzed the change, setting, and distribution of gullies on Mount Rainier where floods were transformed to debris flows during a large storm in 2006. Analysis of debris flow gullies from one storm has allowed us to infer the geomorphic processes of and conditions necessary for this unique style of debris flow initiation, in which floodwaters are transformed to debris flow by progressive entrainment of sediment. Seven debris flows initiated from proglacial areas of separate basins during the 2006 storm. Debris flows were observed with expanded gullies upstream, implying that gully expansion provides the source material for these debris flows. In addition, estimates of sediment volumes entrained relative to estimates of flood discharges suggest that bulking from gully walls is volumetrically plausible.

This manner of debris flow initiation by gully collapse requires both sufficient sediment and energy. Detailed analysis of gully change suggests that debris flow gullies must have abundant and unstable material along the gully length. A slope-drainage area trend produced from seven 2006 debris flow gullies indicates that debris flow initiation requires slopes over ~20^{o} near the gully head, but has little dependence on drainage area. High measured infiltration rates, however, suggest that glaciers play a major role in generating the minimum runoff necessary for debris flow initiation. Availability of sediment and water thus make proglacial areas the most favorable zones for debris flow initiation.

Spatial patterns of recent debris flows suggest that initiation occurs near high-elevation glacier termini, with relatively high gradients. Relatively high gradients in DFB proglacial areas compared to NDFB are consistent with the high gradients measured in the seven 2006 debris flow gullies. Elevation differences of proglacial areas in the two basin types suggest that glaciers tend to be less extensive in DFB. These differences in proglacial area slope and elevation in debris flow and non-debris flow basins reflects an overall positive slope-elevation trend on the volcanic edifice with concave flanks. These findings suggest that the slope distribution of ice-free areas (where debris flows initiate) changes with glacier size as large glaciers cover the steepest slopes, and small glaciers expose the steepest slopes. Variations in the available slope influenced by glaciers in space and time thus should correspond with variations in the activity of debris flows. This model suggests that temporal glacier change can influence debris flow occurrence, as threshold slopes are exposed by glacier retreat. This interpretation contrasts with interpretations invoking debris generation as the result of excess sediment exposed during periods of glacier retreat (Chiarle et al., 2007; Ballantyne, 2002). In the 2006 storm, additional sediment exposed by retreating glaciers appears to have had little influence on spatial patterns of debris flow occurrence, which may suggest that the apparently supply-unlimited basins of Mount Rainier are insensitive to increased amounts of debris supply. These findings have implications for debris flow hazards in basins experiencing glacial and climatic change.

2.9 Figures

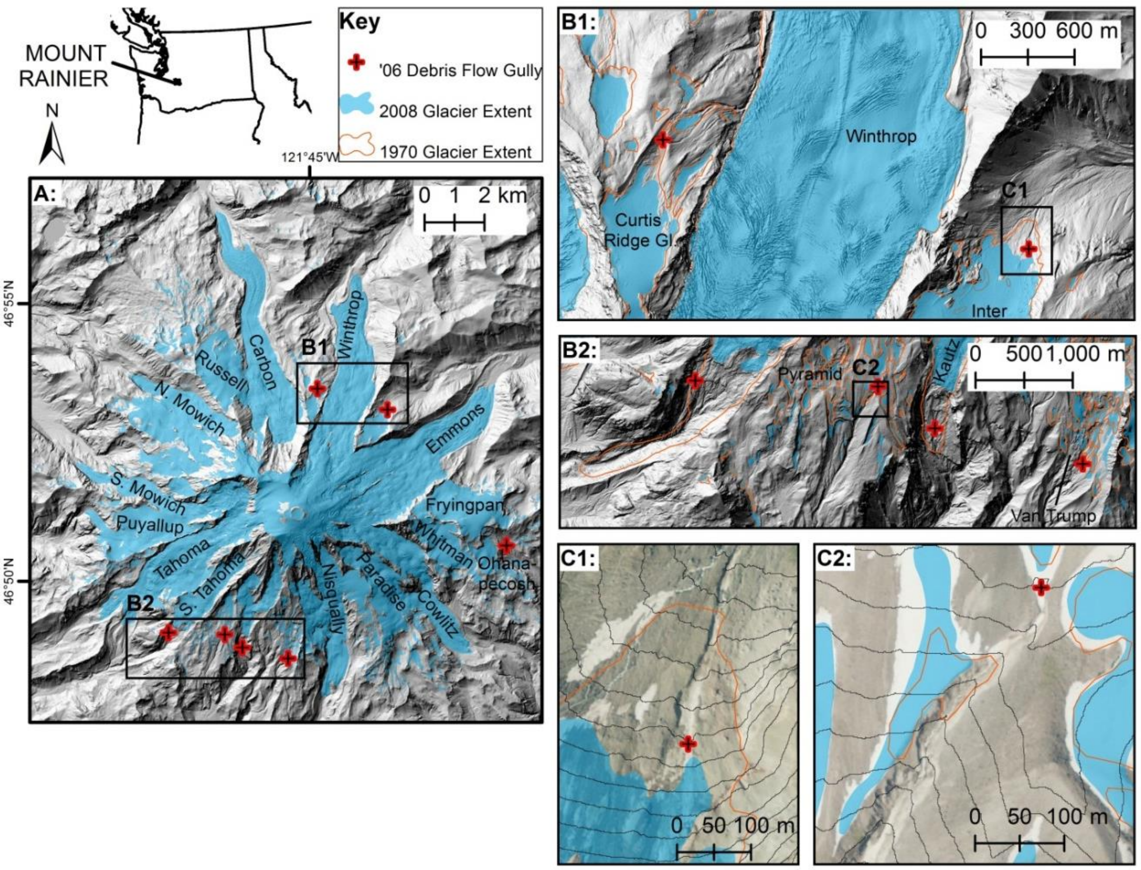

Figure 2-1 Location map of Mount Rainier and debris flow gullies from the 2006 storm. Panel A contains a hillshaded elevation map of Mount Rainier with the extents of insets shown. Panels B1 and B2 contain hillshaded DEMs produced from ALSM data with select debris flow gullies and associated glacier names shown. Panels C1 and C2 show 10-m elevation contours, glacier outlines, debris flow gullies overlain on 2009 NAIP aerial imagery.

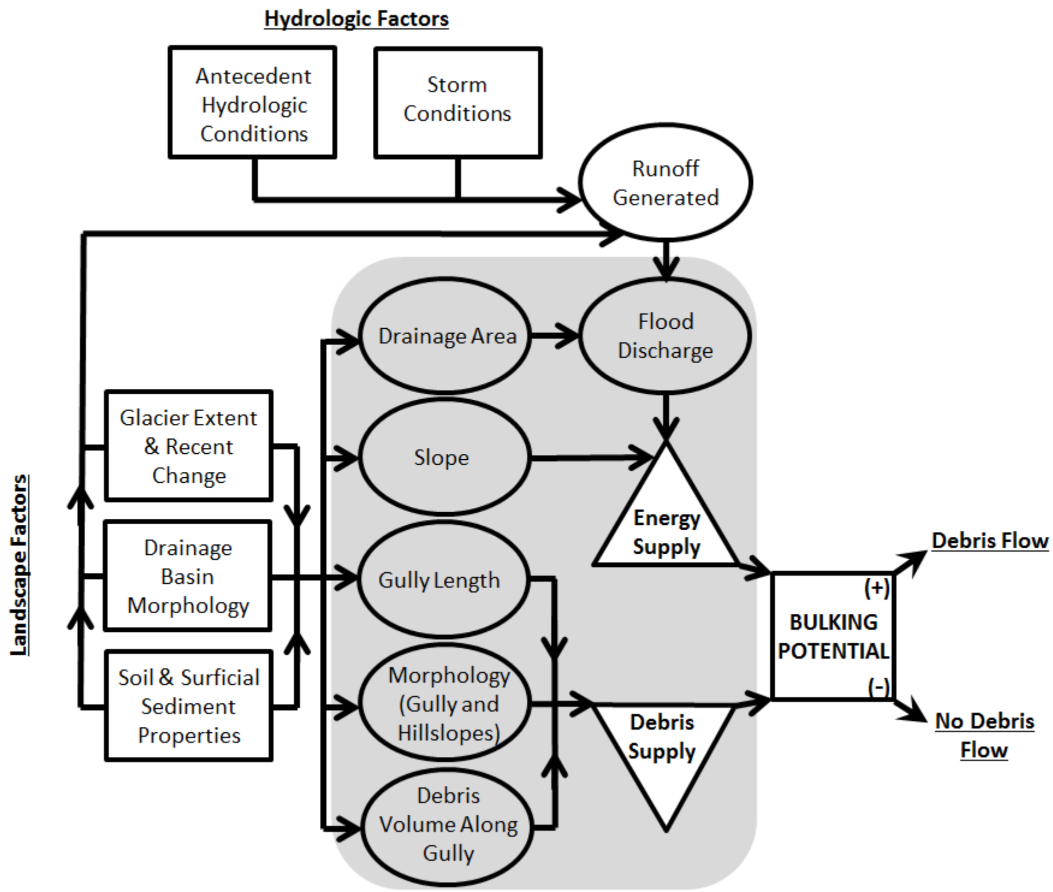

Figure 2-2 Schematic illustration of controls on the transformation of floodwaters to debris flows in glaciated catchments. Rectangular boxes indicate fundamental hydrologic and landscape factors that set conditions for bulking. Ellipses indicate direct (within grey box) and indirect (outside grey box) controls on bulking. Triangles are categories of direct controls that determine bulking potential (square box). Bulking potential can be sufficient (+) or insufficient (-) to generate debris flows.

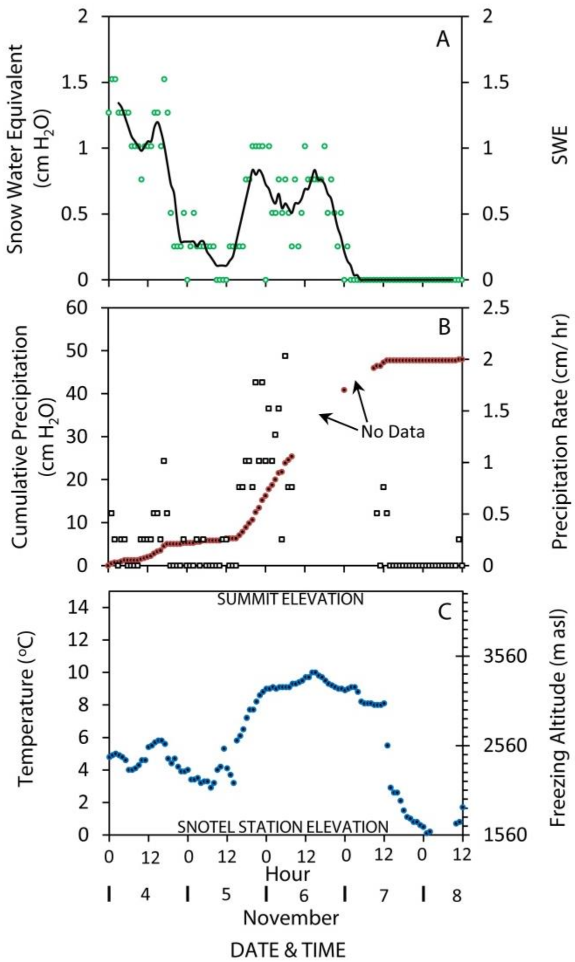

Figure 2-3 Figure showing snow water equivalent (SWE, with running average, A), precipitation (B), and temperature (C) collected at the Paradise SNOTEL station (NRCS, 1,560 masl; 46.78◦, -121.75◦) in a period spanning the November 2006 storm. Hourly SWE measurements (green) and running average (black) are shown in Panel A. Cumulative precipitation (red) and hourly precipitation rates (black) are shown in panel B. Freezing altitudes (Panel C, right vertical axis) are estimated based on a temperature lapse rate of 5.5 degrees Celsius per km altitude.

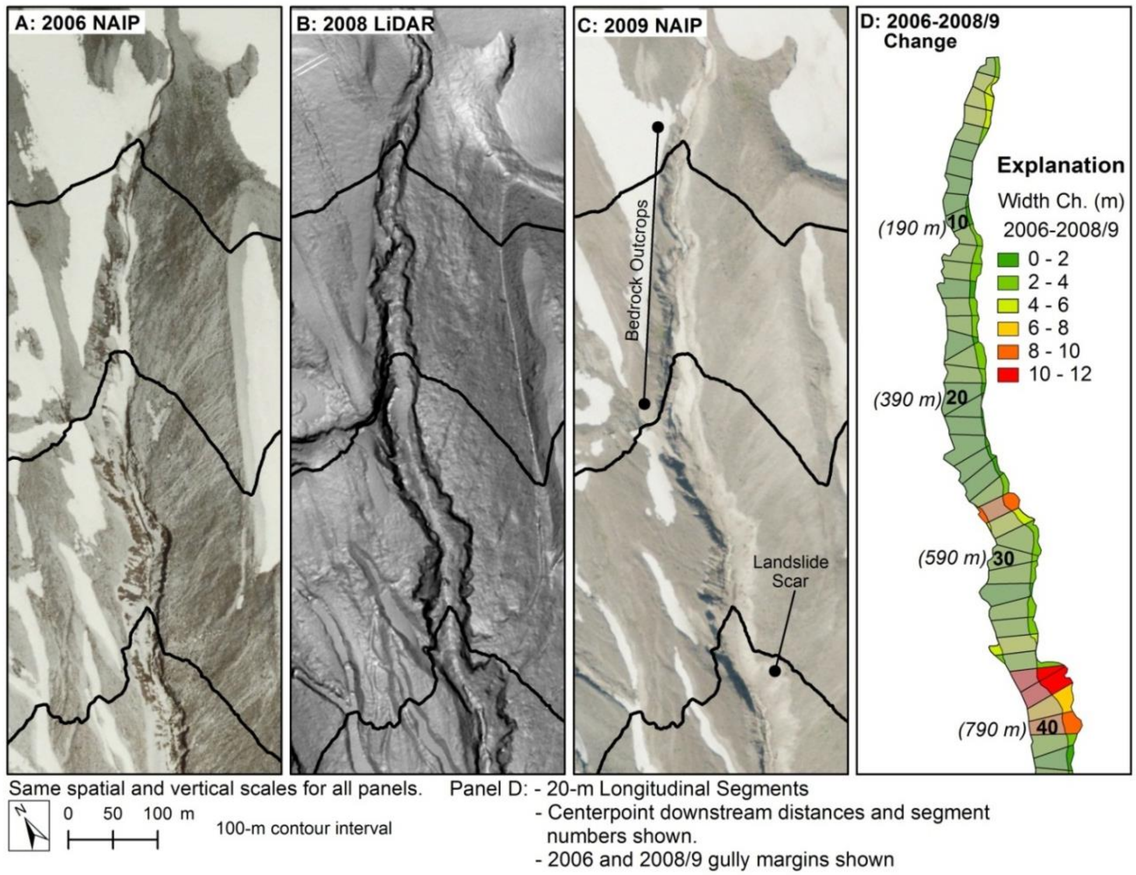

Figure 2-4 Time-series of remote sensing data for the Pyramid gully with data sources shown.The ALSM-DEM in Panel B has a greyscale color corresponding to slope with low slopes in light and steep slopes dark. In panel D, 2006 and 2008 gully outlines are shown. Every tenth segment is labeled with distance downstream from the gully head and a segment number, which correspond to Figure 2-8 segments.

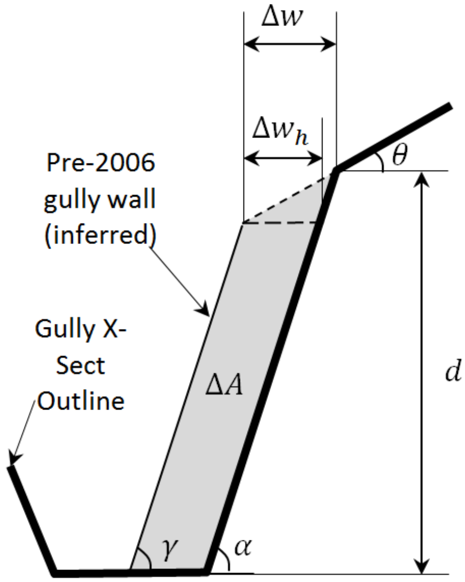

Figure 2-5 Schematic diagram of gully geometry used to convert width change ($\Delta \boldsymbol{w}$) measured from aerial imagery to gully volume change. We assumed that gully bottom elevation and gully wall slope ($\boldsymbol{\gamma}$, before debris flow, $\boldsymbol{\alpha}$ after debris flow) remained unchanged. Hillslope slope ($\boldsymbol{\theta}$), gully depth (d), and gully wall slope ($\boldsymbol{\alpha}$) were measured from 2008 ALSM data. We calculated the width change in the horizontal plane ($\Delta \boldsymbol{w_h}$) using $\Delta \boldsymbol{w_h} = \frac{\Delta \boldsymbol{w} \cdot (\boldsymbol{tan\alpha} - \boldsymbol{tan\theta}) \cdot \mathbf{sin}(\mathbf{90} - \boldsymbol{\alpha})}{\boldsymbol{sin\alpha}}$, cross sectional area change ($\Delta \boldsymbol{A}$) using $\Delta \boldsymbol{A} = \Delta \boldsymbol{w} \cdot \boldsymbol{sin\alpha} \cdot (\frac{\boldsymbol{d}}{\boldsymbol{sin\alpha}} - \frac{\Delta \boldsymbol{w} \cdot \boldsymbol{tan\theta}}{\mathbf{2}\boldsymbol{d}})$, and average volume change ($\Delta \boldsymbol{V}$) for each segment by multiplying $\Delta \boldsymbol{A}$ by segment length (20 m).

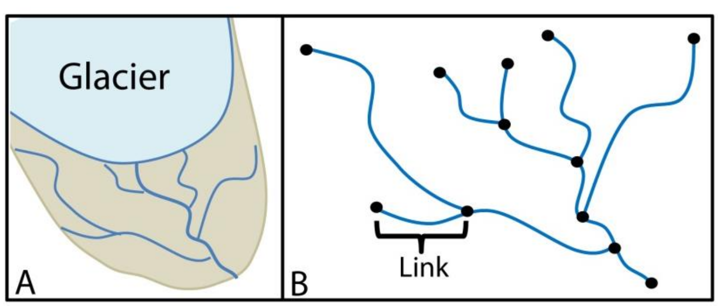

Figure 2-6 Schematic of drainage network clipped proglacial area (A). Panel B shows the drainage networks divided into links at tributary junctions, each of which we extract slope and drainage area.

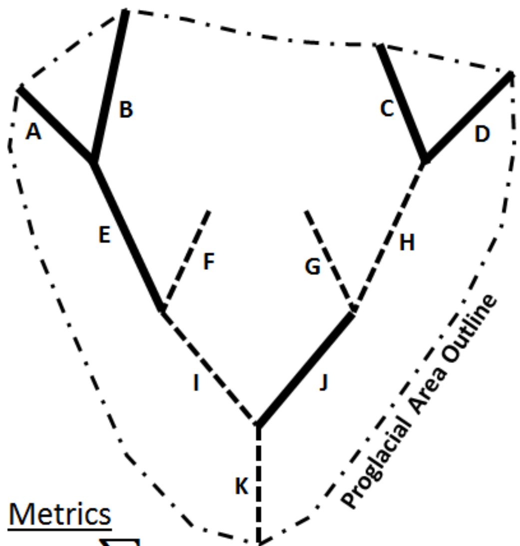

Metrics

$$NL = \sum (l_A, l_B, l_C, l_D, l_E, l_J)$$

$$LCC = \sum (l_B, l_E)$$

Figure 2-7 Example calculations of metrics used to analyze slope and drainage area distributions in drainage networks. Bold links (endpoints defined by tributary junctions) indicate those with slope and drainage above a given partition. Dashed links (length, *l*) are below the partition.

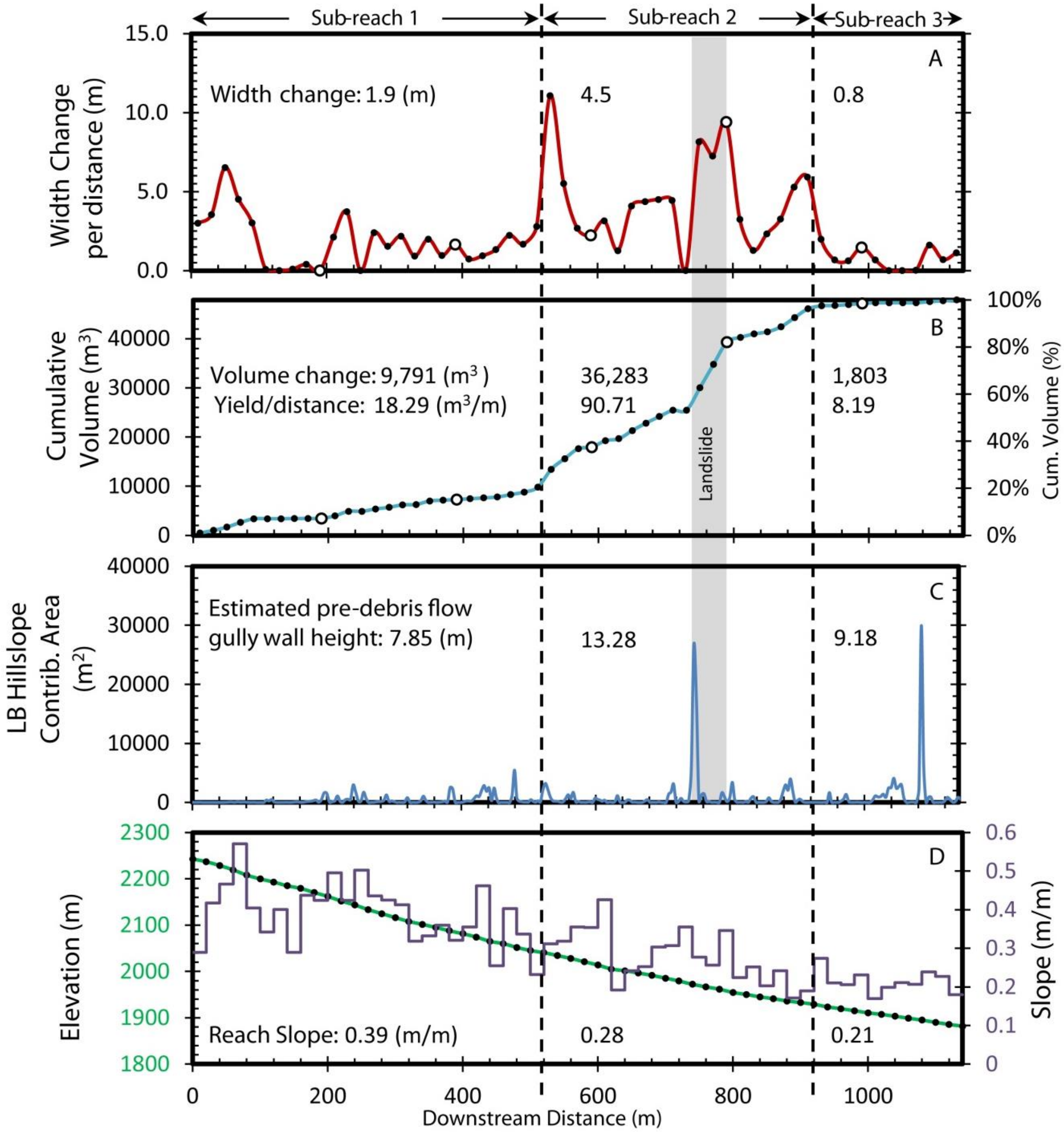

Figure 2-8 Plots of horizontal width change per distance (panel A), cumulative volume change (panel B), hillslope contributing area from the left bank of the Pyramid gully (panel C, proxy for hillslope concavity), and slope (stepped) and elevation (green) with downstream distance in the Pyramid debris flow gully (panel D) estimated for each segment. Sub-reaches are shown to delineate distinct trends in volume change per unit gully length. Each panel contains average metrics for each sub-reach. Note left bank contributing area (panel C) is extracted along a gully-parallel transect shifted approximately 20-m laterally from the gully bottom. Gully wall heights shown are estimates of pre-debris flow gully wall height figured trigonometrically (Figure 2-5). The landslide extent mentioned in the text is shown. In panels A and B, open circles are every tenth segment allowing for comparison with Figure 2-4.

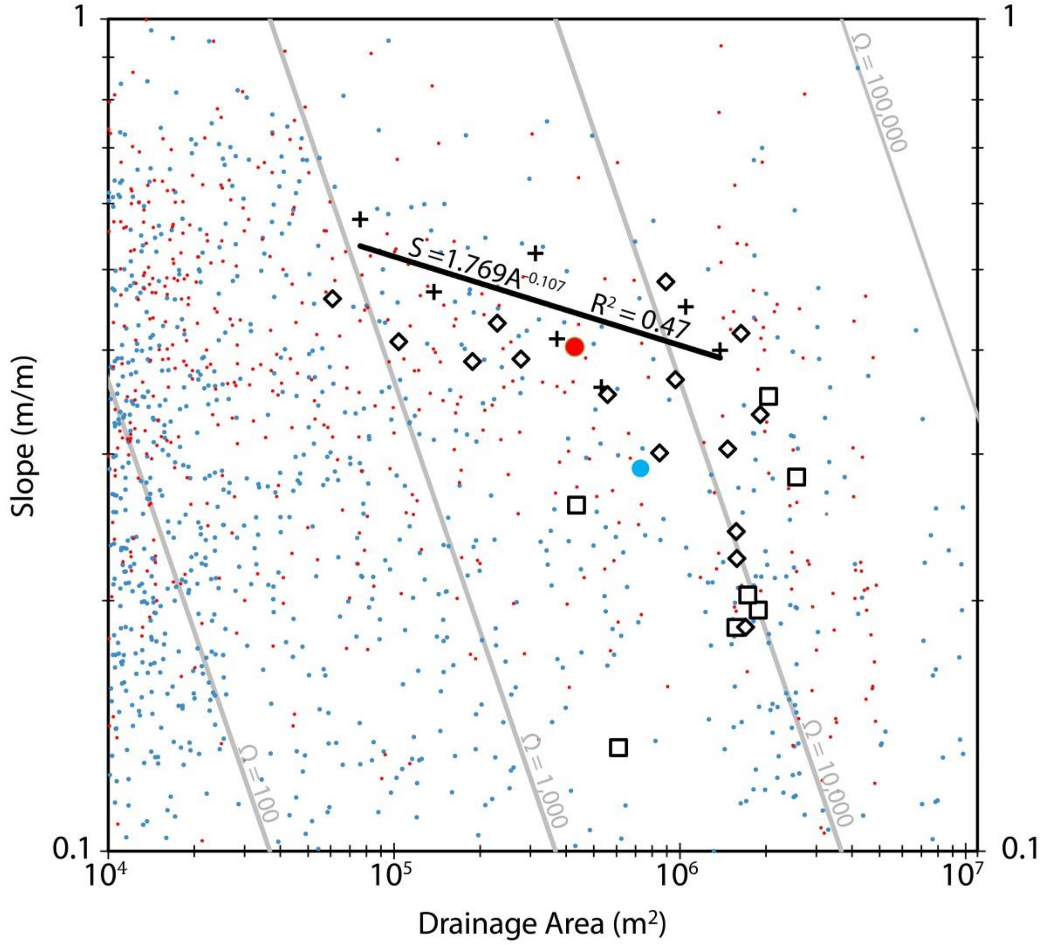

Figure 2-9 Slope-drainage area plot of the upstream limit (crosses), intermediate reaches (diamonds), and downstream limits (squares) of debris flow gullies. Small circles represent all extracted links of drainage networks in proglacial areas in DFB (red, n = 7 basins) and NDFB (blue, n = 15 basins). Large circles of the same colors indicated the length-weighted average of slope and drainage area for the two basin types. The solid line indicates a power regression of the upstream limit dataset. Contours of equal stream power (Ω) are shown [W/m] in grey and based on the stream power equation, $\Omega = \rho_w gQS$, where equation 1 from the text is substituted for water discharge and net runoff generation (rainfall intensity minus infiltration rate) is assumed to be 1 cm/m^2. Other variables in the stream power equation include the density of water (ρ_w), the acceleration due to gravity (g), and slope (S).

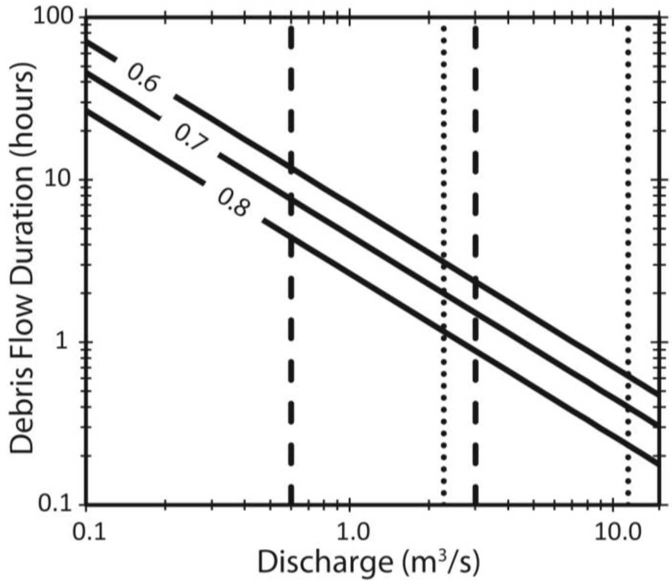

Figure 2-10 Plot of estimated discharge at Pyramid debris flow gully outlet versus calculated debris flow duration. Relationships of discharge to duration are shown for three volumetric sediment concentrations (0.6-0.8). Dashed lines show discharge at rainfall intensities of 0.5 to 2.5 cm/hr (approx. observed range in 2006 storm) for the scenario where runoff is only generated on impervious glacier surfaces. Dotted lines show discharge estimates for the same rainfall intensities (0.5 to 2.5 cm/hr) for the scenario where runoff is generated from an entirely impervious (i.e. frozen) catchment area.

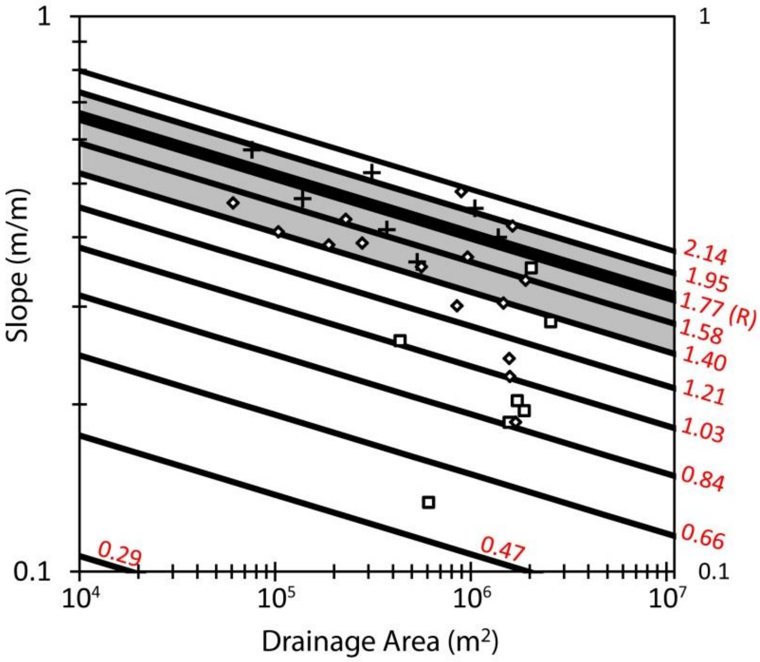

Figure 2-11 Slope-drainage area graph showing partitions (black lines) used to analyze slope and drainage area of drainage networks in proglacial areas. Crosses, diamonds, and squares refer to upstream limits, intermediate reaches, and downstream limits of debris flow gullies (n = 7, see Figure 2-9). Partition values are shown in red adjacent to individual lines and represent the value of the steepness coefficient of slope drainage area partitions aligned parallel to the power law regression equation ($S = 1.769\ A^{-0.107}$) for the upstream limit dataset (Snyder et al., 2000). Partition (steepness) coefficients also correspond to horizontal axis values in Figure 2-12. The grey shaded zone approximately encompasses the observed low concavity trend in debris flow gullies (corresponds to grey box in Figure 2-12).

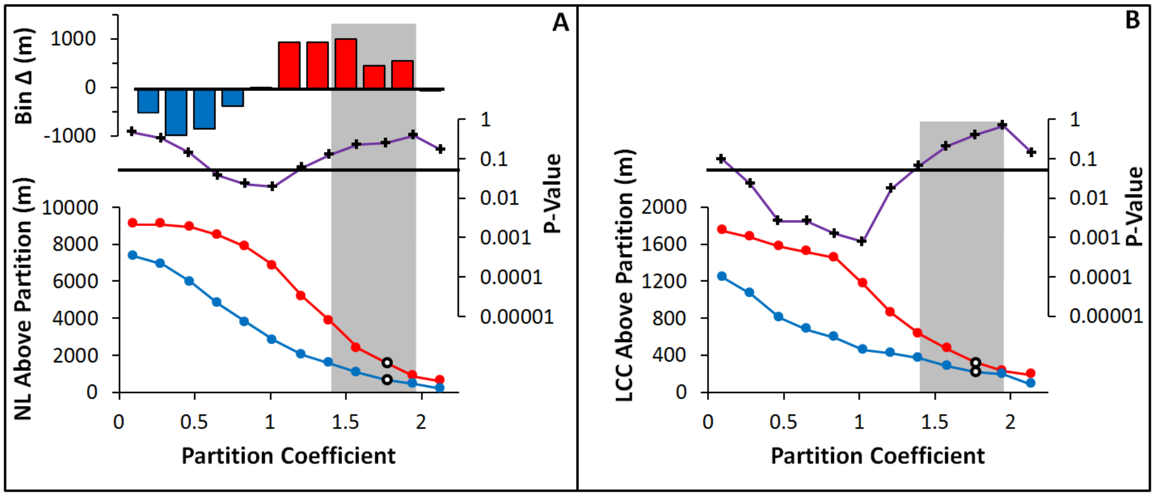

Figure 2-12 Partition graphs for two defined metrics of Network Length (NL, panel A) and Longest Connected Channel (LCC, panel B), which are described in text and in Figure 2-7. Partition coefficients define partitions in slope-drainage area space shown in Figure 2-11. Metric values always represent a length of the drainage network with slope and drainage area above a partition. Red lines are debris flow basin data, blue lines are non-debris flow basin data, and purple lines are two-tail p-values (assuming unequal variances) for each partition. The p-value vertical axis is logarithmic to display differences between the two metrics. Black horizontal lines indicate a p-value of 0.05. Grey boxes indicate the zone of slope and drainage area observed in the low-concavity trend of debris flow gullies. Panel A contains a bar graph showing the difference in length within bins defined by adjacent partitions where positive values show a greater length in DFB, and negative values show a greater length in NDFB.

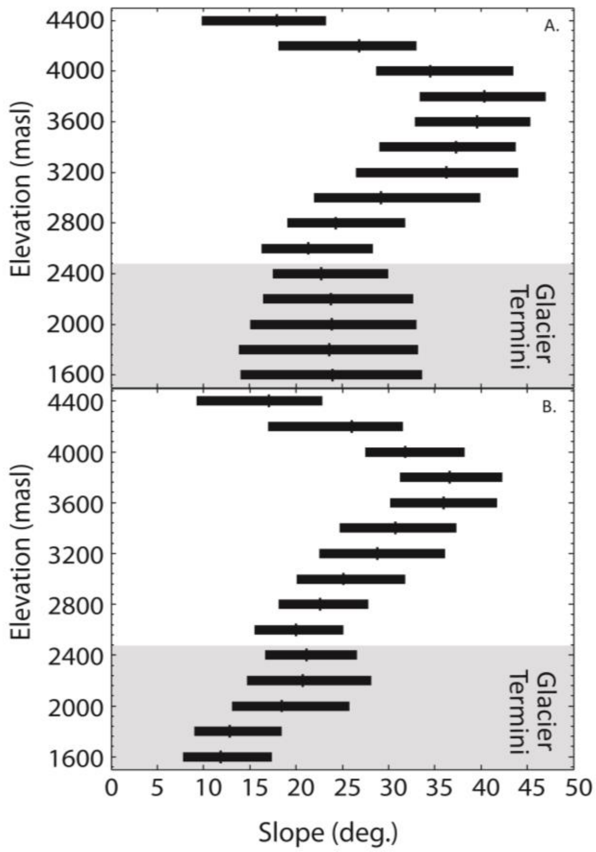

Figure 2-13 Box plots of 200-m elevation bins of slope. Median slope (tick) and 25th and 75th percentile slopes (box ends) are shown for each elevation bin. Elevations of glacier termini are shown. A: Slope-elevation data are extracted from a DEM of entire volcano. B: Slope-elevation data are extracted from only 1970 glacier extents, which effectively selects for valley bottoms where debris flows initiate.

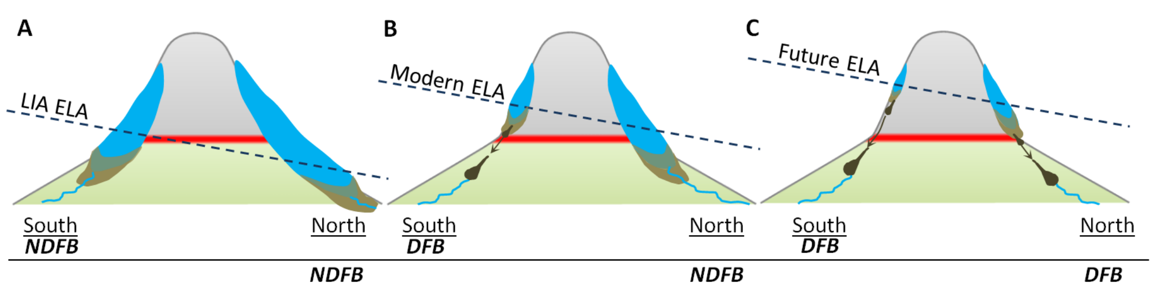

Figure 2-14 Conceptual diagram of spatial and temporal variation in glacier extent and its control on debris flow occurrence in a supply-unlimited basin. Equilibrium line altitudes (ELAs) and corresponding glacial extents are shown for the Little Ice Age (LIA, A), present day (B), and for a future scenario when ELAs are higher (C). In basins where the glacier terminus is above the critical slope angle for debris flow initiation (red line), debris flows occur (DFB). Glacial termini below the critical slope angle have proglacial areas dominated by fluvial transport.

2.10 Tables

Table 2-1 Characteristics of the proglacial areas (PGAs) studied.

Glacier Name	PGA Area (km^2)	Total Extracted Network Length (m)	Drainage Density (m/m^2)	PGA Elevation (masl) Min	Mean	Max	PGA Mean Slope (m/m)	PGA Max Drainage Area (km^2)	1970-2007/8 Glacier Retreat (m) *
NDFB									
Cowlitz	1.02	9,393	0.0092	1,491	1,640	1,905	0.40	15.564	475
Emmons	0.18	2,867	0.0158	1,469	1,498	1,579	0.26	8.803	-130
Flett	0.81	8,166	0.0101	1,954	2,081	2,255	0.45	0.659	115
Fryingpan (East)	0.44	4,866	0.0110	1,778	1,943	2,074	0.37	2.050	110
Fryingpan (West)	0.71	8,789	0.0123	1,773	1,918	2,156	0.38	2.737	110
Nisqually	0.59	3,966	0.0068	1,343	1,547	1,846	0.66	12.081	300
North Mowich	0.81	8,901	0.0110	1,480	1,683	2,209	0.63	8.613	230
Paradise	2.09	21,168	0.0101	1,774	1,979	2,253	0.35	2.502	75
Puyallup	0.12	2,669	0.0224	1,599	1,722	1,868	0.65	2.634	90
Russell	2.21	19,364	0.0088	1,744	2,053	2,400	0.38	1.546	120
South Mowich	0.24	2,935	0.0122	1,482	1,653	1,893	0.61	7.191	260
South Mowich (south terminus)	0.12	1,762	0.0145	1,378	1,499	1,729	0.64	2.357	260
Tahoma	0.35	3,495	0.0101	1,503	1,634	1,803	0.40	5.246	45
Tahoma (west terminus)	0.61	7,717	0.0126	1,485	1,656	1,841	0.47	9.793	45
Whitman	0.56	7,178	0.0129	1,972	2,243	2,454	0.56	3.305	60
Mean	**0.72**	**7,549**	**0.0120**	**1,615**	**1,783**	**2,018**	**0.48**	**5.672**	**144**
DFB									
Curtis Ridge **	0.43	4,547	0.0105	2,110	2,354	2,600	0.53	2.633	75
Inter	0.32	5,441	0.0171	1,964	2,109	2,322	0.49	1.218	210
Kautz	0.96	11,661	0.0121	1,501	1,951	2,417	0.69	4.868	70
Ohanapecosh	1.26	17,342	0.0137	1,687	2,031	2,531	0.56	3.584	140
Pyramid	0.84	9,661	0.0115	1,878	2,205	2,474	0.42	1.645	150
South Tahoma	0.77	8,802	0.0115	1,496	1,832	2,274	0.70	3.120	300
Van Trump	0.61	6,761	0.0111	1,820	2,116	2,450	0.48	1.731	135
Mean	**0.74**	**9,174**	**0.0125**	**1,779**	**2,085**	**2,438**	**0.55**	**2.685**	**154**
p-value	**0.935**	**0.477**	**0.682**	**0.137**	**0.003**	**0.000**	**0.179**	**0.0304**	**0.8361**

* Data from Sisson et. al (2011); negative retreat values indicate advance

** Unnamed glacier located on west-bounding ridge of the Winthrop Glacier

3 Debris flow occurrence and its influence on the Kautz Creek valley (Mount Rainier, Washington) during a 1,000 years of climate and glacier fluctuations

Nicholas T. Legg[a], Andrew J. Meigs[a], Gordon E. Grant[b], Paul Kennard[c]

[a] Oregon State University, College of Earth, Ocean, and Atmospheric Sciences, Corvallis, OR 97331, USA

[b] USDA, Forest Service, Pacific Northwest Research Station, 3200 Jefferson Way, Corvallis, OR 97331, USA

[c] Mount Rainier National Park, 55210 238th Ave E, Ashford, WA 98304, USA

3.1 Abstract

The second study uses a variety of dating techniques to reconstruct a chronology of debris flows in the Kautz Creek valley on the southwest flank of Mount Rainier (Washington). Dendrochronologic dating of growth disturbances combined with lichenometric techniques constrained five debris flow ages from 1712 to 1915 AD. We also estimated ages of three debris flows ranging in age from ca. 970 to 1661. Run-out distances served as a proxy for debris flow magnitude, and indicate that at least 11, 2, and 1 debris flow(s) have traveled at least 1, 3, and 5 km from the valley head, respectively since ca. 1650. Valley form reflects the frequency-magnitude relationship indicated by the chronology. In the upper, relatively steep valley, discrete debris flow snouts and secondary channels are abundant, suggesting a process of debris flow conveyance, channel plugging, and channel avulsion. The lower valley is characterized by relatively smooth surfaces, an absence of bouldery debris flow snouts, few secondary channels, and relatively old surface ages inferred from the presence of tephra layers. We infer that the lower valley is deposited on by relatively infrequent, large magnitude, low-yield strength debris flows like an event in 1947, which deposited wide, tabular lobes of debris outside of the main channel. Debris flows during the Little Ice Age (LIA) predominantly traveled no further than the upper valley. Stratigraphic evidence suggests that the main Kautz Creek channel was filled during the LIA, enhancing debris flow deposition on the valley surface and perhaps reducing run-out lengths. Diminished areas and gradients in front of glaciers during the LIA also likely contributed to decreased run-out lengths. These findings suggest that changes in debris flow source and depositional zones resulting from temperature and glacier cycles influence the

magnitude and run-out distances of debris flows, and the dynamics of deposition in valley bottoms.

3.2 Introduction

Debris flows are a primary geomorphic process as well as a dangerous natural hazard in mountain terrains around the world (Iverson et al., 1997). Debris flows occur in many mountainous settings; in this paper we focus on debris flows that initiate high on the flanks of glaciated stratovolcanoes in the Cascade Range of the northwestern United States. Recent and unusually extensive debris flow events in this setting have raised questions as to whether changing climate is increasing the potential for debris flow initiation and run-out. Whether or not this is occurring, its potential causes and consequences are key issues facing managers of mountain environments in this region. But factors controlling debris flow occurrence remain poorly understood.

The lack of suitable debris flow records limits our ability to assess the frequency and magnitudes of debris flows, and put recent debris flows into context. On Mount Rainier in Washington State, the location of this study, existing archival debris flow records span few decades, are incomplete, and are compiled across basins with seemingly different debris flow potentials (Copeland, 2009). With exception of pioneering studies on Mount Shasta that used tree rings to reconstruct debris flow ages, no detailed efforts to construct debris flow (non-lahar) chronologies in valley bottoms of the Cascade volcanoes have been completed (Hupp, 1984; Hupp et al., 1987). In addition to simply understanding debris flow occurrence through time, these studies reveal depositional patterns that affect the short- and long-term evolution of the geomorphology and forest ecology of valley bottoms (Hack and Goodlett, 1960).

The natural setting on Cascade volcanoes is an ideal natural laboratory for studying coupling between erosional processes in upper catchments with evolution of depositional settings in valleys downstream. Large glaciers erode the weak upper flanks of these volcanoes at rapid rates, causing large quantities of sediment to be transported through valleys (Czuba et al., 2012; Mills, 1976). Debris flows and floods deliver sediment to valley bottoms on annual to decadal scales; valleys that are often wide and favorable for stratigraphic preservation (Driedger and Fountain, 1989; Scott et al., 1995; Copeland, 2009). In addition, old protected forests with relatively little influence from wildfire provide a record of disturbance through time (Stoffel and Bollschweiler, 2008; Dunwiddie, 1986). These environmental factors allow high-resolution coupling of valley bottom records of geomorphic processes with climate and glacier changes that may drive erosion and sediment production in the upper catchments, connections that are often studied over thousands of years as opposed to hundreds (e.g. Dühnforth et al., 2008; Ritter et al., 1995).

In this study, we use field evidence to develop a debris flow chronology in the Kautz Creek drainage basin on the southwest flank of Mount Rainier (Figure 3-1). At least six debris flows have occurred in Kautz Creek in the past century, including the largest of historical record on Mount Rainier. Of the valleys radiating from the volcano, the Kautz valley is relatively wide with a roughly trapezoidal cross-sectional shape, leading to high potential for preservation of debris flow deposits. We use a combination of radiocarbon dating, tephra layers deposited within in the stratigraphic succession, dendrochronology, and lichenometry to establish ages of debris flows. The resulting chronology is correlated with precipitation indexes, local temperature reconstructions and moraine stabilization ages dated here and in previous studies (Burbank, 1981; Burbank, 1982; Heliker et al., 1984; Sigafoos and Hendricks, 1972; O'Neal, 2005; Graumlich and Brubaker, 1986; Viau et al., 2012; MacDonald and Case, 2005). This combination of high-resolution climate and glacier reconstructions provides a unique opportunity to link high frequency oscillations in valley sedimentation processes with changes in erosional processes in upper catchments.

3.3 Background – Volcanic and Glacial History of Mount Rainier

Mount Rainier, a stratovolcano of andesite-dacite composition, is the highest peak (4,392 m asl) in the Cascade Range and supports the greatest volume of glacier ice in the lower United States (Driedger and Kennard, 1984; Hildreth, 2007). Rivers drain radially from glaciers that vary in extent with aspect and run through valleys of differing widths, gradients, and form. Varying valley morphologies may relate to the suite of processes that have shaped the volcanoe since its construction ca. 500 ka (Hildreth, 2007). The edifice was built on deeply dissected terrain, and some of the ridges radiating from the summit, including the east-bounding ridge of Kautz Creek Valley, were formed when lava flowed and solidified between early glaciers (Lescinsky and

Sisson, 1998). Ancestral topography, eruptive products, alluvial fill, glaciers, and constructional topography thus combine to shape valleys and provide a context for the variation in morphology of valleys radiating from Mount Rainier.

Mass movement processes on Mount Rainier include debris flows initiated by precipitation, debris flows initiated by glacier outburst flood, and lahars (Scott et al., 1995; Vallance and Scott, 1997; Crandell, 1971b). While definitions of lahars and debris flows lie on a continuum, lahars are typically unrelated to glacier, climate, and hydrological processes focused on here; therefore, we attempt to distinguish between lahar and debris flow deposits using sedimentology and volumes. Lahars tend to be cohesive, relatively high clay-content debris flows that typically result from flank collapse of the volcanic edifice. Conversely, debris flows on the Cascade volcanoes typically have low-clay content and cohesiveness because they mobilize surficial debris from which clay has been winnowed. Whereas lahars have return intervals of greater than 500 years and travel tens of kilometers from the summit, debris flows have been recorded numerous times in the previous century and typically travel less than ten kilometers from the summit (Scott et al., 1995). Hydrologically-induced debris flows initiate when runoff generated from precipitation or glacier outburst floods incorporate surficial sediment (Walder and Driedger, 1994b; Walder and Driedger, 1994a; Walder and Driedger, 1995; Vallance et al., 2003).

Eruptive products and lahars preserved in valley bottoms can complicate the record of landscape responses to glacial and climatic drivers studied here. Recent eruptive periods of Mount Rainier have been dated at, 2,200 to 2,600, 1,500, and 1,000 BP (Sisson and Vallance, 2009), yet eruptive products or lahars dating from these time periods have not been documented in the Kautz Creek valley. The Summerland (2,200 to 2,600 ybp) eruptive period is capped by the C tephra and probably induced the National lahar which traveled to the west from the summit (Mullineaux, 1974). The 1,500 ybp eruption is associated temporally with the Twin Creek lahars which initiated from the northeast flank of Mount Rainier and ran out to the Puget Sound (Sisson and Vallance, 2009). Finally, an ash deposit found near the White River (northeast flank) was dated at 1,040 ±410 cal year BP (Hoblitt et al., 1995). The closest associated lahar deposit in time is the Fryingpan lahar assemblage, which ran out to the north east and was dated at 1,120 ± 70 cal year BP (Zehfuss et al., 2003). Lahars or tephras with similar ages have not been documented on the southwest side of the Mount Rainier.

Tephra layers sourced from Mount Saint Helens (~75 km to the south-southwest) are present in the study area as well, and serve as temporal markers in strata and on landforms. Notable ash layers for this study include layer W, which represents two closely spaced eruptions tree-ring dated at 531 and 533 BP (1480 to 1482 AD), and layer Y at 3,500 BP (Vallance and Scott, 1997; Yamaguchi, 1985).

A series of moraine studies around the mountain document Neoglacial glacier fluctuations on Mount Rainier(Burbank, 1982; Burbank, 1981; Sigafoos and Hendricks, 1972; O'Neal, 2005). Moraine ages predominantly date to the Little Ice Age (LIA) period extending from ca. 1600-1850, with terminus positions typically 1-2 km down valleys of current termini. Multiple moraines in valleys suggest that glaciers fluctuated throughout the LIA, while on average larger than present glaciers. Moraine ages are not known in the Kautz drainage. As discussed later, periods of moraine stabilization across the volcano, as indicated by clusters of moraine ages, coincide with warming trends in the temperature record (Graumlich and Brubaker, 1986). Since moraines stabilize when glaciers recede away from a previously stable terminus position, moraine ages should coincide with warming temperature trends. These correlations in moraine stabilization and temperature support temperature-sensitivity of glaciers and a robust temperature reconstruction (Meier, 1984). In the previous century, glaciers have generally retreated with exception of a period in the 1960s and 1970s, and have lost 14% of their volume from 1970-2007/8 (Heliker et al., 1984; Sisson et al., 2011).

3.4 Methods

This study used a combination of geomorphic mapping, surface dating of landforms, and stratigraphic sequences to reconstruct the chronology of prehistoric debris flows, fluvial processes, and glacier terminus positions in the Kautz Creek basin. Geomorphic mapping on high-resolution topography derived from airborne laser swath mapping (ALSM) provides a basis for interpretation of valley form. We use a series of surficial and stratigraphic dating methods including dendrochronology, lichenometry, and radiocarbon dating techniques to establish temporal constraint on the natural archives in the Kautz Valley.

High-resolution ALSM data allow detailed landform mapping and measurement of vertical elevation change. The ALSM data used here were collected in October 2008 and August 2012 (both obtaining 7 points/m^2) and subsequently processed into 1-m gridded digital elevation models (DEMs) of the bare earth and digital surface models (DSM) of the forest canopy. The repeat ALSM surveys allowed us to measure vertical elevation change between survey dates by generating DEM of difference (DOD) maps. We also used DSMs of the forest canopy to evaluate relative forest and landform ages where boundaries in forest age coincided with landform boundaries.

Spatial distributions of debris flow deposits and their characteristics allowed us to qualitatively evaluate the nature and frequency of debris flow deposition in the Kautz Valley. We utilized bare-earth DEMs with one-meter elevations contours and DSMs of tree canopies overlain at a 1:1,000 scale for field mapping. DSMs of tree canopies provided visual representation of relative forest ages and aided with landform identification in the field. In active channels, we mapped the distribution of major debris flow deposits from the most recent debris flow that occurred in 2006. Outside of active channels where forest cover had not degraded surface features, we mapped debris flow snouts and levees in the field and using ESRI ArcGIS. We defined levees as narrow and roughly linear features in map view that are composed of grains with no preferred orientation. We classified debris flow snouts as any deposit with no obvious orientation of grains or fluvial features (Whipple and Dunne, 1992). We primarily mapped these landforms in the field, but supplemented mapping with imagery and ALSM DEMs in the office. Finally, we used historical aerial imagery to map former channel positions and aid with geomorphic surface age determination.

Where trees appeared impacted or buried by debris flow deposits in the field, we employed dendrochronologic techniques to determine debris flow disturbance ages. We cored the impacted (typically uphill) and un-impacted sides of trees using a 24-inch increment borer, which allowed us to core to the pith in all but the largest trees. We marked sampled trees on DSMs of the forest canopy height, on which individual trees were identifiable. Debris flows can bury, scar, or tilt trees, and the associated growth disturbances record debris flow events (Figure 3-3) (Bollschweiler et al., 2007; Stoffel and Bollschweiler, 2008). Stem burial abruptly suppresses annual growth; scarring results in creation of traumatic resin ducts; and tilting causes eccentric growth resulting in asymmetric ring-width patterns between the two opposite core samples. In conifers such as Douglas fir (Pseudotsuga menziesii), mountain hemlock (*Tsuga mertensiana*), western hemlock (*Tsuga heterophylla*), grand fir (*Abies grandis*), and silver fir (*Abies amabilis*) sampled here, compression wood grows on the underside of a tilted tree. Alternatively, debris flows clear swaths of a forest that leave adjacent uninjured trees with additional light and nutrients. Enhanced growing conditions release growth in these survivors and mark the timing of debris flows (Stoffel et al., 2005).

Laboratory processing of tree cores included sample preparation, sample screening, and cross dating. We prepared core samples using standard techniques and examined samples associated with a single debris flow deposit for growth disturbances of roughly common age (Speer, 2010). On samples with roughly contemporaneous disturbances, we measured ring widths using a scope and Velmex measuring stage with one micron precision. We then checked our sample measurements with the statistical cross-dating program COFECHA to identify approximate locations of missing or false rings, and corrected measurements accordingly (Grissino-Mayer, 2001; Holmes et al., 1986). Finally, we compared disturbances to existing master tree-ring chronologies to confirm that observed disturbances were not climatically induced (Earle et al., 1987; Peterson and Peterson, 2001). Where a common non-climatic disturbance was present in two or more samples associated with a single debris flow deposit, we assigned the associated deposit the age of common growth disturbance. Where only one tree was available for a single deposit, we compared disturbance ages with the associated lichen landform age (lichenometric techniques discussed below). Where a disturbance age was within error of the lichenometric age, we assigned the deposit the age of the tree growth disturbance. We assigned a lower certainty to deposits meeting the latter criteria. Even with statistical checks for cross-dating accuracy, debris flow dates have an approximate error of ±2 years due the possibility of false or missing rings, measurement error, and uncertainty in the exact year of disturbance onset.

Lichenometric dating also provided a method for estimating landform ages. A diametric growth curve for the abundant species *Rhizocarpon geographicum* at elevations between 1,000 and 1,760 masl was developed by Porter (1981), updated by O'Neal and Schoenenberger (2003) and extended by O'Neal et al. (in review). Measurement of the largest lichen diameter on a landform permits age estimation of landforms to least 300 years in age with an approximate error of ±10 years on surfaces younger than 150 years, and with increasing error on older surfaces. On many debris flow deposits, we suspect errors are greater than published error estimates due to competition with moss and shading from adjacent forests (we assume ±15 and ±20 years on surfaces of 0 to 150, and >150, respectively). We also measured lichen diameters on glacial moraines, and assume the published error ranges apply based on minimal moss coverage and shading at higher elevations.

Stratigraphic sequences exposed in banks and soil pits revealed change in valley sedimentation through time. We measured and described stratigraphy in vertical sections and used sedimentological descriptions, and infrequently sediment size analysis by sieving and pebble counts, to interpret the nature of stratigraphic layers (Costa, 1988; Pierson, 2005; Scott et al., 1995; Wolman, 1954). Sedimentological boundaries or buried organic soil horizons marked layer contacts, and tephra layers and radiocarbon dating constrained absolute horizon ages. Whenever possible, we collected radiocarbon samples from the outermost rings of buried tree stumps in growth position to estimate death dates and infer ages of overlying deposits. We also sampled organic material incorporated in layers representing individual fluvial or debris flow layers to estimate maximum ages. Radiocarbon samples were submitted for analysis using Atomic Mass Spectrometer (AMS) techniques and calibrated using the INTCAL09 curve (Reimer et al., 2009). When multiple age constraints were present within individual sections, we used stratigraphic modeling in the OxCal program to adjust raw age probabilities of radiocarbon results to reflect age constraints imposed by tephra layers and other radiocarbon samples in stratigraphic succession (Ramsey, 1995).

To obtain a snapshot of landform ages and infer geomorphic disturbance through time, we dug soil pits at randomly sampled locations to determine the presence or absence of the Mount Saint Helens Layer W (1480-1482 AD). We randomly selected 55 locations using ArcGIS10 from areas of unknown surface age (surfaces originating prior to the 1947 debris flow, discussed below), and dug to the first encounter of mineral soil. At each location, we dug a maximum of three pits within an approximate 10-meter radius to prevent false negatives that may have resulted from spotty ash coverage. In pits where mineral soil was encountered above the ash layer, we classified the surface as younger than 1482, meaning deposition covered or erosion removed the layer. Where the Layer W was encountered, we classified the surface as older than 1480.

We integrated results from all dating methods to form a chronology of debris flows and sedimentation in the Kautz Valley and correlated with climate and glacier data. For temperature, we combined instrumental records (1914-2010; Western Regional Climate Center) of mean annual temperature with a tree-ring reconstructed mean annual temperature record (1590-1979) for Longmire (Graumlich and Brubaker, 1986). We performed a linear regression for the period of 1914 to 1979 and corrected the tree-ring reconstructed temperatures according to the linear regression equation.

3.5 Landforms – Physical Characteristics and Distribution

The general form of the Kautz Valley varies with distance from its head at the Box Canyon (Figure 3-1). Longitudinal valley gradients range from approximately 7^{o} at the valley head below the bedrock-walled (but alluviated) Box Canyon, to 2^{o} at the confluence with the Nisqually River (Figure 3-2). Kautz Creek runs the length of the broad valley as a cobble and boulder-rich alluvial channel averaging about 50 meters in width (Figure 3-3). No major tributaries enter Kautz Creek until about river kilometer (RK) 4, where Pyramid Creek joins (Figure 3-1). Pyramid Creek enters the valley from river right near the valley head and runs down the right side of the valley until meeting Kautz Creek. Based on this configuration, most of the sediment in the main channel is derived from the headwaters with limited lateral contributions. A cross-sectional convexity characterizes the upper valley above RK 9, with the bed of the main Kautz Creek channel sitting as much as 15 meters above the valley sides. In the following discussion, we refer to the Kautz Creek channel as the main channel and to other channels (abandoned and active) that run across the valley floor as secondary channels. We also use the term valley floor for the valley bottom outside of the main channel. For ease of discussion, we also define the upper, middle, and lower valleys to extend from the Box Canyon to RK 8, RK 8 to RK 5, and RK 5 to the Nisqually confluence, respectively.

Active deposition occurs on the valley floor, despite some factors suggesting a disconnection from the main channel. The main channel bed sits on average 5.4 meters below the adjacent forested valley surface, suggesting minimal exchange of water and sediment between the main channel and adjacent valley surfaces. During field work, however, summer stream flows actively ran across the valley floor in a narrow channel that appeared to run through a faint former channel feature (Figure 3-1). DEM of difference maps reveal that this channel conveyed sediment into the forest between 2008 and 2012.

Debris flow landforms were commonly composed of open-framework boulders with little matrix at the surface (Figure 3-3). Debris flow lobes had surface gradients along their long axes ranging from 7^{o} to 15^{o} and generally exceeded the surrounding valley floor slope. Intermediate grain diameters averaged approximately 40 cm, with boulders greater than a meter in diameter common. Below the surficial layer of open framework boulders (usually 1-2 boulder diameters thick), boulders and cobbles were supported in a dense matrix of sand, silt, and clay (Figure 3-3). Due to little fine matrix at the surface, debris flow deposits often had minimal forest growth and were therefore easily identified using aerial photographs, DSMs of forest canopies, and in the field. Debris flow landform mapping may thus be biased toward un-forested open framework deposits.

Debris flow landforms vary in abundance and character longitudinally and transversely in the Kautz Valley (Figure 3-4). Mapped debris flow landforms were abundant downstream of the Box Canyon (RK 11) to approximately RK 8, where longitudinal valley and channel gradients range from 6^{o} to 7^{o} (Figure 3-2 and Figure 3-4). Debris flow lobes commonly appear to have spilled from secondary channels, many of which are now inactive and forested. In some cases, debris flow lobes appear “frozen” in place in secondary channels (Figure 3-4). Other secondary channels lose their expression where broad boulder fields are present. Secondary channels form a discontinuous, network sub-parallel to the valley trend, creating a rough surface appearance (Figure 3-4). Secondary channels range in morphology from incised into the valley surface to being perched on top of the valley surface with constructed channel banks (Figure 3-5). Below approximately RK 8, debris flow lobes and levees become markedly less abundant, and the valley surface takes on a smooth surface character with fewer secondary channels. In this lower zone, secondary channel cross sections reveal subtle to non-existent levees.

3.6 Historical Debris Flows in Kautz Creek

Historical debris flows have known times of deposition and provide examples of debris flow magnitudes, styles, and sedimentological characteristics.

3.6.1 1947 Debris Flow

Kautz Creek was the site of the largest debris flow on Mount Rainier in recorded history. On October 1, 2, and 3, 1947, intense rain fell and induced flooding and debris flows in Kautz Creek. High water washed out the entrance bridge, which was followed by a series of debris flows. The first debris flow occurred between 10 and 11 PM; the first of a number of pulses that occurred through the night of October 2 to 3. The debris flows reportedly had the “consistency of wet concrete, carrying along vegetation and boulders as large as [4 meters] in diameter” (Crandell, 1971b). Grater (1947) observed a large canyon cut into glacial material upstream of the box canyon following the event, and hypothesized that debris flow pulses resulted from temporary damming behind the Box Canyon (Figure 3-1 and Figure 3-6). Grater (1947) estimated that the event mobilized greater than 40 million cubic meters of material. Czuba et al. (2012) estimated a sediment volume change of approximately 9 million m^3 between 1945 and 1956 in the Alder Reservoir located downstream on the Nisqually River.

The debris flows and floods of the 1947 storm profoundly changed the Kautz Valley. Reconnaissance following the storm found that a reach of the former channel was abandoned and left perched above a newly cut 10- to 25-m deep channel (Figure 3-1, Figure 3-3, and Figure 3-6). Today, the former channel sits approximately 6 m above the active channel. Though originally thought to have cut a completely new channel by Grater (1947), Crandell (1971) indicated that the valley topography suggested that flows had enlarged a pre-existing, unoccupied channel. Based on valley gradients, Crandell inferred that channel incision was accomplished by floodwaters as opposed to debris flows. Flooding also cut secondary channels through the forest (Figure 3-5). In the upper part of the valley, debris flow deposits remained mostly confined to the channel, with minor localized spill over. In the lower portion of the valley (below ~ RK 6), wide lobes of debris spilled from the channel, inundating large areas of the forest and forming a debris fan at the confluence with the Nisqually River (Figure 3-1 and Figure 3-6).

3.6.2 Other Debris Flows

In contrast with the 1947 event, subsequent debris flows in 1975, 1985, 1986, 2005, and 2006 were mostly confined to channels (Richardson, 1968; Driedger and Fountain, 1989; Copeland, 2009). The 1975 debris flow initiated near the Kautz Glacier, crossed the drainage divide, and traveled down the Van Trump drainage to the east. Detailed maps of the 1985 and 1986 deposits were not available, and their deposits were not identifiable in the field, suggesting their impact outside of the active channel was small. The 1975, 1985, and 1986 debris flows all occurred during warm periods in summer months, suggesting they were initiated from glacier outburst floods. The 2005 debris flow occurred during a storm in late fall after intense precipitation (Copeland, 2009)

On November 6 and 7, 2006, an atmospheric river storm approaching from the southwest hit Mount Rainier and dropped approximately 45 cm of rain over a 36-hour period (Neiman et al., 2008). We identified 2006 deposits in active channels and in localized areas where the debris flows spilled into and killed forests (Figure 3-1 and Figure 3-3). In places where the 2005 debris flow filled the main channel, the 2006 debris flowed into and killed forests. The 2006 debris flow traveled downstream in the main channel to approximately RK 3 and caused an avulsion in the active channel, rerouting normal stream flow following the storm to the east side of the 1947 debris fan (Figure 3-1). Whereas atmospheric river storms like that of 2006 storms have conditions favorable for debris flow initiation (Chapter 2), storms that are not classified as atmospheric rivers likely also create conditions favorable for debris flow initiation.

3.7 Little Ice Age Moraine Ages – Lichenometric Data

Lichenometric age estimates of previously undated moraines above the Box Canyon in Kautz Creek provided temporal constraint on glacier positions (Figure 3-7). Using an established growth curve, we estimate three moraine ages of 1637 , 1768 , and 1839 (maximum lichen diameters of 165 mm, 108 mm, and 77 mm respectively) , which fall within periods of moraine stabilization found for other glaciers on Mount Rainier (Sigafoos and Hendricks, 1972; Burbank, 1981; O'Neal, 2005; O'Neal et al., in review). These moraine ages represent minimum ages, because relatively few lichens were present.

3.8 Landforms – Relative and Absolute Ages

The distribution of forest properties, tephra layer W, and lichen measurements of debris flow landforms provide relative landform ages along the valley length. Forest structure varies longitudinally along the valley. In the upper valley, DEMs of the forest canopy and aerial photographs indicate mixed forest age classes and numerous forest clearings coincident with debris flow lobes. In the lower valley outside of young forests on the 1947 debris flow deposit, old-growth forests persist, suggesting limited geomorphic disturbance. The spatial distribution of Layer W was spotty in the upper valley, consistent with the patchwork of debris flow deposits mapped (Figure 3-1 and Figure 3-4). With exception of an area in the middle valley, all surfaces older than the 1947 deposit appear to have been stable since prior to 1480. We observed no other ash layers in soil pits. At all locations where we positively identified Layer W, we encountered it in the first pit dug. We dug three pits in sample locations where we encountered no Layer W at the boundary between organic and mineral soil. These observations gave us confidence that there were few to no false negatives. Lichenometric measurements on boulder deposits provide relative age constraints on the distribution of debris flow deposit ages in the upper valley. Figure 3-4 indicates the maximum lichen diameter measured on debris flow deposits. Spatially-scattered lichen diameters and corresponding age estimates suggest that secondary channels have conveyed debris flows away from the main channels (pre-1947 and current) through time. In the discussion below, we use lichenometric data in conjunction with tree-ring dating to constrain absolute deposit ages and spatial extents in the upper valley. Using surficial dating methods, we estimated absolute debris flow dates of 1915, 1868, 1782, and 1718. We established two (1915 and 1868) with high confidence and two with moderate confidence (1782 and 1718) (Table 3-1). Consistent growth disturbances in tree ring samples KD-036 and KD-195 constrained the 1915 deposit age (Appendix A). The associated debris flow snout was located approximately 100 meters west of the main channel at RK ~8.6 (Figure 3-4). The maximum lichen diameter (50 mm) yielded a date estimate of 1901 ± 15 years. Contemporaneous growth disturbances in tree ring samples KD-033, KD-187, and KD-188 constrained the 1868 deposit age (Appendix A and Figure 3-4). The associated boulder snout was located approximately 100 meters west of the main channel at RK ~8.3, with castes of trees present (Figure 3-3), suggesting that enough time had passed since deposition for full decay (Figure 3-4). The maximum lichen diameter (68 mm) yielded a date estimate of 1860 ± 15 years. A growth disturbance in sample KD-175 in 1782 was within error of a lichenometric age estimate of 1789 ± 20 years (99 mm diameter) (Figure 3-8). A boulder "eddy" on the lee side of the sampled tree indicated that deposition of the associated boulder snout (25 m west of the main channel at RK 9.6) had impacted the tree (Figure 3-4). The tilting direction indicated by opposite tree cores in Figure 3-8 was consistent with the direction of inferred boulder transport. Nearby, a tree (sample KD-176) was abruptly tilted in 1718, within error of a lichenometric date of 1731 ± 20 years (124 mm diameter) on an adjacent boulder levee (Figure 3-4; Figure 3-8). We observed similar boulder eddy consistent with impact by debris flow levee deposition.

Despite environmental factors associated with shading and moss affecting lichen growth, lichenometric age estimates of deposits with known ages are within reasonable error of the published lichenometric growth curve (Figure 3-9) (O'Neal and Schoenenberger, 2003; O'Neal et al., in review). Measurements of maximum lichen diameter at discrete locations along the 1947 debris flow deposit in the upper valley coupled with lichen sizes on four deposits with tree-ring age constraint show growth rates consistent with the published curve. The minor deviations that are present suggest that lichen growth rates may tend to be relatively rapid in the first hundred years of growth, and slower thereafter as demonstrated by lichens on the 1718 and 1782 deposits underestimating deposit age given by tree rings. The pattern of relatively early rapid growth followed by slower growth may relate to shading that causes lichens to grow relatively quickly until moss coverage increases to a point where it competes with and overgrows lichens. This interpretation is supported by our observation that moss coverage tended to be greater on older deposits. Appendix B details lichen measurements in this study.

Good fits of measured lichen diametric growth rates to published lichen growth rates allowed us to use lichen sizes to constrain the age of landforms without dendrochronologic age constraint. According to lichen age estimates, we assigned each debris flow landform an age of known debris flow ages (1915, 1868, 1782, or 1712) or an unknown age (Figure 3-10). We assigned a known age when a deposits lichenometric age estimate fell within error of the lichenometric age estimate on a tree-ring dated deposit. For lichenometic age estimates outside of error of all tree-ring dated deposits, we categorized deposits ages as unknown. We secondarily used the location of a deposit with respect to other deposits of the same age to decide age categories. Figure 3-10 reveals that we assigned ages to 20 of 29 debris flow landforms that originally had only lichenometric age constraint.

Depositional patterns of the four dated debris flows record run-out paths of each (Figure 3-4). The 1915 deposit appears to have predominantly traveled down the pre-1947 main channel. The 1868 deposit flowed along the pre-1947 channel, and a secondary channel that diverges from the pre-1947 main channel at ~RK 9.5. Deposits of the 1782 debris flow indicate that it traveled along the pre-1947 main channel as well. Deposits of the 1718 debris flow are limited in extent, but suggest that the debris flow may have traveled down a channel that pre-existed the current main channel that was reoccupied in 1947 (Crandell, 1971b). The seemingly realistic run-out paths where individual debris flows follow predominantly a single channel adds confidence to age assignments of sets of debris flow deposits.

Figure 8 shows two sets of unknown deposits ages that fell out of error range of the tree-ring dated deposits. One set of six deposits have individual lichenometric date estimates of 1821, 1821, 1828, 1828, 1837, and 1844 (lichen diameters of 85 mm, 85 mm, 82 mm, 82 mm, 78 mm, and 75 mm). Overlapping error bars make it impossible to determine how many events are actually represented by these deposits, but at least one debris flow is likely. For simplicity, we assume the set of deposits represent one event with an age of the mean of the six lichenometric estimates (1829). Spatially, five of deposits are located along the pre-1947 main channel and secondary channels that diverge from its upper reach (~ RK 9.5), suggesting a run-out path roughly consistent with routes of the predating 1782 and postdating 1868 debris flows. Another cluster of unconstrained deposits have lichenometric estimates of 1910, 1920, and 1922; however, they are young outliers relative to nearby deposits, and are scattered spatially relative to the 1915 deposit (temporally closest). Due to these uncertainties, we left their ages unassigned.

3.9 Physical Stratigraphy

Valley stratigraphy of debris flow and fluvial layers provided a means to evaluate temporal change in valley deposition (Figure 3-11). Stratigraphic column C, located along the right bank of the main channel at RK 7.6, revealed the greatest number of individual layers and provides a logical section to present sedimentological descriptions and facies definitions (Figure 3-4).

The uppermost layer of the section was composed of poorly sorted cobbles and boulders supported in a massive matrix ranging in size from gravel to clay. Course framework grains tended to be sub-angular to-sub rounded, whereas gravel, granule, and sand-sized particles were commonly angular. We observed no sedimentary structures such as cross- or planar-bedding within the layer. We interpreted the uppermost layer as a debris flow based on descriptions of debris flows in the literature that include course clasts supported in matrix, massive bedding with no sedimentary structures, and changing roundness with clast size (Pierson, 2005; Costa, 1988). We defined a debris flow facies (DF) for further discussions of similar layers (Figure 3-11). Underlying the uppermost layer was an organic horizon with a buried stump in growth position, consistent with a buried forest layer. The growth position stump may also support abrupt burial by the layer above. Below was a sequence of four layers composed of sand and gravel with buried organic layers at their contacts. Clast-supported mixed sand, gravel and intermittent cobbles characterized the uppermost and lowermost layers in the sequence. Cross beds were present, and clasts were generally sub-angular to sub-round. Based on sedimentary structures and clast-support indicative of water-lain deposits, we interpreted these layers as fluvial deposits. Grain size coarseness suggests that these deposits were laid by relatively energetic flows either in or proximal to channels, causing us to define a second facies of channelized fluvial deposits (FC, Figure 3-11). The middle two layers in the sequence of layers were dominated by sand with cross beds and intermittent zones of massive bedding. We interpreted these layers as fluvial deposits that occurred adjacent to channels, likely from overbank floods, and defined a third facies of fluvial sand (FS). Below the sequence of sand and gravel was a layer of matrix-supported gravel and cobbles that we interpreted as DF facies. The layer's lower contact was defined as an abrupt sedimentologic boundary without buried organic material. The layer below was predominantly sand with few sedimentary structures that we classified as facies FS. A sharp sedimentologic boundary marked the contact with the layer below, which was composed of matrix-supported boulders and cobbles that we classified as a debris flow. The debris flow deposit sat on a organic horizon with a layer of white pumice and grey sand consistent with descriptions of the Tephra Layer W that was erupted from Mount Saint Helens in cal. years 1480 and 1482 (Vallance and Scott, 1997; Yamaguchi, 1985). Below was a layer of matrix-supported cobbles and boulders that we interpreted as a debris flow. The debris flow layer's lower contact was marked by an organic horizon underlain by a clast-supported sand and gravel layer that we interpreted as facies FC. The layer's lower contact was marked by a sharp change to a sand layer with occasional sedimentary structures that we interpreted as facies FS. Below were two layers of matrix-supported boulders and cobbles interpreted as debris flows (Figure 3-11).

In addition to those identified in column C, we identified two facies in column E located in a cut bank of a head-cut secondary channel (~ RK 5.3) in the lower valley (Figure 3-1 and Figure 3-11). The type-layer for the first facies (2.7-3.1 m depth) was composed of sand with cross-bedding and occasional finely laminated silt layers. We interpreted the layer as fluvial in nature (FSSi). We defined a second facies based on a brown silt layer (3.1-3.4 m depth) with intermittent inter-beds of fine sand (FSiS). We interpreted that both facies originated from low-energy fluvial deposition, possibly by a secondary channel that ran across the valley floor.

In the lowermost layer in column E, we analyzed sediment size to evaluate the deposit layer's origin. The layer's extent down valley and a buried forest exposed in the main channel of similar elevation suggested a large volume debris flow and begged questions about whether the deposit recorded a high-clay lahar or debris flow. Simple settling tests of the sieved fine fraction (>4 Φ) revealed that a majority of fine fraction was silt, with approximately 70% of sediment volume settling within 30 minutes. Hand texturing of the fine fraction also indicated minor plasticity and correspondingly minor clay content. Vallance and Scott (1997) found that lahars tend to exceed 0.05 in the fraction of clay to sand plus silt plus clay. Our measurements reveal this fraction to be less than 0.02, suggesting that event mobilized clay-poor sediments characteristic of surficial sediment sources.

3.10 Stratigraphic Evidence for Debris Flow Ages

Because individual layers were often poorly exposed, we were not able to physically trace and correlate their extents down valley. Absolute age data provided by radiocarbon analysis and tephra layers, however, allow temporal correlation. Tephra layer W was observed in all stratigraphic columns presented here, and thus serves as a common temporal marker. In young layers at the surface of stratigraphic sections where radiocarbon techniques are ineffective, we used aerial imagery and approximate forest characteristics as a proxy for surficial layer ages. Working down-section, we discuss absolute and relative age data to correlate and interpret the ages of layers.

Aerial imagery, DSMs of forest canopy height, and forest characteristics provided a relative age constraint on the surficial layer in stratigraphic sections (Figure 3-11). Aerial imagery captured in 1965 suggested that the surface of sections B and E were within deposits of the 1947 debris flow. The 1965 aerial imagery showed a relatively young forest at the surface of section C, but mature enough to suggest earlier surface disturbance than the 1947 debris flow. We thus interpreted the surface debris flow to represent the 1915 debris flow dated using tree-ring techniques. Mature forests growing at sections A and C indicated that surficial debris flows were at least in the hundreds of years in age.

Three radiocarbon ages, tephra layer W, and relative ages constrain the age of a debris flow that occurred in the late 1600s. Radiocarbon samples KRC-04C, KRC-05B, and KRC-06B (sections A, B, and C respectively) provided calibrated calendar age ranges (95%) of 1,466-1,636 cal. years; 1,490-1,603 (74.2%) 1,611-1,645 (21.2%) cal. years; and 1,642-1,681, 1,763-1,801, 1,938-1,955 cal. years, respectively (Table 3-2). Samples KRC-04C and KRC-05B were organic fragments incorporated into debris flow layers in sections A and B, and thus provide maximum debris flow ages. The latter sample from section C was collected from the outermost rings of a buried stump in growth position. Outer rings on the stump appeared normal in growth suggesting that the tree was abruptly buried and killed. In column C, the debris flow layer discussed here is overlain by a sequence of fluvial layers separated by organic horizons and further overlain by the 1915 debris flow, suggesting that the debris flow of interest is at least a few hundred years in age. Based on the apparent time represented above in section C, and the correlation with the layer upstream, we interpret the debris flow age range to coincide with the first calendar range of 1,642-1,681 for sample KRC-06B. An absence of layer W on the valley floor surface with mature to old growth forests implies that the debris flow spilled from the main channel between RK 7.3 and 6.2 (Figure 3-1) and represents the surficial debris flow layer in column D (Figure 3-11).

Absolute age data in stratigraphic columns A, B, and C suggest that a debris flow occurred in the early 1400s (Figure 3-11). Tephra Layer W overlies the debris flow layer in all sections. In columns A and C, samples KRC-04A and KRC-06C collected from an organic horizon below the debris flow have consistent calibrated dates of 1,295-1,400 AD. Modeling the bounding radiocarbon and tephra ages yield a deposit date of 1,416 ± 61 AD (Ramsey, 1995).

Radiocarbon dates of the outer rings from growth position stumps constrain the age of a debris flow layer exposed in columns C, D, and E (Figure 3-11). Radiocarbon samples KRC-06E, 12-KS-04A, and 12-KS-09 (columns C, D, and E respectively) yield calibrated dates 895-1,018 AD, 906-1,033 AD, and 827-987 AD. Because these samples approximately represent death dates of the respective tree stumps, we interpret the layers age by the youngest radiocarbon result of the three samples (12-KS-04A) of 970±64 AD.

The debris flow with a calendar date of 970±64 AD (1,041±64 BP) coincides temporally with volcanic and tectonic events that confound its origin. The Mount Rainier eruption dated at 1,040 ±410 BP is within error of the debris flow (Hoblitt et al., 1995). Our sediment size data, however, indicate that the debris flow likely was not a lahar induced from flank collapse, which mobilize clay-rich sediment and can result from eruptions (Vallance and Scott, 1997). Rather, volcanic activity could have melted glaciers and induced a large debris flow of surficial debris. In addition, a roughly contemporaneous large magnitude earthquake dated at 1,000 to 1,100 cal. years BP on the Seattle Fault (Puget Sound, Washington, 60 km west-northwest) is connected with landslides and rock avalanches in the Puget Sound and the Olympic Mountains (Atwater and Moore, 1992; Jacoby et al., 1992; Schuster et al., 1992). As discussed later, the debris flow also corresponds with the Medieval Warming Period when temperatures were likely similar to the recent century (Viau et al., 2012). Regardless of its origin, the ca. 970 AD debris flow is consistent in timing with arrival of a sediment pulse at the Nisqually River delta into the Puget Sound (Barnhardt and Sherrod, 2006). The authors of that study were not able to unequivocally constrain the sediment pulse's origin, but speculated that it was a result of a large debris flow or lahar originated from Mount Rainier.

3.11 Interpretation of Valley Form and Process

Debris flow run-out lengths represent a spectrum in frequency and magnitude of debris flow deposition along the Kautz Valley. Rickenmann (1999) found a simple empirical relationship between debris flow volume and run-out length on fans, despite dependence of debris flow run-out distance on other factors including peak discharge, velocity and channel cross-sectional area. Distance traveled down-valley thus served as a proxy for debris flow volume or magnitude. For historical debris flows, we measured this distance based on the furthest location downstream where the deposit would have been preserved outside of the main channel. This approach allows for integration of historical with prehistorical records and comparison of events on roughly the same relative length scale. We measured the run-out distance of reconstructed events at the furthest extent downstream. In cases where debris flows ran out beyond the valley, we assumed the debris flow stopped at the confluence with the Nisqually River. Run out lengths are detailed in Table 3-3**Error! Reference source not found.**, but in general reveal 9, 2, and 2 debris flows that ran out 1-3 km, 3-5 km and 5-11 km, respectively from the Box Canyon. These data show a magnitude-frequency gradient with valley length despite the fact that the record of small magnitude events is likely incomplete before about 350 years BP due to the temporal limits on surficial dating of small magnitude debris flows (discussed in detail below). For just the last 350 years (removing the ca. 970 and ca. 1412, AD events), the record contains 9, 1, and 1 debris flows that ran out 1-3 km, 3-5 km, and 5-11 km, respectively.

We observed longitudinal variation in nature of deposits that indicates a downstream gradient in the nature and frequency of debris flow deposition, from frequent, patchy deposition in the upper valley to infrequent, large magnitude deposition in the lower valley. Key data and observations include downstream gradients in the nature and abundance of debris flow landforms, the morphology and quantity of channels, valley convexity in cross section, and surface roughness of the valley bottom as observed in Figure 3-1 and Figure 3-4. These measures vary downstream and correspond with a nearly monotonic decrease in valley gradient with downstream distance (Figure 3-2).

The coincidence of debris flow deposits and secondary channels in the upper valley suggest a process of debris flow conveyance, channel plugging, and channel avulsion. Abundant debris flow levees and lobes spill from and line secondary channels in the upper valley as observed by depositional patterns with respect to secondary channels in Figure 3-4. Debris flow deposits also coincide with abrupt channel ends, indicating that debris flows plug channels (Figure 3-4). Channel plugging drives avulsion and scouring of new channels, which explains the network of discontinuous channels on the valley bottom. The rough appearance of the upper valley thus reflects the mosaic of debris flow landforms and secondary channels. Valley convexity is consistent with near-channel deposition by debris flows, with the greatest rate of deposition occurring along the valley axis as the main channel emerges from and is fixed to the mouth of the Box Canyon at the head of the valley (Figure 3-4).

We interpret that secondary channels in the upper valley generally originate from fluvial erosion, but are influenced by debris flows. Longitudinal slopes in the upper valley are approximately 6^{o} to 7^{o} , which are slopes which are slopes where debris flows have been found to deposit (Pierson, 1980; Benda and Cundy, 1990). An absence of observed erosion from recent debris flows, debris flow lobes in channels (Figure 3-4), and the numerous debris flow layers on top of organic layers in stratigraphy (Figure 3-11) confirm that un-channelized and channelized debris flows generally deposit material in the upper valley. By process of elimination, channels are likely water-scoured. Channels often have sharp-crested, narrow, boulder-rich levees, suggesting debris flow passage (Figure 3-5). In extreme cases, channels beds and banks sit above the surrounding valley surface, suggesting that successive debris flows occasionally construct channels as they travel between their own levees across the valley surface (Figure 3-5) (Sharp, 1942; Whipple and Dunne, 1992).

Variation in the form of debris flow lobes along the valley surface may suggest deposition of debris flows with a range of flow rheology and yield strength. Whereas the control of yield strength on debris flow depositional form is disputed, Whipple and Dunne (1992) attributed a variation in debris flow deposits to variations in yield strength (Iverson, 2003). In the upper valley, debris flow lobes range from distinct and steep-snouted (Figure 3-4) to non-distinct boulder fields with a surface slopes equaling that of the surrounding valley surface. Steep, distinct lobes that freeze in channels or spill a short distance from channels suggest high yield strength debris flows that are only mobile at high gradients (Whipple and Dunne, 1992). On the other hand, the observed non-distinct, low-gradient snouts suggest low-yield strength debris flows with greater mobility.

As compared to the upper valley, the lower valley is dominated by infrequent deposition of large volume debris flows with a different surface character. The 1947 debris flow deposit and a geomorphic surface lder than Layer W generally comprise the lower valley surface, suggesting infrequent resurfacing by debris flows (Figure 3-1). Figure 3-6 shows an image of the smooth 1947 deposit shortly after the event. A smooth surface appearance with few debris flow snouts like the upper valley suggests that only deposition of low yield strength debris flows occurs. These apparent low yield strength debris flows are mobile to lower gradients (2^o-3^o in this case), and spill from channels as wide, tabular, lobate deposits as indicated by the depositional pattern of the 1947 deposit (Figure 3-1) (Whipple and Dunne, 1992).

The spatial variation in geomorphic surface expression of the 1947 deposit suggests that debris flow pulses within the event had varying flow properties that dictated their distance traveled down valley. The main 1947 debris flow deposit in the lower valley is consistent with a low yield strength debris flow, with its wide, tabular deposits (Figure 3-1), but not incompatible with high yield strength pulses during the event. Steep, boulder lobes deposited adjacent to the main channel in the upper valley suggest that high yield strength pulses also occurred (Figure 3-4). The suggested range in yield strengths along the valley may relate to a range of volumetric sediment concentration (sediment to sediment and water) debris flows, which is conceivable considering that flooding and debris flows were observed during the 1947 storm. Others have document pulses of varying sediment concentration or downstream dilution in debris flows elsewhere (e.g. Pierson, 1986; Pierson and Scott, 1985).

The nature and distribution of landforms suggest that the Kautz valley has evolved in a manner consistent with arid debris flow fans, where frequent deposition occurs via a network of channels on upper fans, and mobile, low yield strength debris flows travel to the lower fan and spill from channels creating smooth surfaces (i.e. Whipple and Dunne, 1992; Hooke, 1967). While this type of valley seems unique for humid valleys in the Pacific Northwest, the similarity with a fan at a fault-bounded mountain front seems to be the fixed point source of sediment and water at the valley head with limited tributary inputs below. The Kautz valley thus provides an example of evolution of a relatively steep mountain valley where lateral influences from tributaries and mass movement processes have little influence (cf. Grant and Swanson, 1995).

3.12 Interpretation of Debris Flow Occurrence with Respect to Glacier and Climate Fluctuations

The chronology of debris flows reconstructed here spans the LIA, permitting examination of debris flow occurrence across a period of changing climate and glacier extent. The LIA was generally a cool period when glaciers were extensive relative to present day (Figure 3-1, Figure 3-2, and Figure 3-12), but oscillated in their extent. In the Kautz drainage, LIA moraines cluster spatially just upstream of the Box Canyon, providing a set of snapshots in time of terminus positions. In periods between moraine ages, however, temperature oscillations suggest that glaciers also waxed and waned. Because maritime glaciers like those of Mount Rainier are sensitive to temperature, as indicated by moraine stabilization times coinciding with warming trends across Mount Rainier, temperature serves as a proxy for relative glacier extent between moraine ages (Meier, 1984; Oerlemans, 2005). Thus, relatively warm periods in the LIA likely caused the Kautz glacier terminus to recede to positions up-valley of the set of LIA moraines. In the warmest periods within the LIA, like the 1600s, similar temperatures to the 20th century suggest glaciers receded back to positions comparable to the 20th century. With changes in glacier extent along a concave valley profile (Figure 3-2), the sources and production rates of sediment likely would have changed.

Whereas average metrics of debris flow occurrence suggest that temperature and inferred glacier extent throughout the LIA had little influence on debris flow occurrence, the timing and magnitudes of individual events may suggest differently. We compare 1650-1900, generally corresponding with the LIA, to the period from 1900 to present day. The chronology contains 5 and 7 debris flows in the two periods, respectively, with corresponding average frequencies of 2 and 3.4 debris flows per century. In run-out length, the average magnitudes for the two time periods are 2.4 and 3 km from the Box Canyon. These simple statistics suggest that average climate and glacier extent have equivocal effects on debris flow occurrence across the two periods, particularly when considering that the record of smallest events is likely biased toward the present day. Thus, average metrics of debris flow frequency seem inadequate to assess changes in debris flow occurrence through time. Conversely, the timing and run-out lengths of individual debris flows may correspond systematically to the temperature record. The debris flow record presented in Figure 3-12 shows an apparent co-occurrence of individual debris flows and warm periods. Three warm periods with dated moraines in the drainage have corresponding debris flows (ca. 1661 AD, ca. 1782 AD, and ca. 1829 AD). In addition, other debris flows (ca. 1712 AD, ca. 1868 AD) occur during short-lived warming periods that have no associated moraines. Two effects of warmer climate may explain the correspondence between debris flows and warm periods: (1) retreat of the Kautz Glacier exposed debris at increased gradients and led to debris flows, or (2) elevated snow-lines during warm periods exposed material for debris flow initiation. The first effect depends on the temperature sensitivity of the Kautz Glacier, which is suggested to be high by moraine ages and work by others on maritime glaciers (Meier, 1984; Oerlemans, 2005). If the Kautz Glacier receded up-valley during these short-lived warm periods, expanded periglacial areas with abundant debris at increased gradients may have driven debris flow production. Elevated perennial snow-lines also may have had similar effects in enlarging debris flow source areas, as has been suggested by Stoffel and Beniston (2006). Whereas debris flows seem to correlate with the temperature record, individual debris flows occur across a range of indices for Pacific Decadal Oscillation Index, which correspond to multi-decadal hydro-climatological oscillations in the Pacific Northwest (MacDonald and Case, 2005). The seeming lack of systematic correspondence of debris flows with hydroclimate contrasts with some studies of debris flow occurrence in the European Alps where they are apparently linked (cf. Schneuwly-Bollschweiler and Stoffel, 2012).

Debris flow magnitudes also appear to correspond roughly with the magnitude of temperature change from the LIA minimum. Because of suggested temperature sensitivity of Mount Rainier glaciers, the total temperature change from the LIA minimum temperature can serve as a rough proxy for the up-valley distance to a glacier terminus. The timing of the largest debris flow events coincide with the warmest periods. The 1947 AD event occurred when the Kautz Glacier had down-wasted and receded up-valley to positions near present day (Grater, 1947). The ca. 1661 AD event falls within the warmest period in the LIA (Figure 3-12). The large magnitude ca.

970 AD event falls within the Medieval Warming Period, when local pollen reconstructions suggest temperatures were similar to the 20th century (Viau et al., 2012). In comparison, debris flow run-out lengths are consistently shorter in the brief, relatively warm periods in the LIA. In these periods, a relatively large Kautz Glacier would have limited the size and average slopes of ice-and snow-free source areas for debris flows. Figure 3-13 shows a correlation of temperature and run-out distance.

Depositional records imply LIA channel conditions in the Kautz valley that inhibited debris flow run-out during the LIA. In stratigraphic section C, a sequence of relatively thin fluvial layers overlie the 1661 debris flow layer, and underlie the 1915 debris flow layer, constraining the sequence's age to the LIA (Figure 3-14). The sequence of fluvial layers, which we interpret as a set of flood layers, is anomalous for the stratigraphic record observed in Kautz valley (Figure 3-11). Two possible interpretations of the flood sequence are (1) that the LIA was wetter, with more frequent or larger floods, or (2) that increased glacial sediment yield (or dryer climates) caused filling of channels to create smaller cross-sectional areas, which promoted overbank deposition more frequently. PDO indexes oscillated during the LIA, but were not on average different than the 20th century (MacDonald and Case, 2005). Regional tree-ring and lake sediment reconstructions of precipitation suggest that the LIA on average was similar to or relatively drier than the 20th century (Steinman et al., 2012; Graumlich, 1987). In addition, cooler temperatures suggest that rain-on-snow-induced flooding may have been reduced, causing LIA hydrographs to be less flashy (Harr, 1981). These records suggest that increased flood magnitudes are an unlikely explanation of the set of flood layers. Larger glaciers during cool periods tend to erode at greater rates, yielding greater amounts of sediment relative to warmer periods with smaller glaciers (e.g. Hallet et al., 1996). This increased total sediment production often causes aggradation downstream (Dühnforth et al., 2008; Ritter et al., 1995). Aggraded channels with lower cross-sectional areas thus can promote deposition on fan or valley surfaces. The latter scenario of infilled channels promoting flooding therefore seems more plausible. Debris flow depositional patterns also support our interpretation of aggraded channels and enhanced deposition on the valley floor. Of the five debris flows (1661, 1712, 1782, 1829, and 1868) in the LIA, only the 1661 debris flow, which occurred during the warmest period in the LIA, traveled to stratigraphic section C (Figure 3-11). The other debris flows deposited on the upper valley surface, often along secondary channels (Figure 3-4). Taken together, these two lines of evidence suggest strongly that debris flows did occur during the LIA, but that their run-out lengths were limited.

In the Kautz Valley, glacier extent appears to influence both debris flow source areas and channel conditions in depositional areas, which in turn have effects on debris flow run-out lengths and depositional patterns. Whether these two effects cooperate or compete depends on the response times associated with each. The coincidence of debris flows with short-lived warm periods within the LIA suggests that debris flows occurred as a rapid response to expanded and steeper source areas resulting from glacier retreat of the Kautz glacier and from elevated snowlines. Based on the pronounced concavity of the Kautz basin above the Box Canyon, enlarged debris flow source areas would have had increased average slopes. Rickenmann (1999) found that debris flows travel distances related positively to the product of material volume of a debris flow times the vertical elevation difference between the source and depositional area. Steeper slopes and increased volumes of sediment that were exposed in the warmest periods imply that debris flows should have run out relatively further, an inference supported by relatively long run-out lengths in the ca. 970, 1661, and 1947 AD debris flows (Figure 3-12 and Figure 3-13). As discussed previously, large glaciers produce relatively large amounts of sediment transported by fluvial processes, which can aggrade rivers and promote overbank deposition. Overbank deposition of material from a debris flow as it travels downstream may also reduce the material volume available to be conveyed downstream, potentially reducing debris flow run-out distances (Dühnforth et al., 2007). The response time of channels to glacier change, however, appears longer than the response of debris flow occurrence. Deposition of the 1915 debris flow on the valley surface may suggest that the main channel was relatively filled until at least that time (Figure 3-4). Large scale incision of approximately 10 meters during 1947 flooding may represent the point in time when channels evacuated fill from the LIA. Subsequent deposition on the valley surface outside of main channels has been relatively minimal (see 2006 deposit in Figure 3-1). That much of the incision that occurred in 1947 remains likely reflects reduced sediment production from the relatively smaller Kautz Glacier of the post-LIA climate.

These effects of glaciers on debris flow source areas and downstream channels interpreted here can cooperate or compete in conveying debris flows to downstream areas. In the LIA, short term warm periods saw debris flows while the channels were adjusted to the prevailing glacial climate, causing small volume debris flows to be conveyed a relatively short distance downstream as debris flows spilled from channels. Current conditions with large sediment-mantled areas in front of glaciers perched at relatively high elevations and steep slopes above the deposition setting, making large run-out distances more likely (Rickenmann, 1999). In addition, entrenched channels convey debris flows downstream, further enhancing debris flow run-out distances. This may suggest that recent debris flows like the one in 2006 have been conveyed further downstream with respect to its volume than debris flows in the LIA.

3.13 Completeness of the Reconstructed Debris Flow Record

We have reconstructed an approximately 1,100-year chronology of debris flows using a combination absolute and relative age data on surficial deposits and in stratigraphic sections. Using the surficial dating, we estimated ages of five debris flows (1718, 1782, 1829, 1868, and 1915 AD) of generally shorter run-out lengths. Absolute age data in stratigraphic sections constrained ages of three deposits (970, 1412, and 1661 AD) that ran-out further. The contrast in ages and apparent magnitudes extracted from surficial and stratigraphic methods suggests that the recent record within the age of living trees is more complete. Although we cannot rule out the possibility that our chronology missed events, the distribution of lichen age estimates of deposits on the upper valley suggest that few were missed from the upper valley surface in the last approximately 300 years (Figure 3-10). The smallest events which did not overtop channels were likely missed by our efforts. The record in strata, though incomplete for smaller magnitude events, likely has few missing events of larger magnitude. The distribution of Tephra W on the valley surface suggests that the lower channel below about RK 8 has been stable in planform since earlier than 1480. Because deposition in the lower valley has relatively little dependence on a network of secondary channels, strata exposed in existing cut banks should preserve a relatively complete record of debris flows sourced from the main channel and primary depositional locus. As discussed above, channel conditions may also influence the record completeness, as noted by others (Dühnforth et al., 2007). Filled channels, however, seem to have improved the record completeness through the LIA because the deposits are distributed across the surface and have not been buried.

3.14 Conclusions

This study builds a chronology of 14 debris flows extending 1,100 years BP in a relatively steep valley on the flanks of Mount Rainer. We have demonstrated that debris flow records are best reconstructed using a variety of surficial and stratigraphic techniques. Due to temporal limitations of the surficial dating techniques used, the chronology is most complete for the past 300 to 350 years. Since 1650 AD, at least 12 debris flows have occurred from the upper Kautz basin, 11 of which traveled to the Kautz Valley below the Box Canyon. Run-out distances served as a proxy for debris flow magnitude, and indicate that at least 11, 2, and 1 debris flow(s) have traveled at least 1, 3, and 5 km from the valley head, respectively since ca. 1650, indicating a frequency-magnitude relationship. The largest of these events was the 1947 event, which was estimated at 40 million m^3 volume (Crandell, 1971a). The only other event of similar magnitude to the 1947 was one dated at ca. 970 AD that had a contemporaneous sediment pulse downstream at the Puget Sound (Barnhardt and Sherrod, 2006). We compare 1650-1900, generally corresponding with the LIA, to the period from 1900 to present day. Five and seven debris flows occurred in the two periods, respectively, with corresponding average frequencies of 2 and 3.4 debris flows per century. In run-out length, the average magnitudes for the two time periods are 2.4 and 3 km from the Box Canyon. Considering unavoidable biases toward the present in any reconstructed chronology, debris flow activity differences indicated by these averages are equivocal.

The geomorphic form and process of Kautz Valley is unique for the Pacific Northwest region, despite commonality with debris flow fans in arid environments. The Kautz Valley has limited lateral inputs from tributaries, creating a longitudinal gradient in geomorphic process dominated by debris flow deposition that varies in frequency and magnitude, as observed in the chronology. Debris flows deposit relatively often and in limited spatial extent in the upper valley, where secondary channels control debris flow depositional patterns. Depositional tracks of individual dated debris flows demonstrate the control of secondary channels on debris flow deposition. Variable form of deposits suggests that debris flows with variable rheology deposit on the relatively steep slopes of the upper valley. The lower valley, however, is dominated by relatively infrequent but widespread deposition by seemingly mobile debris flows that overwhelm the main channel and produce a smooth valley surface character.

The Kautz Creek chronology suggests relationships between the timing and run-out distance of individual debris flows with temperature and inferred glacier extent. Individual debris flows coincide temporally with relatively warm periods and inferred smaller glaciers. Kautz Creek's concave longitudinal profile requires that gradients in ice-free areas become steeper with decreased glacier sizes and elevated snow-lines. In the LIA, small magnitude debris flows occur during relatively warm periods either when glaciers retreated up-valley or snow coverage was less, exposing steeper gradients in ice-free areas. LIA debris flows, however ran-out relatively short distances compared to warmer periods before and after the LIA. Shorter run-out lengths appear to result from a combination of (1) relatively small areas and slopes of zones in the fronts of glaciers relative to warm periods like the MWP and the 20th century, and (2) from enhanced deposition of debris flows outside of the main channel as a result of filled channels during glacial times. Stratigraphic records and debris flow depositional patterns support filled channels during the LIA. Whereas we cannot fully deconvolve source area and depositional controls on the observed run-out distances, these results suggest that the hazards to debris flow prone areas change with temperature and glacier oscillations in steep catchments.

3.15 Figures

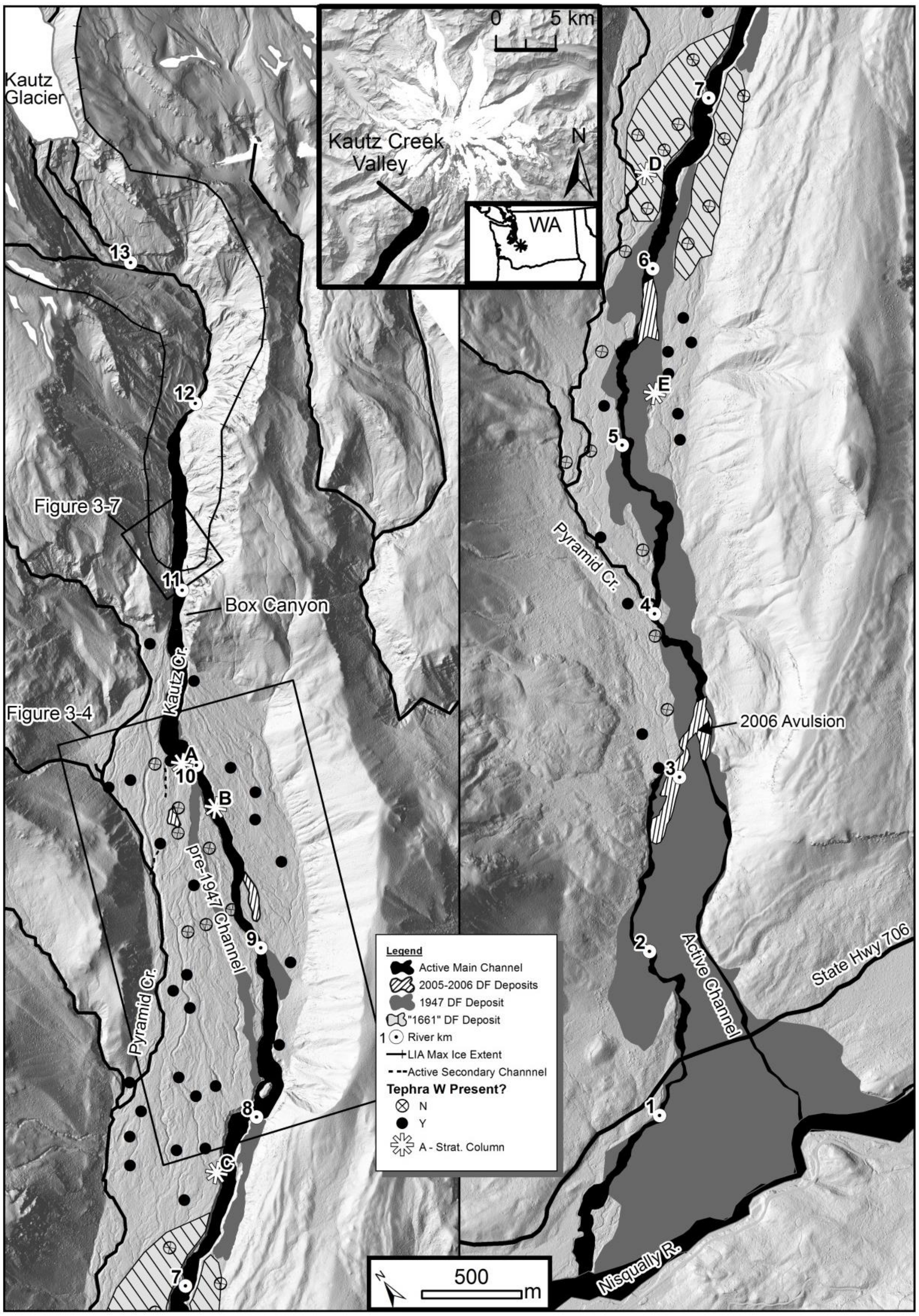

Figure 3-1 ALSM-generated hillshade map of the Kautz Creek drainage basin with select debris flow deposit extents shown. Scale and orientation are identical for the left and right panes.

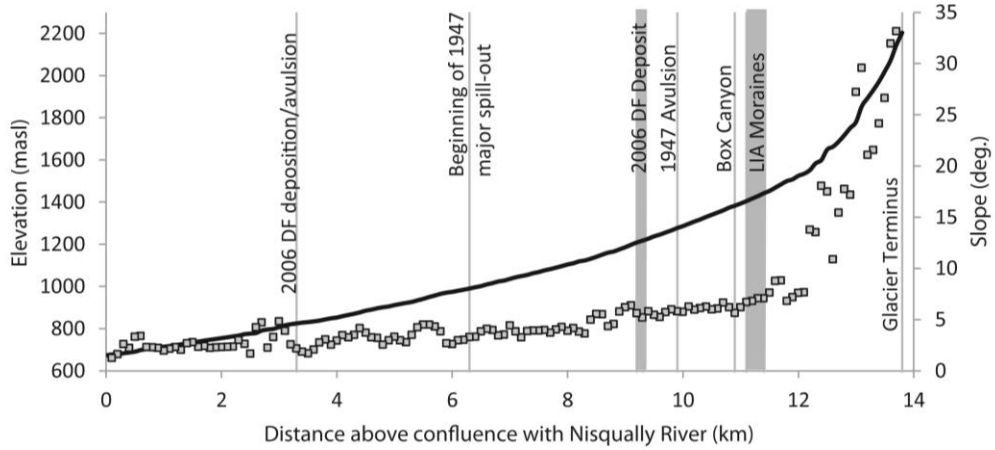

Figure 3-2 Longitudinal profile (black line) and gradient (black boxes, estimated from 200-m segments) of Kautz Creek with key locations marked as grey vertical bars.

Figure 3-3 Photographs taken (2011) of select landforms and deposits in the Kautz Valley. A: Area inundated by 2006 deposit with 1-m diameter damaged tree in foreground (image location: Figure 5). B: A western hemlock tree impacted by debris flow boulders. C: A tree cast (60-cm diameter) in a debris flow snout. Note matrix-supported cobbles below the open-framework surface. D: Kautz Creek flows below the Box Canyon (in distance). E: A debris flow layer overlying the Tephra Layer W (1480-1482) in outcrop. F: A debris flow snout composed of open-framework boulders.

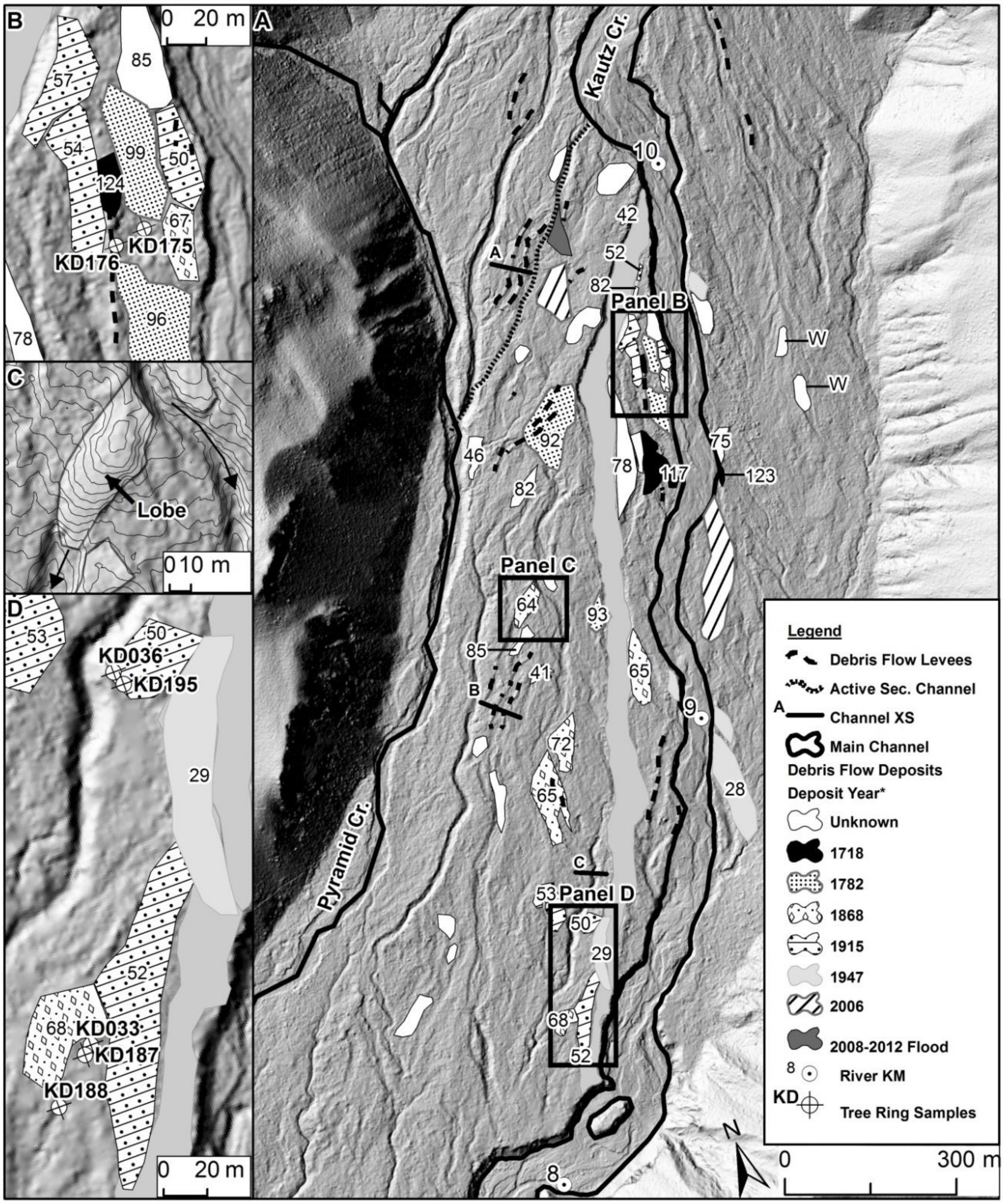

Figure 3-4 Geomorphic map of the upper Kautz Valley with insets of geomorphic and landform dating details. Panel A shows dated and undated debris flow deposits with the maximum measured lichen diameter (mm). Tephra W was found on deposits labeled. Cross section transects of Figure 3-5 are shown. Panel B shows detailed landforms, lichen measurements, and key tree ring samples for the ca. 1718 and 1782 debris flows (Figure 3-8 shows tree ring width data). Panel C shows an example of a channel-plugging debris flow lobe with the plugged and avulsed channels shown. Panel D shows key tree ring samples used for establishing two debris flow ages (ca. 1868 and 1915).

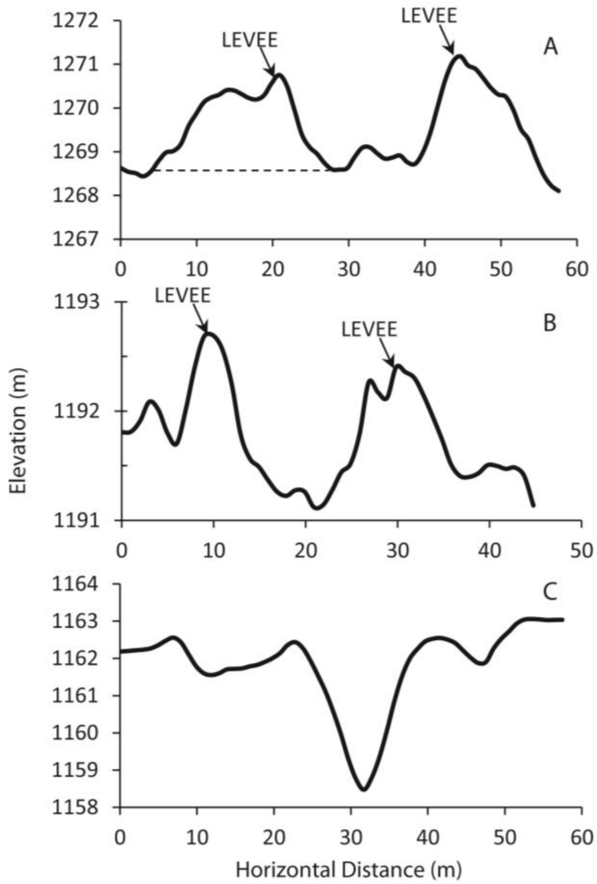

Figure 3-5 Selected channel cross sections extracted from ALSM DEMs (locations shown on Figure 3-4) that demonstrate variability of secondary channel form on the upper valley, with a channel bed above the surrounding surface (A), a channel with pronounced levees (B), and a channel entrenched into the valley surface. Panel C shows a channel incised by 1947 flooding, with approximate forest ages suggesting no disturbance since the event. The channel thus represents a young channel with little debris flow passage. Forest age indicates channels in Panels A and B are relatively old.

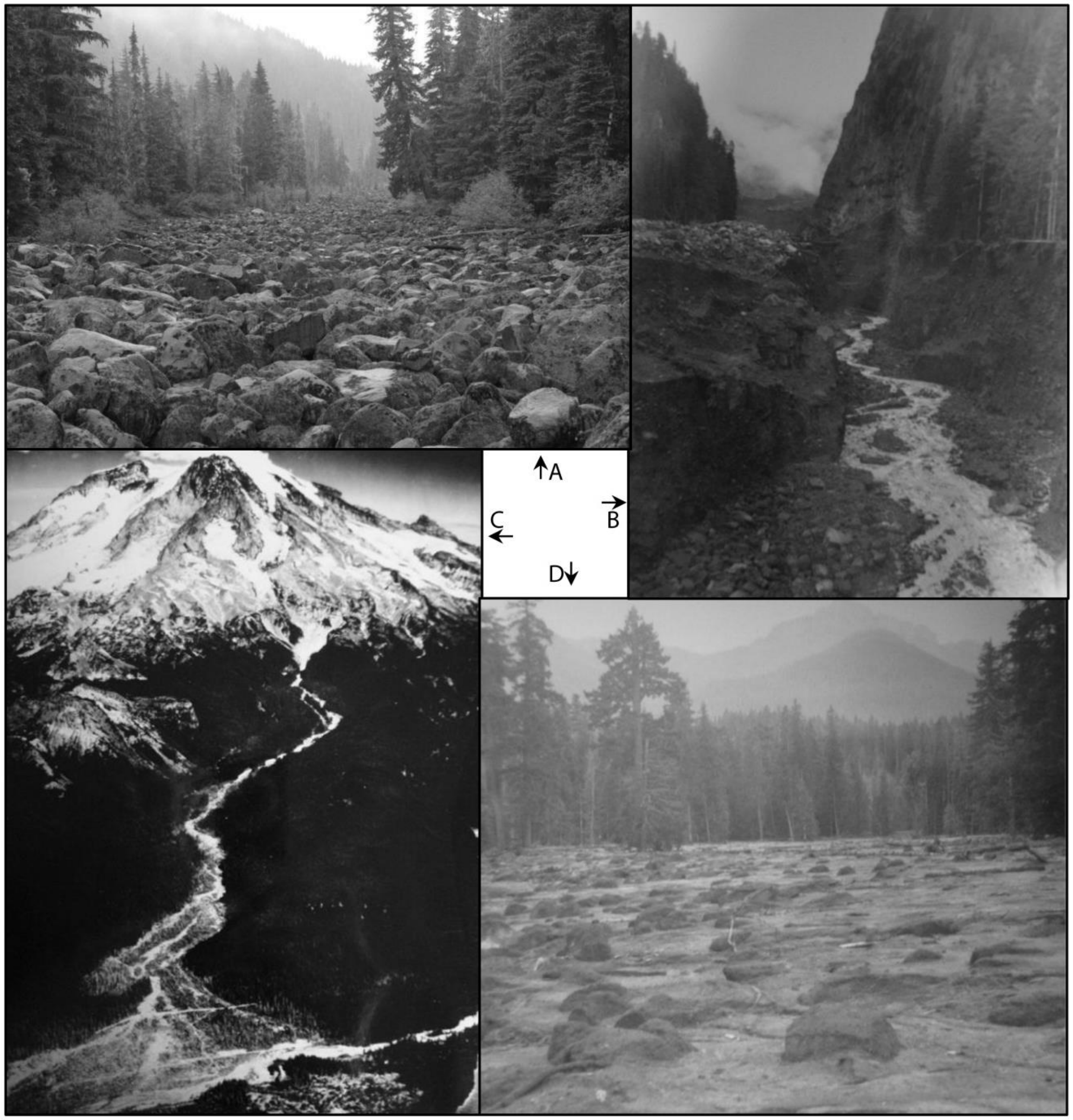

Figure 3-6 Recent (A) and historical photographs (NPS Archives) of 1947 debris flow landforms. A: Looking down the former Kautz Creek channel. Note coverage of open-framework boulders. B: Looking upstream at incision from 1947 storm just below the Box Canyon visible in background (Potts, 1947). C: Oblique aerial photograph of Kautz Valley (unknown photographer, 1957). D: 1947 debris flow deposit in the lower Kautz Valley (unknown photographer, 1947).

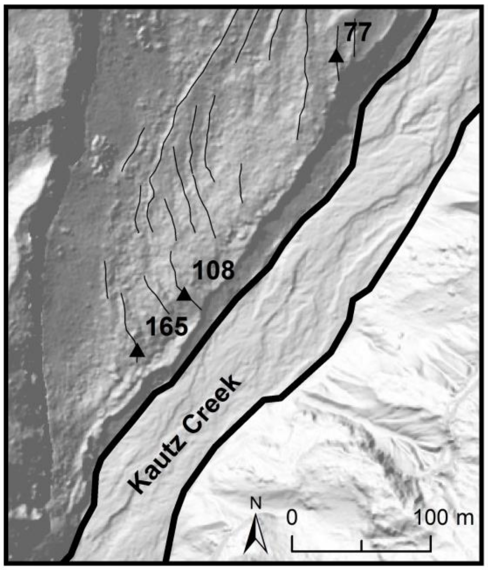

Figure 3-7 Map of LIA moraine crests (thin black lines) above the Box Canyon. The largest lichens measured are indicated in mm and correspond with moraine stabilization calendar dates of 1637 AD (165 mm), 1768 AD (108 mm) and 1839 AD (77 mm) based on the linear growth curve of (O’Neal et al., in review; O’Neal and Schoenenberger, 2003)

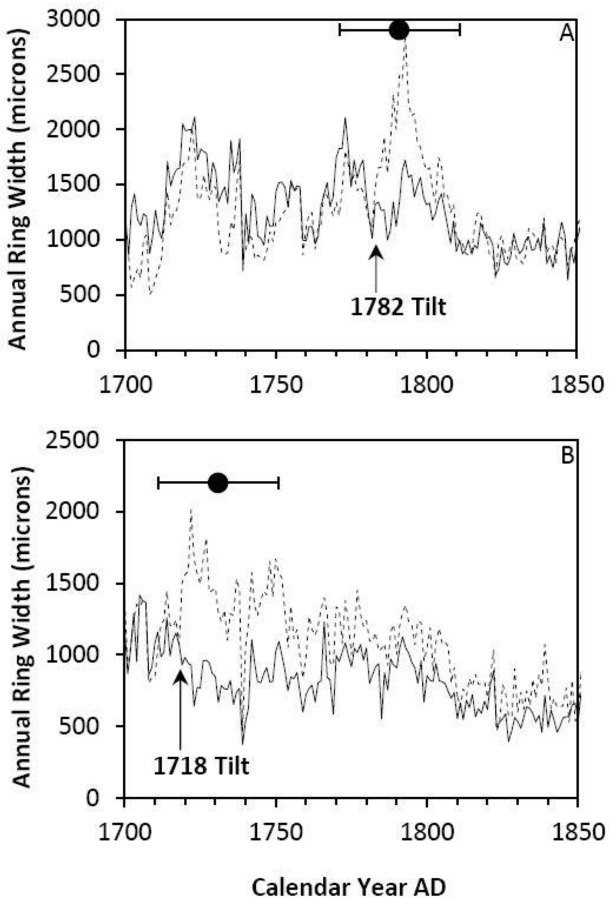

Figure 3-8 Measured annual growth of increment cores from trees KD-175 (A) and KD-176 (B) with lichenometric age estimates (black dots with error bars) of debris flow deposits that impacted each tree. Growth for the impacted (solid lines) and un-impacted (dashed) are shown. Divergence in annual growth in cores of opposite orientation indicates tilting.

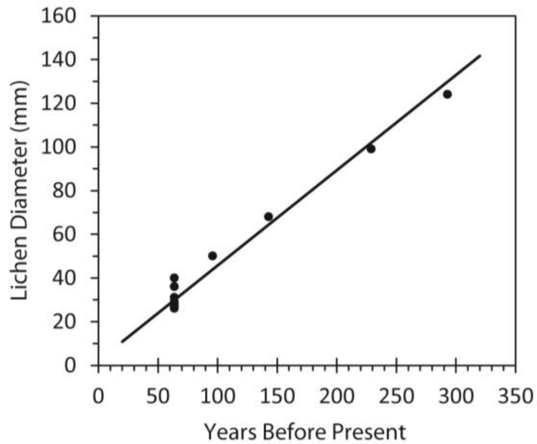

Figure 3-9 **L**ichen diameter versus time plot showing measured lichen sizes on deposits of known age (dots) with the published growth curve (black line) for the Pacific Northwest (O'Neal et al., in review; O'Neal and Schoenenberger, 2003).

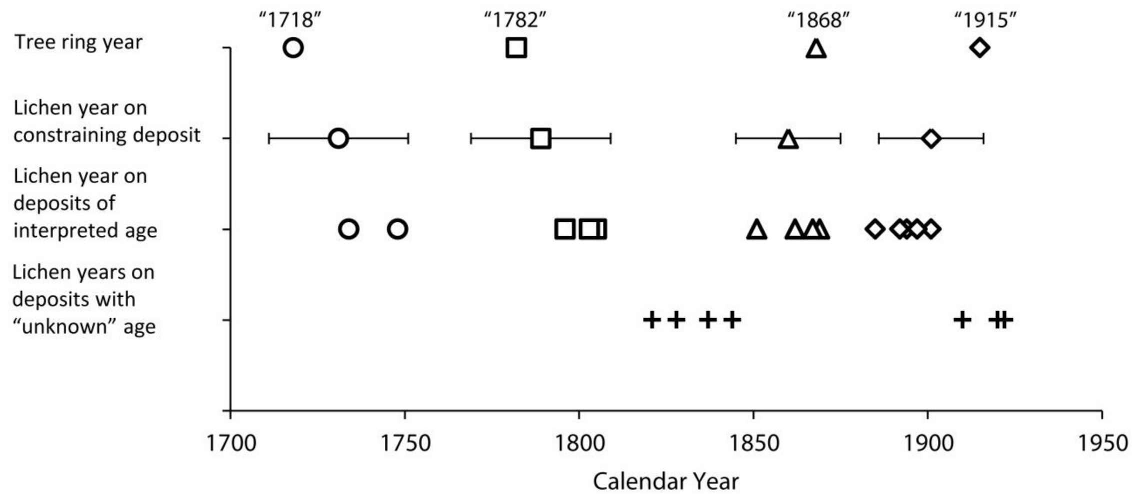

Figure 3-10 Plot showing the four tree ring-dated deposit ages, the four corresponding estimates of age using published growth curves, and lichenometric age estimates of all other boulder deposits with lichen measurements. The latter group is classified according to the four deposit ages or as unknown age in the lowest row. This plot allowed us to interpret ages of boulder deposits systematically.

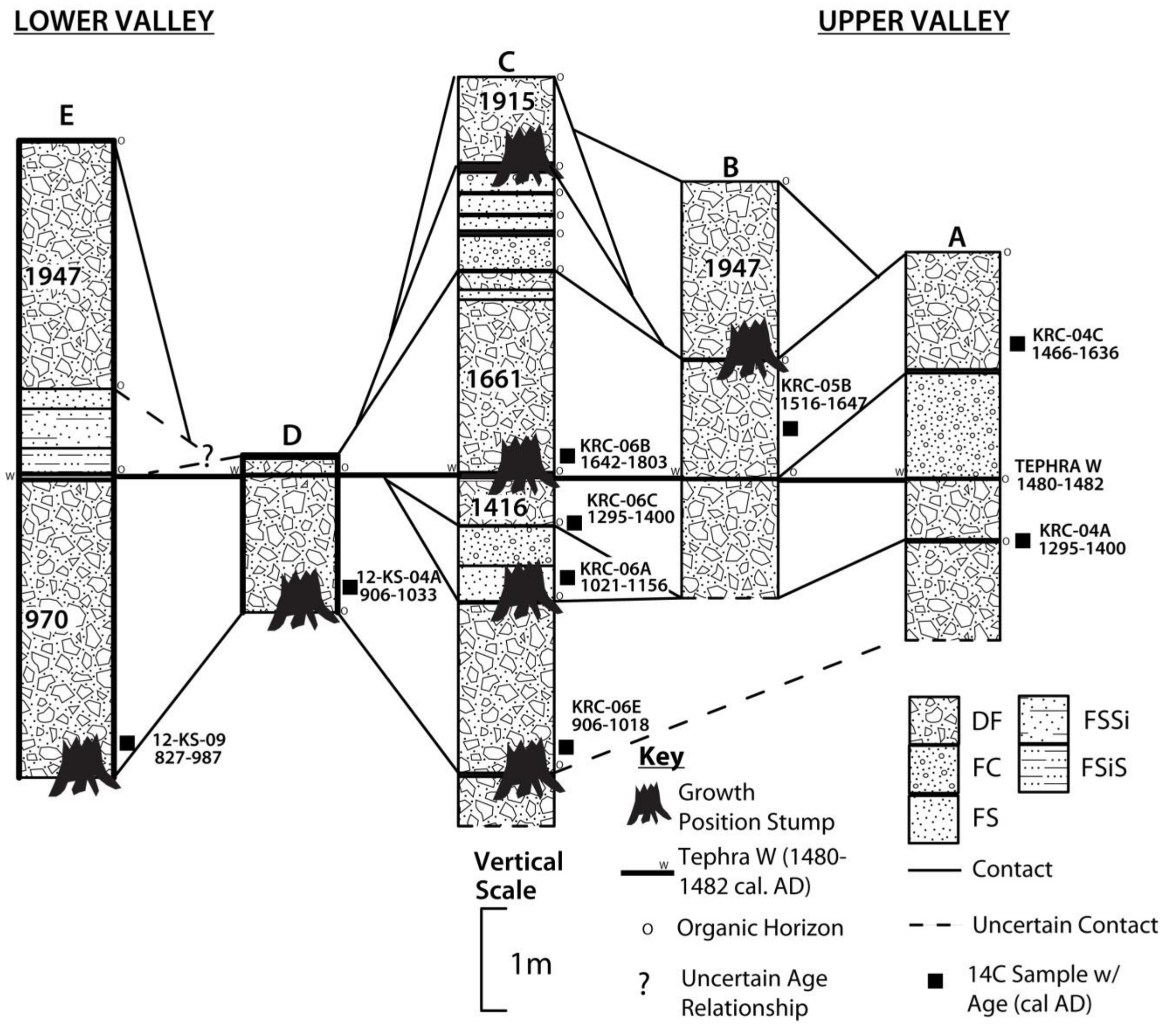

Figure 3-11 Fence diagram of stratigraphic columns shown on Figure 3-1. Interpreted debris flow calendar ages corresponding with those shown in Table 1 are shown. Sedimentological units include debris flow (massive, poorly sorted, matrix-supported; DF), fluvial channel deposit (clast-supported gravel, cobbles and boulders with stratification, FC), fluvial sand (sand with stratification, FS), fluvial sand with silt (FSSi), and fluvial silt with sand (FSiS). Radiocarbon ages calibrated with stratigraphic modeling are shown. Where sample depths are adjacent to buried stumps, samples were collected from the outermost annual growth rings.

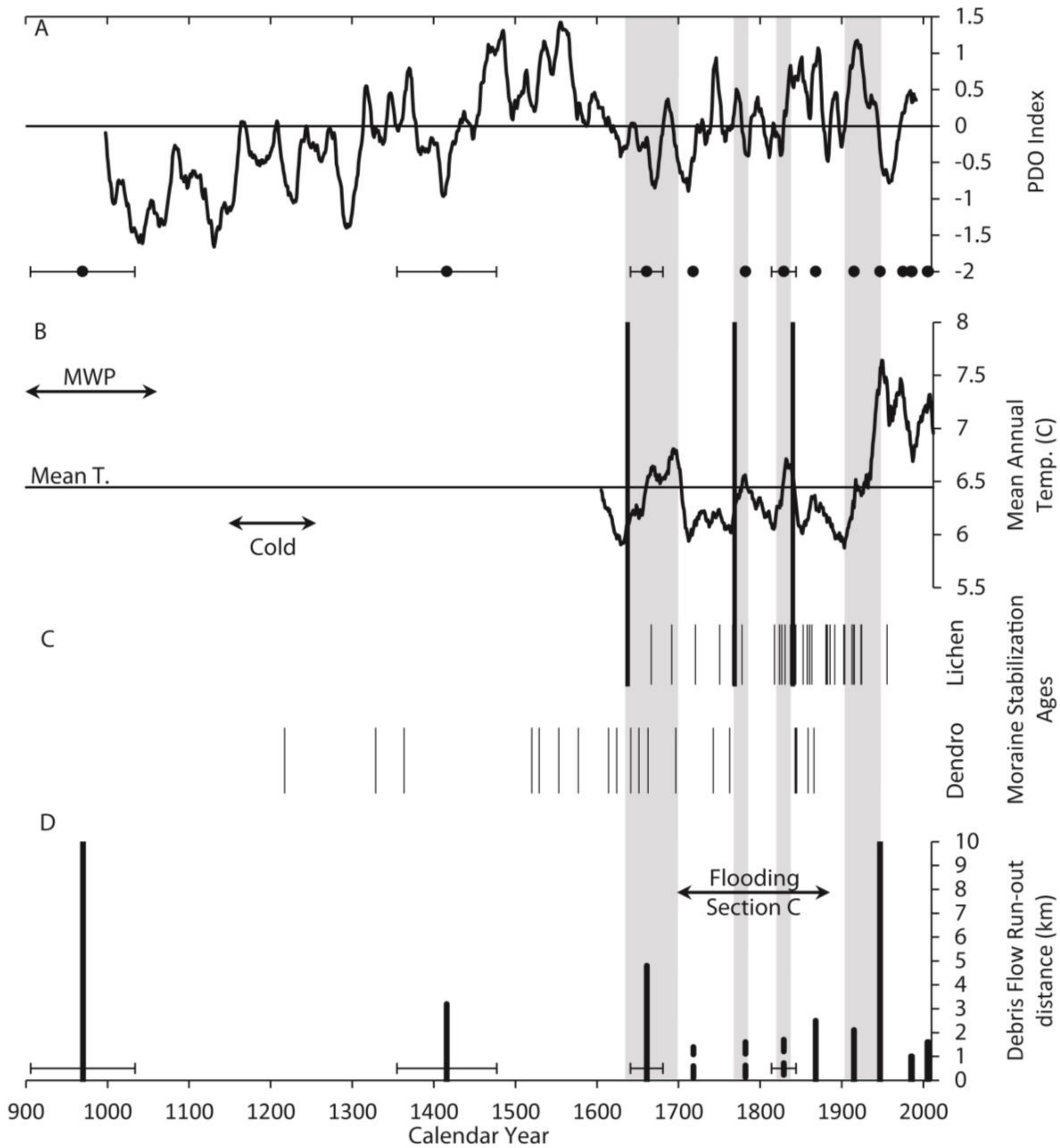

Figure 3-12 Summary diagram of climate, glacier positions, and debris flows for the last 1,100 calendar years. Panel A shows a tree ring reconstructed index for Pacific Decadal Oscillation (PDO) where positive values indicate decreased winter precipitation and snowpack and negative values indicate the reverse conditions (MacDonald and Case, 2005). Debris flow ages are also shown. Panel B shows a running average (15-year trailing) of annual temperature (Graumlich and Brubaker, 1986)reconstructed from tree rings. The 15-year choice is based on glacier response time estimated for Mount Rainier glaciers according to empirical relationships (Oerlemans, 2005; Oerlemans, 2001). Vertical grey areas define selected warming trends according to tree ring temperature reconstruction. Periods of warm (Medieval Warming Period (MWP)) and cold temperature anomalies derived from a pollen temperature reconstruction in the coastal region are also shown (Viau et al., 2012). Panel C shows moraine stabilization ages as determined from lichenometry (Burbank, 1981; O'Neal, 2005) and the oldest tree growing on moraines (Sigafoos and

Hendricks, 1972; Burbank, 1981). Bolded vertical lines denote lichenometric moraine ages for the Kautz basin (this study). Panel D shows reconstructed and recorded debris flows and periods of flood sedimentation. Broken lines indicate moderate confidence debris flows, solid lines show high confidence ages. Error bars (95%) shown. We use debris flow run-out distance as a proxy for debris flow volume. Note that the 1975 debris flow is not shown in Panel D (like it is in Panel A) because it ran-out along Van Trump Creek to the east of Kautz Valley.

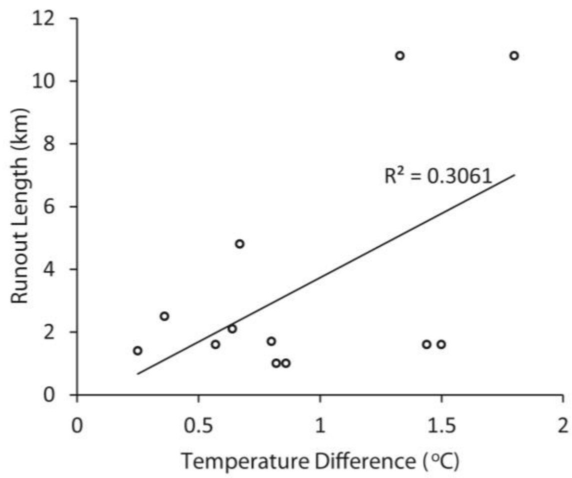

Figure 3-13 Plot of temperature difference (from the date of the debris flow to the minimum temperature during the LIA) versus run-out length from the valley head. The 1416 event is not included due to poor temperature constraint. The temperature for the ca. 970 event during the Medieval Warming Period was estimated using the average of the 20th century. Temperature is a proxy for glacier extent.

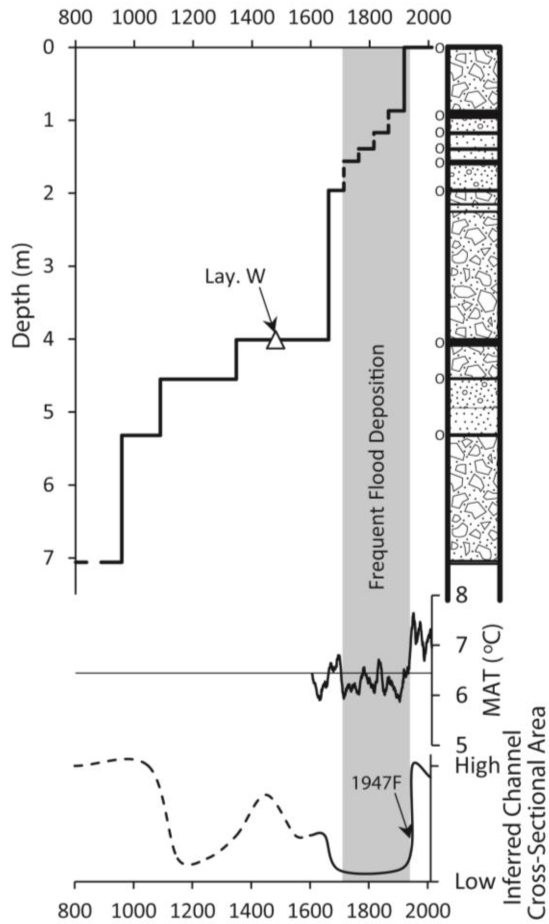

Figure 3-14 Time versus depth plot of stratigraphic column C (patterns defined in Figure 3-11, O means an organic horizon was observed). Lower plots show a combined instrumental and tree-ring reconstruction of mean annual temperature (MAT) and inferred channel cross sectional area which relates to the capacity of channels to convey floods and debris flows. We interpret the cross-sectional area based on the incidence of flooding recorded in debris flows, and from inferred sediment production as a result based on temperature and glacier records (Figure 3-11). We interpret a period of frequent flood deposition coinciding with the LIA to be a result of filled channels as a result of increased stream transported sediment flux produce from large glaciers.

3.16 Tables

Table 3-1 Reconstructed Debris Flow Ages and Age Constraints

Calendar Year (AD)	Age Error	Certainty that a debris flow	Age Constraint(s)***
2006	0	High	A
2005	0	High	A
1986*	0	High	A
1985*	0	High	A
1975*	0	High	A
1947	0	High	A
1915	2	High	D
1868	2	High	D
1829	15	Medium	L
1782	2	Medium	D/L
1718	2	Medium	D/L
1661	20	High	S
1416	61	High	S
970	64	High	S

* Occurred during hot and dry weather, suggesting the debris flow was induced by glacier outburst flood.
** The 1975 debris flow crossed the drainage basin divide and traveled down the Van Trump drainage (Driedger and Fountain, 1989).
*** Age constraints included, archives (A), dendrochronologic distrubance (D), lichenometric age estimates (L), and stratigraphic section (S).

Table 3-2 Summary of Radiocarbon Samples

Sample ID	Material	Stratigraphic Section	Sample Depth (m)*	Uncalibrated 14C Age (14C YBP)	Calibrated Date Range (calAD, 95% Conf.)	Stratigraphically Modeled Age (calAD, 95% Conf.)	Sample Position***
KRC-04A	Wood	A	2.95	615±30	1295-1400	1295-1400	OH
KRC-04C	Wood	A	1	345±25	1466-1636	1498-1531 (11.6%); 1537-1641 (83.8%)	OF
KRC-05B	Charcoal	B	2.5	315±25	1490-1603 (74.2%); 1611-1645 (21.2%)	1516-1647	OF
KRC-05C	Wood	B	2.5	375±25	1447-1524 (62.6%); 1559-1564 (1.1%); 1571-1631 (31.7%)	**	OF
KRC-06A	Wood	C	5.3	965±30	1018-1155	1021-1156	BTGP
KRC-06B	Wood	C	4	225±25	1642-1681 (44.2%); 1763-1801 (39.2%); 1938-1955 (12.0%)	1642-1681 (55.6%) 1763-1803 (39.8%)	BTGP
KRC-06C	Wood	C	4.6	615±25	1295-1400	1295-1400	OH
KRC-06D	Wood	C	7.1	1110±25	887-990	**	BTGP
KRC-06E	Wood	C	7.1	1080±25	895-925 (26.3%); 936-1018 (69.1%)	896-927 (21.9%; 936-1018 (73.5%)	BTGP
12-KS-04A	Wood	D	1	1030±25	906-912 (1.1%); 972-1033 (94.3%)	906-912 (1.1%); 972-1033 (94.3%)	BTGP
12-KS-09	Wood	E	4.5	1130±25	827-840 (1.6%); 865-987 (93.8%)	827-840 (1.6%); 865-987 (93.8%)	BTGP

* Sample depth from top of stratigraphic column
** Sample not stratigraphically modeled because another sample provided younger maximum age.
*** Denotes sample position which determines the type of age provided by the sample. Samples are collected from buried organic horizons (OH), organic fragments (OF) incorporated into debris flow layers, and the outer rings of buried trees in growth position (BTGP).

Table 3-3 Table of Debris Flow Run-Out Distances

Year (AD)	Maximum Distance Downstream (RK)	Runout Distance (from Box Canyon, km)
2006	9.2	1.6
2005	9.2	1.6
1986*	9.5	1
1985*	9.5	1
1947	0	10.8
1915	8.7	2.1
1868	8.3	2.5
1829	9.1	1.7
1782	9.2	1.6
1718	9.4	1.4
1661	6	4.8
1416	7.6	3.2
970**	0	10.8

* Assumed small distance
** Traveled at least to valley mouth based on Barnhardt and Sherrod, 2006

4 Conclusions

This work details an effort to constrain the initiation mechanisms of recent debris flows and contextualize their occurrence by reconstructing a debris flow chronology on Mount Rainier. Our approach spans different spatial and temporal scales to provide insights into to (1) debris flow initiation mechanisms, (2) debris flow activity over the last 1,000 years and its implications valley bottom evolution, and (3) influences of climate and glacier extent on debris flow occurrence and run-out. We discuss our conclusions accordingly, below.

We analyzed the change, setting, and distribution of gullies on Mount Rainier where floods were transformed to debris flows during a large storm in 2006. Analysis of debris flow gullies from one storm has allowed us to infer the geomorphic processes of and conditions necessary for this unique style of debris flow initiation, in which floodwaters are transformed to debris flow by progressive entrainment of sediment. Seven debris flows initiated from proglacial areas of separate basins during the 2006 storm. Gully expansion provides the source material for these debris flows. In addition, estimates of sediment volumes entrained relative to estimates of flood discharges suggest that material from gully walls is volumetrically sufficient. This manner of debris flow initiation requires both sufficient sediment and energy. Detailed analysis of gully change suggests that debris flow gullies must have abundant and unstable material along the gully length. A slope-drainage area trend produced from seven 2006 debris flow gullies indicates that debris flow initiation requires slopes over ~20^{o} near the gully head, but has little dependence on drainage area. High measured infiltration rates, however, suggest that glaciers play a major role in generating the minimum runoff necessary for debris flow initiation. Availability of sediment and water thus make proglacial areas favorable zones for debris flow initiation in the catchments of Mount Rainier.

This study builds a chronology of 14 debris flows extending 1,100 years BP in a relatively steep valley on the flanks of Mount Rainer. We have demonstrated that debris flow records are best reconstructed using a variety of surficial and stratigraphic techniques. Due to temporal limitations of the surficial dating techniques used, the chronology is most complete for the past 300 to 350 years. Since 1650 AD, at least 12 debris flows have occurred from the upper Kautz basin, 11 of which traveled to the Kautz Valley below the Box Canyon. Run-out distances served as a proxy for debris flow magnitude, and indicate that at least 11, 2, and 1 debris flow(s) have traveled at least 1, 3, and 5 km from the valley head, respectively since ca. 1650, indicating a frequency-magnitude relationship. The largest of these events was the 1947 event, which was estimated at 40 million m^3 volume (Crandell, 1971a). The only other event of similar magnitude to the 1947 was one dated at ca. 970 AD that had a contemporaneous sediment pulse downstream at the Puget Sound (Barnhardt and Sherrod, 2006). We compare 1650-1900, generally corresponding with the LIA, to the period from 1900 to present day. Five and seven debris flows occurred in the two periods, respectively, with corresponding average frequencies of 2 and 3.4 debris flows per century. In run-out length, the average magnitudes for the two time periods are 2.4 and 3 km from the Box Canyon. Considering unavoidable biases toward the present in any reconstructed chronology, debris flow activity differences indicated by these averages are equivocal.

The geomorphic form and process of Kautz Valley reflects the frequency and magnitude relationships observed in the chronology of dated events. Debris flows deposit relatively often and in limited spatial extent in the upper valley, where secondary channels control debris flow depositional patterns. Depositional tracks of individual dated debris flows demonstrate the control of secondary channels on debris flow deposition. Variable form of deposits suggests that debris flows with variable rheology deposit on the relatively steep slopes of the upper valley. The lower valley, however, is dominated by relatively infrequent but widespread deposition by mobile debris flows that overwhelm the main channel, producing a smooth valley surface character.

The first study revealed spatial patterns of recent debris flows that suggest initiation occurs near high-elevation glacier termini, with relatively high gradients. Relatively high gradients in DFB proglacial areas compared to NDFB are consistent with the high gradients measured in the seven 2006 debris flow gullies. Elevation differences of proglacial areas in the two basin types suggest that glaciers tend to be less extensive in DFB. These differences in proglacial area slope and elevation in debris flow and non-debris flow basins reflects an overall positive slope-elevation trend on the volcanic edifice with concave flanks. These findings suggest that the slope distribution of ice-free areas (where debris flows initiate) changes with glacier size as large glaciers cover the steepest slopes, and small glaciers expose the steepest slopes. Variations in the available slope influenced by glaciers in space and time thus influence the activity of debris flows. This model suggests that temporal glacier change can influence debris flow occurrence, as threshold slopes are exposed by glacier retreat. This interpretation contrasts with interpretations invoking debris flow occurrence generation as the result of excess sediment exposed during periods of glacier retreat (Chiarle et al., 2007). In the 2006 storm, additional sediment exposed by retreating glaciers appears to have had little influence on spatial patterns of debris flow occurrence, which may suggest that the apparently supply-unlimited basins of Mount Rainier are insensitive to increased amounts of debris supply. These findings provide context for our debris flow chronology constructed in Kautz Creek, which spans periods of variable glacier extent.

The Kautz Creek chronology suggests relationships between the timing and run-out distance of individual debris flows with temperature and inferred glacier extent. Individual debris flows coincide temporally with relatively warm periods and inferred smaller glaciers. Kautz Creek's concave longitudinal profile requires that gradients in ice-free areas become steeper with decreased glacier sizes and elevated snow-lines. In the LIA, small magnitude debris flows occur during relatively warm periods either when glaciers retreated up-valley or snow coverage was less, exposing steeper gradients in ice-free areas. LIA debris flows, however ran-out relatively short distances compared to warmer periods before and after the LIA. Shorter run-out lengths appear to result from a combination of (1) relatively small areas and slopes of zones in the fronts of glaciers relative to warm periods like the MWP and the 20th century, and (2) from enhanced deposition of debris flows outside of the main channel as a result of filled channels during glacial times. Stratigraphic records and debris flow depositional patterns support filled channels during the LIA. Whereas we cannot fully deconvolve source area and depositional controls on the observed run-out distances, these results suggest that the hazards to debris flow prone areas change with temperature and glacier oscillations in steep catchments.

REFERENCES

Anderson, R.S., 2004, Strong feedbacks between hydrology and sliding of a small alpine glacier: Journal of Geophysical Research, v. 109, no. F3.

Atwater, B.F., and Moore, A.L., 1992, A tsunami about 1000 years ago in Puget Sound, Washington: SCIENCE-NEW YORK THEN WASHINGTON-, v. 258, p. 1614–1614.

Ballantyne, C.K., 2002, Paraglacial geomorphology: Quaternary Science Reviews, v. 21, no. 18-19, p. 1935–2017.

Barnhardt, W.A., and Sherrod, B.L., 2006, Evolution of a Holocene delta driven by episodic sediment delivery and coseismic deformation, Puget Sound, Washington, USA: Sedimentology, v. 53, no. 6, p. 1211–1228.

Benda, L.E., and Cundy, T.W., 1990, Predicting deposition of debris flows in mountain channels: Canadian Geotechnical Journal/Revue Canadienne de Geotechnique, v. 27, no. 4, p. 409–417.

Bollschweiler, M., Stoffel, M., Ehmisch, M., and Monbaron, M., 2007, Reconstructing spatio-temporal patterns of debris-flow activity using dendrogeomorphological methods: Geomorphology, v. 87, no. 4, p. 337–351.

Bovis, M.J., and Jakob, M., 1999, The role of debris supply conditions in predicting debris flow activity: Earth surface processes and landforms, v. 24, no. 11, p. 1039–1054.

Burbank, D.W., 1981, A chronology of late Holocene glacier fluctuations on Mount Rainier, Washington: Arctic and Alpine Research, v. 13, no. 4, p. 369–386.

Burbank, D.W., 1982, Correlations of Climate, Mass Balances, and Glacial Fluctuations at Mount Rainer, Washington, USA, Since 1850: Arctic and Alpine Research, v. 14, no. 2, p. 137–148.

Cannon, S.H., and Gartner, J.E., 2005, Wildfire-related debris flow from a hazards perspective: Debris-flow Hazards and Related Phenomena,, p. 363–385.

Cannon, S.H., and Reneau, S.L., 2000, Conditions for generation of fire-related debris flows, Capulin Canyon, New Mexico: Earth Surface Processes and Landforms, v. 25, no. 10, p. 1103–1121.

Chiarle, M., Iannotti, S., Mortara, G., and Deline, P., 2007, Recent debris flow occurrences associated with glaciers in the Alps: Global and Planetary Change, v. 56, no. 1-2, p. 123–136.

Copeland, E.A., 2009, Recent Periglacial Debris Flows from Mount Rainier, Washington [Master's]: Oregon State University, 111 p.

Costa, J.E., 1988, Rheologic, geomorphic, and sedimentologic differentiation of water floods, hyperconcentrated flows, and debris flows: Flood Geomorphology.,, p. 113–122.

Crandell, D.R., 1971a, Postglacial lahars from Mount Rainier volcano, Washington: USGS Professional Paper, v. 677, p. 75.

Crandell, D.R., 1971b, Postglacial lahars from Mount Rainier volcano, Washington:.

Czuba, J.A., Czuba, C.R., Magirl, C.S., and Voss, F.D., 2010, Channel-conveyance capacity, channel change, and sediment transport in the lower Puyallup, White, and Carbon Rivers, western Washington:.

Czuba, J.A., Magirl, C.S., Czuba, C.R., Grossman, E.E., Curran, C.A., Gendaszek, A.S., and Dinicola, R.S., 2011, Sediment load from major rivers into Puget Sound and its adjacent waters: US Geological Survey, Wasington Water Science Center.

Czuba, J.A., Olsen, T.D., Czuba, C.R., Magirl, C.S., and Gish, C.C., 2012, Changes in sediment volume in Alder Lake, Nisqually River Basin, Washington, 1945-2011: United States Geological Survey OFR - 2012-1068, i–30 p.

Driedger, C.L., and Fountain, A.G., 1989, Glacier outburst floods at Mount Rainier: Washington State, USA: Annals of Glaciology, v. 13, p. 51–55.

Driedger, C.L., and Kennard, P.M., 1984, Ice volumes on Cascade volcanoes: Mount Rainier, mount Hood, Three sisters, and mount Shasta: US Dept. of the Interior, Geological Survey.

Dühnforth, M., Densmore, A.L., Ivy-Ochs, S., and Allen, P.A., 2008, Controls on sediment evacuation from glacially modified and unmodified catchments in the eastern Sierra Nevada, California: Earth Surface Processes and Landforms, v. 33, no. 10, p. 1602–1613.

Dühnforth, M., Densmore, A.L., Ivy-Ochs, S., Allen, P.A., and Kubik, P.W., 2007, Timing and patterns of debris flow deposition on Shepherd and Symmes creek fans, Owens Valley, California, deduced from cosmogenic 10Be: Journal of Geophysical Research, v. 112, no. F3.

Dunwiddie, P.W., 1986, A 6000-year record of forest history on Mount Rainier, Washington: Ecology, v. 67, no. 1, p. 58–68.

Earle, C.J., Brubaker, L.B., and Segura, G., 1987, Douglas Fir Tree Ring Master Chronology for Tahoma Creek Trailhead, WA: 1411-1987:.

Fitts, C.R., 2002, Groundwater science: Academic Press.

Gabet, E.J., and Bookter, A., 2008, A morphometric analysis of gullies scoured by post-fire progressively bulked debris flows in southwest Montana, USA: Geomorphology, v. 96, no. 3-4, p. 298–309.

Gabet, E.J., and Sternberg, P., 2008, The effects of vegetative ash on infiltration capacity, sediment transport, and the generation of progressively bulked debris flows: Geomorphology, v. 101, no. 4, p. 666–673.

Grant, G.E., and Swanson, F.J., 1995, Morphology and processes of valley floors in mountain streams, western Cascades, Oregon: Geophysical Monograph Series, v. 89, p. 83–101.

Grater, R.K., 1947, Report on Kautz Creek Flood: National Park Service Memorandum, 1–3 p.

Graumlich, L.J., 1987, Precipitation variation in the Pacific Northwest (1675–1975) as reconstructed from tree rings: Annals of the Association of American Geographers, v. 77, no. 1, p. 19–29.

Graumlich, L.J., and Brubaker, L.B., 1986, Reconstruction of annual temperature (1590-1979) for Longmire, Washington, derived from tree rings: Quaternary Research, v. 25, no. 2, p. 223–234.

Van de Griend, A., and Arwert, J., 1983, The mechanism of runoff generation from an alpine glacier during a storm traced by oxygen: Journal of Hydrology, v. 62, no. 1-4, p. 263–278.

Grissino-Mayer, H.D., 2001, Research report evaluating crossdating accuracy: a manual and tutorial for the computer program COFECHA: Tree-ring research, v. 57, no. 2, p. 205–221.

Hack, J.T., and Goodlett, J.C., 1960, Geomorphology and forest ecology of a mountain region in the central Appalachians: US Govt. Print. Off.

Hallet, B., Hunter, L., and Bogen, J., 1996, Rates of erosion and sediment evacuation by glaciers: A review of field data and their implications: Global and Planetary Change, v. 12, no. 1-4, p. 213–235.

Harr, R.D., 1981, Some characteristics and consequences of snowmelt during rainfall in western Oregon: Journal of Hydrology, v. 53, no. 3, p. 277–304.

Heliker, C., Johnson, A., and Hodge, S., 1984, Nisqually Glacier, Mount Rainier, Washington, 1857-1979: A Summary of the Long-Term Observations and a Comprehensive Bibliography: USGS Open-file Report 83-541 1984. 20 p, 4 Fig, 5 Tab, 84 Ref.,.

Hildreth, W., 2007, Quaternary magmatism in the Cascades-Geologic perspectives: US Geological Survey professional paper, , no. 1744, p. 1–125.

Hoblitt, R.P., Walder, J.S., Driedger, C.L., Scott, K.M., Pringle, P.T., and Vallance, J.W., 1995, Volcano Hazards from Mount Rainier, Washington: US Department of the Interior, US Geological Survey.

Holmes, R.L., Adams, R., and Fritts, H., 1986, Quality control of crossdating and measuring: a users manual for program COFECHA: Tree-ring chronologies of western North America: California, eastern Oregon and northern Great Basin.,, p. 41–49.

Hooke, R.L.B., 1967, Processes on arid-region alluvial fans: The Journal of Geology,, p. 438–460.

Hungr, O., Morgan, G.C., and Kellerhals, R., 1984, Quantitative analysis of debris torrent hazards for design of remedial measures: Canadian Geotechnical Journal, v. 21, no. 4, p. 663–677.

Hupp, C.R., 1984, Dendrogeomorphic evidence of debris flow frequency and magnitude at Mount Shasta, California: Environmental Geology, v. 6, no. 2, p. 121–128.

Hupp, C.R., Osterkamp, W.R., and Thornton, J.L., 1987, Dendrogeomorphic evidence and dating of recent debris flows on Mount Shasta, northern California:.

Istanbulluoglu, E., Tarboton, D.G., Pack, R.T., and Luce, C., 2003, A sediment transport model for incision of gullies on steep topography: Water Resources Research, v. 39, no. 4.

Iverson, R.M., 2003, The debris-flow rheology myth, *in* Debris flow Mechanics and Mitigation Conference, Mills Press, Davos, p. 303–314.

Iverson, R.M., 1997, The physics of debris flows: Reviews of Geophysics, v. 35, no. 3, p. 245–296.

Iverson, R.M., Reid, M.E., and LaHusen, R.G., 1997, Debris Flow Mobilization From Landslides: Annual Review of Earth and Planetary Sciences, v. 25, no. 1, p. 85–138.

Jacoby, G.C., Williams, P.L., and Buckley, B.M., 1992, Tree ring correlation between prehistoric landslides and abrupt tectonic events in Seattle, Washington: SCIENCE-NEW YORK THEN WASHINGTON-, v. 258, p. 1621–1621.

Lamb, M.P., Scheingross, J.S., Amidon, W.H., Swanson, E., and Limaye, A., 2011, A model for fire-induced sediment yield by dry ravel in steep landscapes: Journal of Geophysical Research, v. 116, no. F3.

Lancaster, S.T., Nolin, A.W., Copeland, E.A., and Grant, G.E., 2012, Periglacial debris-flow initiation and susceptibility and glacier recession from imagery, airborne LiDAR, and ground-based mapping: Geosphere, v. 8, no. 2, p. 417–430.

Larsen, M.C., Wieczorek, G.F., Eaton, L.S., and Torres-Sierra, H., 2001, The rainfall-triggered landslide and flash-flood disaster in northern Venezuela, December 1999, *in* Proceedings of the Seventh Federal Interagency Sedimentation Conference, p. 9–16.

Lescinsky, D.T., and Sisson, T.W., 1998, Ridge-forming, ice-bounded lava flows at Mount Rainier, Washington: Geology, v. 26, no. 4, p. 351–354.

MacDonald, G.M., and Case, R.A., 2005, Variations in the Pacific Decadal Oscillation over the past millennium: Geophysical Research Letters, v. 32, no. 8.

Meier, M.F., 1984, Contribution of Small Glaciers to Global Sea Level: Science, v. 226, no. 418, p. 1418–1421.

Meyer, G.A., and Wells, S.G., 1997, Fire-related sedimentation events on alluvial fans, Yellowstone National Park, USA: Journal of Sedimentary Research, v. 67, no. 5, p. 776–791.

Meyer, G.A., Wells, S.G., and Jull, A.J.T., 1995, Fire and alluvial chronology in Yellowstone National Park: climatic and intrinsic controls on Holocene geomorphic processes: Geological Society of America Bulletin, v. 107, no. 10, p. 1211–1230.

Mills, H.H., 1976, Estimated erosion rates on Mount Rainier, Washington: Geology, v. 4, no. 7, p. 401.

Montgomery, D.R., and Dietrich, W.E., 1989, Source areas, drainage density, and channel initiation: Water Resources Research, v. 25, no. 8, p. 1907–1918.

Moore, R.D., Fleming, S.W., Menounos, B., Wheate, R., Fountain, A., Stahl, K., Holm, K., and Jakob, M., 2009, Glacier change in western North America: influences on hydrology, geomorphic hazards and water quality: Hydrological Processes, v. 23, no. 1, p. 42–61.

Mote, P.W., 2003, Trends in snow water equivalent in the Pacific Northwest and their climatic causes: Geophysical Research Letters, v. 30, no. 12, p. 1601.

Mote, P.W., Parson, E.A., Hamlet, A.F., Keeton, W.S., Lettenmaier, D., Mantua, N., Miles, E.L., Peterson, D.W., Peterson, D.L., and Slaughter, R., 2003, Preparing for climatic change: the water, salmon, and forests of the Pacific Northwest: Climatic Change, v. 61, no. 1, p. 45–88.

Mullineaux, D.R., 1974, Pumice and other pyroclastic deposits in Mount Rainier National Park, Washington: US Government Printing Office.

Neiman, P.J., Ralph, F.M., Wick, G.A., Kuo, Y.H., Wee, T.K., Ma, Z., Taylor, G.H., and Dettinger, M.D., 2008, Diagnosis of an intense atmospheric river impacting the Pacific Northwest: Storm summary and offshore vertical structure observed with COSMIC satellite retrievals: Monthly Weather Review, v. 136, no. 11, p. 4398–4420.

O'Connor, J.E., Hardison, J.H., and Costa, J.E., 2001, Debris flows from failures of Neoglacial-Age moraine dams in the Three Sisters and Mount Jefferson wilderness areas, Oregon: US Dept. of the Interior, US Geological Survey.

O'Neal, M.A., 2005, Late Little Ice Age Glacier Fluctuation in the Cascade Range of Washington and northern Oregon [Dissertation]: University of Washington, 115 p.

O'Neal, M.A., Legg, N.T., Hanson, B., Morgan, D.J., and Rothgeb, A., in review, Lichenometric Dating of Rock Surfaces in the northern Cascade Range, USA: Geografiska Annaler. Series A, Physical Geography,.

O'Neal, M.A., and Schoenenberger, K.R., 2003, A Rhizocarpon geographicum growth curve for the Cascade Range of Washington and northern Oregon, USA: Quaternary Research, v. 60, no. 2, p. 233–241.

Oerlemans, J., 2005, Extracting a Climate Signal from 169 Glacier Records: Science, v. 308, no. 5722, p. 675–677, doi: 10.1126/science.1107046.

Oerlemans, J., 2001, Glaciers and climate change: Taylor & Francis.

Peterson, D.W., and Peterson, D.L., 2001, Mountain hemlock growth responds to climatic variability at annual and decadal time scales: Ecology, v. 82, no. 12, p. 3330–3345.

Pierson, T.C., 2005, Distinguishing between debris flows and floods from field evidence in small watersheds: US Dept. of the Interior, US Geological Survey.

Pierson, T.C., 1980, Erosion and deposition by debris flows at Mt. Thomas, north Canterbury, New Zealand: Earth Surface Processes, v. 5, no. 3, p. 227–247.

Pierson, T.C., 1986, Flow behavior of channelized debris flows, Mount St. Helens, Washington: Hillslope processes,, p. 269–296.

Pierson, T.C., and Scott, K.M., 1985, Debris Flow to Hyperconcentrated Streamflow: Water resources research, v. 21, no. 10, p. 1511–1524.

Porter, S.C., 1981, Lichenometric studies in the Cascade Range of Washington: establishment of Rhizocarpon geographicum growth curves at Mount Rainier: Arctic and Alpine Research, v. 13, no. 1, p. 11–23.

Porter, S.C., 1989, Some geological implications of average Quaternary glacial conditions: Quaternary Research, v. 32, no. 3, p. 245–261.

Ramsey, C.B., 1995, Radiocarbon calibration and analysis of stratigraphy: the OxCal program: Radiocarbon, v. 37, no. 2, p. 425–430.

Reimer, P.J., Baillie, M.G.L., Bard, E., Bayliss, A., Beck, J.W., Blackwell, P.G., Ramsey, C.B., Buck, C.E., Burr, G.S., and Edwards, R.L., 2009, IntCal09 and Marine09 radiocarbon age calibration curves, 0–50,000 years cal BP:.

Richardson, D., 1968, Glacier outburst floods in the Pacific Northwest: US Geologic Survey Professional Paper, , no. 600-D, p. D79–D86.

Rickenmann, D., 1999, Empirical relationships for debris flows: Natural Hazards, v. 19, no. 1, p. 47–77.

Ritter, J.B., Miller, J.R., Enzel, Y., and Wells, S.G., 1995, Reconciling the roles of tectonism and climate in Quaternary alluvial fan evolution: Geology, v. 23, no. 3, p. 245.

Santi, P.M., dewolfe, V.G., Higgins, J.D., Cannon, S.H., and Gartner, J.E., 2008, Sources of debris flow material in burned areas: Geomorphology, v. 96, no. 3, p. 310–321.

Schneuwly-Bollschweiler, M., and Stoffel, M., 2012, Hydrometeorological triggers of periglacial debris flows in the Zermatt valley (Switzerland) since 1864: Journal of Geophysical Research, v. 117, no. F2, doi: 10.1029/2011JF002262.

Schumm, S.A., 1979, Geomorphic thresholds: the concept and its applications: Transactions of the Institute of British Geographers,, p. 485–515.

Schuster, R.L., Logan, R.L., and Pringle, P.T., 1992, Prehistoric rock avalanches in the Olympic Mountains, Washington: SCIENCE-NEW YORK THEN WASHINGTON-, v. 258, p. 1620–1620.

Scott, K.M., Vallance, J.W., and Pringle, P.T., 1995, Sedimentology, behavior, and hazards of debris flows at Mount Rainier, Washington: USGPO.

Seidl, M.A., and Dietrich, W.E., 1993, The problem of channel erosion into bedrock: Catena supplement, v. 23, p. 101–101.

Sharp, R.P., 1942, Mudflow levees: Journal of Geomorphology, v. 5:.

Sigafoos, R.S., and Hendricks, E.L., 1972, Recent activity of glaciers of Mount Rainier, Washington:.

Sisson, T.W., Robinson, J.E., and Swinney, D.D., 2011, Whole-edifice ice volume change A.D. 1970 to 2007/2008 at Mount Rainier, Washington, based on LiDAR surveying: Geology, v. 39, p. 639–642.

Sisson, T.W., and Vallance, J.W., 2009, Frequent eruptions of Mount Rainier over the last 2,600 years: Bulletin of volcanology, v. 71, no. 6, p. 595–618.

Snyder, N.P., Whipple, K.X., Tucker, G.E., and Merritts, D.J., 2000, Landscape response to tectonic forcing: Digital elevation model analysis of stream profiles in the Mendocino triple junction region, northern California: Geological Society of America Bulletin, v. 112, no. 8, p. 1250–1263.

Speer, J.H., 2010, Fundamentals of tree ring research: University of Arizona Press.

Steinman, B.A., Abbott, M.B., Mann, M.E., Stansell, N.D., and Finney, B.P., 2012, 1,500 year quantitative reconstruction of winter precipitation in the Pacific Northwest: Proceedings of the National Academy of Sciences, v. 109, no. 29, p. 11619–11623.

Stock, J., and Dietrich, W.E., 2003, Valley incision by debris flows: Evidence of a topographic signature: Water Resources Research, v. 39, no. 4, p. 1089.

Stoffel, M., and Beniston, M., 2006, On the incidence of debris flows from the early Little Ice Age to a future greenhouse climate: a case study from the Swiss Alps: Geophysical Research Letters, v. 33, no. 16, p. 16404.

Stoffel, M., and Bollschweiler, M., 2008, Tree-ring analysis in natural hazards research? an overview:.

Stoffel, M., Lièvre, I., Conus, D., Grichting, M.A., Raetzo, H., Gärtner, H.W., and Monbaron, M., 2005, 400 years of debris-flow activity and triggering weather conditions: Ritigraben, Valais, Switzerland: Arctic, Antarctic, and Alpine Research, v. 37, no. 3, p. 387–395.

Tarboton, D.G., Bras, R.L., and Rodriguez-Iturbe, I., 2006, On the extraction of channel networks from digital elevation data: Hydrological processes, v. 5, no. 1, p. 81–100.

Vallance, J.W., Cunico, M.L., Schilling, S.P., and Geological Survey, V., 2003, Debris-flow hazards caused by hydrologic events at Mount Rainier, Washington: United States Geological Survey.

Vallance, J.W., and Scott, K.M., 1997, The Osceola Mudflow from Mount Rainier: Sedimentology and hazard implications of a huge clay-rich debris flow: Geological Society of America Bulletin, v. 109, no. 2, p. 143–163.

Viau, A.E., Ladd, M., and Gajewski, K., 2012, The climate of North America during the past 2000years reconstructed from pollen data: Global and Planetary Change, v. 84-85, p. 75–83.

Walder, J.S., and Driedger, C.L., 1995, Frequent outburst floods from South Tahoma Glacier, Mount Rainier, USA: relation to debris flows, meterological origin and implications for subglacial hydrology: Journal of Glaciology, v. 41, no. 137, p. 1–10.

Walder, J.S., and Driedger, C.L., 1994a, Geomorphic change caused by outburst floods and debris flows at Mount Rainier: Washington with emphasis on Tahoma Creek Valley: US Geological Survey Water-Resources Investigations Report,, p. 93–4093.

Walder, J.S., and Driedger, C.L., 1994b, Rapid geomorphic change caused by glacial outburst floods and debris flows along Tahoma Creek, Mount Rainier, Washington, USA: Arctic and Alpine Research, v. 26, no. 4, p. 319–327.

Walder, J.S., and Driedger, C.L., 1994c, Rapid geomorphic change caused by glacial outburst floods and debris flows along Tahoma Creek, Mount Rainier, Washington, USA: Arctic and Alpine Research, v. 26, no. 4, p. 319–327.

Wells, W.G., 1987, The effects of fire on the generation of debris flows in southern California: Rev. Eng. Geol, v. 7, p. 105–114.

Whipple, K.X., and Dunne, T., 1992, The influence of debris-flow rheology on fan morphology, Owens Valley, California: Geological Society of America Bulletin, v. 104, no. 7, p. 887–900.

Whipple, K.X., and Tucker, G.E., 1999, Dynamics of the stream-power river incision model: Implications for height limits of mountain ranges, landscape response timescales, and research needs: Journal of Geophysical Research, v. 104, no. B8, p. 17661–17.

Wolman, M.G., 1954, A method of sampling coarse river-bed material: American Geophysical Union.

Yamaguchi, D.K., 1985, Tree-ring evidence for a two-year interval between recent prehistoric explosive eruptions of Mount St. Helens: Geology, v. 13, no. 8, p. 554–557.

Yang, C.T., 1972, Unit stream power and sediment transport: Journal of the Hydraulics Division, v. 98, no. 10, p. 1805–1826.

Zehfuss, P.H., Atwater, B.F., Vallance, J.W., Brenniman, H., and Brown, T.A., 2003, Holocene lahars and their by-products along the historical path of the White River between Mount Rainier and Seattle: Field Guides, v. 4, p. 209–223.

APPENDIX A: Dendrochronologic Data

Locations of samples shown in graphs below can be found in Figure 3-4.

Tree Samples Constraining Age of the 1915 Deposit

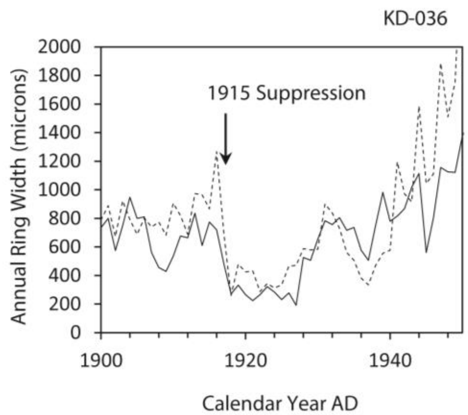

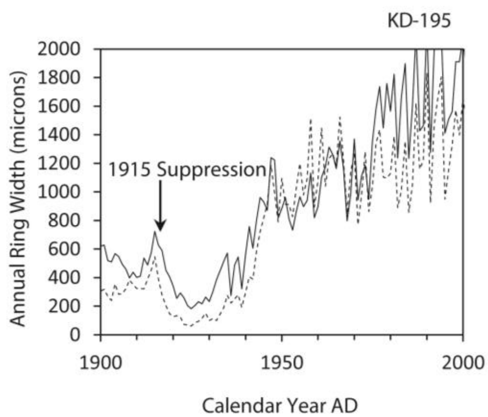

Tree Samples Constraining Age of the 1868 Deposit

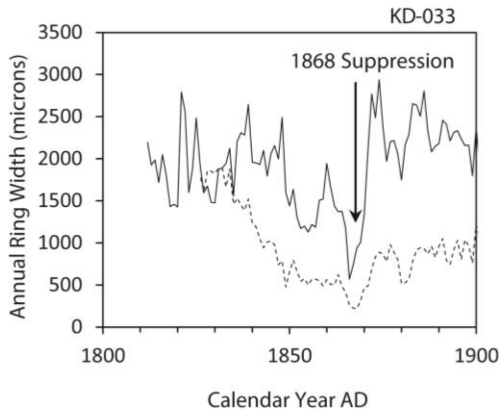

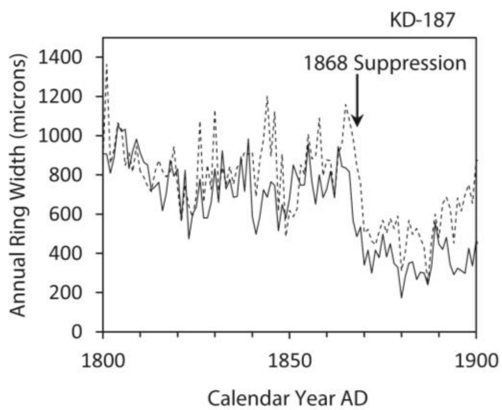

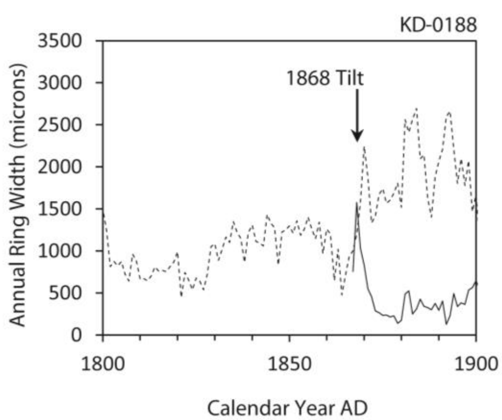

Details of Tree Samples (Locations, Sample Details, Tree Species)
(Ring Width measurements are listed in the following pages.
Ring width measurements were made with Velmex system with 1 micron precision)

Sample_ID	Y (UTM Zone 10N)	X (UTM Zone 10N)	Core ID	Tree Species*	Height of Core Above Ground (in)	Core Orientation (deg.)	Tree Diamater At Core (in)
KD-008	5182239.462	591729.465	A	WH	69	357	27.5
			B	WH	50	194	28
KD-009	5182230.087	591728.6966	A	Ced	22	245	13.5
			B	Ced	17	310	11
KD-010	5182189.72	591786.3357	A	WH	15	39	16
			B	WH	47.5	224	17.5
KD-011	5182185.622	591795.0785	A	WH	48	336	19
			B	WH	38.5	145	18.5
KD-024	5181074.915	591065.3482	A	WH	33.5	82	27
			B	WH	25	257	29
KD-026	5181088.917	591072.2809	A	WH	41	106	26
			B	WH	44	284	26
KD-029	5181127.44	591086.6245	A	WH	26	340	13
			B	WH	47	89	13
			C	WH	44	246	13
KD-033	5181129.899	591079.2478	A	WH	38	50	22
			B	WH	39	219	23
			C	WH	46	321	22
KD-036	5181287.648	591147.7514	B	WH	47	235	22
			D	WH	38	165	31
KD-084	5181970.913	591684.6094	A	WH	42	25	18
			B	WH	42.5	188	18
KD-085	5181972.051	591686.7818	A	Ced	26.5	5	11
			B	Ced	28.5	182	11
KD-086	5181974.12	591689.5748	A	WH	27.5	75	30
			B	WH	39	177	25
KD-087	5181979.602	591687.7128	A	WH	30	290	11.5
			B	WH	35	110	11.5
KD-089	5181989.74	591705.9193	A	WH	23	0	21
			B	WH	32	178	22
KD-090	5182001.636	591698.3677	A	WH	27	30	22
			B	WH	34	229	22
KD-097	5182190.398	591770.7434	A	WH	17	66	12
			B	WH	15	230	13
KD-146	5182482.151	591622.0365	A	SilFir	33	62	20
			B	SilFir	34	236	20
KD-147	5182485.812	591620.7051	A	WH	27	88	29
			B	WH	38	246	33
			C	WH	39	176	33
KD-148	5182487.643	591624.0336	A	WH	21	108	25
			B	WH	30	284	26
KD-149	5182500.791	591626.6964	A	WH	26	120	22
			B	WH	34	310	22
KD-150	5182558.707	591604.0626	A	WH	16.5	84	15
			B	WH	23	74	18
KD-151	5182557.042	591602.5648	A	WH	28	40	26
			B	WH	42	240	28
KD-153	5182488.309	591555.9657	B	SilFir	29	164	11

Details of Tree Samples (Locations, Sample Details, Tree Species)
(Ring Width measurements are listed in the following pages.
Ring width measurements were made with Velmex system with 1 micron precision)

Sample_ID	Y (UTM Zone 10N)	X (UTM Zone 10N)	Core ID	Tree Species*	Height of Core Above Ground (in)	Core Orientation (deg.)	Tree Diamater At Core (in)
KD-154	5182469.336	591553.6357	A	Fir	22	340	13
			B	Fir	29.5	131	29.5
KD-155	5182458.685	591547.6444	A	WH	14	309	17
			B	WH	42.5	124	17
KD-156	5182037.82	591723.6822	A	Dfir	43	4	33
			B	Dfir	44.5	180	35
KD-157	5182030.325	591729.9941	A	WH	38	288	16
			B	WH	45	118	16
KD-158	5182029.931	591721.3153	A	WH	36	308	18
			B	WH	41	115	18
KD-175	5182146.104	591599.3312	A	Dfir	37	74	78
			B	Dfir	53	261	78
KD-176	5182142.936	591582.9834	A	DFIr	42	40	60
			B	Dfir	37	180	60
KD-187	5181126.531	591075.2311	A	Dfir	29	36	40
			B	Dfir	39.5	217	40
KD-188	5181107.981	591055.7251	A	Dfir	25	NNE	27
			B	Dfir	36	SW	27
KD-195	5181280.754	591150.3475	A	Dfir	42	NNE	54
			B	Dfir	43	SSW	54

* Tree Species: Dfir = Douglas Fir, WH = Western Hemlock, SilFir = Silver Fir, Fir = Grand Fir, Ced = Western Red Cedar)

Locations are in UTM Zone 10N coordinates. Locations were precisely located (within 2 meters) using LiDAR generated Digital Canopy Models

All Samples were collected in August and September of 2011

Ring width measurements (in microns) in "Tucson Format" for all samples measured. Samples are not fully cross-dated.

KD008A	1790	707	755	760	744	660	690	651	654	560	593
KD008A	1800	613	516	556	537	521	522	398	477	702	834
KD008A	1810	870	918	962	973	935	923	852	795	628	739
KD008A	1820	471	403	389	389	720	623	547	567	627	634
KD008A	1830	430	409	345	542	547	491	547	636	547	607
KD008A	1840	455	454	681	507	448	576	688	641	436	481
KD008A	1850	557	517	397	615	568	827	606	318	289	312
KD008A	1860	247	386	382	381	371	454	599	658	647	526
KD008A	1870	619	653	582	583	519	412	322	324	391	416
KD008A	1880	420	392	541	543	310	306	343	399	390	351
KD008A	1890	439	309	306	480	471	369	328	261	266	245
KD008A	1900	511	623	701	579	360	419	660	485	564	648
KD008A	1910	393	368	474	403	526	364	369	367	403	373
KD008A	1920	313	485	491	341	383	591	391	421	427	348
KD008A	1930	359	382	338	347	243	255	255	326	253	361
KD008A	1940	392	416	221	361	315	293	461	419	334	424
KD008A	1950	477	396	370	315	414	381	101	176	209	182
KD008A	1960	111	117	163	126	76	141	87	35	66	53
KD008A	1970	31	59	80	105	104	67	79	100	95	104
KD008A	1980	68	86	121	96	112	77	38	145	247	212
KD008A	1990	441	421	209	184	372	411	525	453	575	439
KD008A	2000	335	466	564	260	434	760	666	493	367	388
KD008A	2010	528	-9999								
KD008B	1805	579	641	675	600	688					
KD008B	1810	934	885	979	835	1220	732	1062	1113	1101	1095
KD008B	1820	859	846	564	455	544	553	1037	704	518	479
KD008B	1830	835	785	562	412	679	568	639	631	702	908
KD008B	1840	856	669	705	459	321	405	545	584	536	434
KD008B	1850	541	423	338	488	233	302	378	326	406	469
KD008B	1860	622	588	732	698	762	1037	851	617	718	547
KD008B	1870	530	462	495	509	389	396	373	380	391	540
KD008B	1880	619	341	437	420	527	288	265	398	306	332
KD008B	1890	434	454	405	273	328	283	409	619	656	618
KD008B	1900	603	400	343	596	515	501	381	309	370	377
KD008B	1910	241	412	250	251	186	190	268	227	217	226
KD008B	1920	209	205	301	224	307	387	293	352	363	297
KD008B	1930	297	188	224	298	280	274	305	319	408	296
KD008B	1940	326	199	241	331	250	164	162	296	279	372
KD008B	1950	292	784	1030	797	492	339	360	216	186	233
KD008B	1960	161	148	88	106	82	104	133	122	153	169
KD008B	1970	265	175	204	163	213	224	256	201	207	307
KD008B	1980	249	255	255	339	566	457	549	527	740	734
KD008B	1990	1288	837	981	1567	1867	1872	1682	1470	1529	1858
KD008B	2000	2543	2240	2233	1717	1904	1745	1580	1169	908	862

KD008B 2010 795 -9999

KD009A 1767 220 176 139
KD009A 1770 417 657 543 458 384 221 366 477 481 396
KD009A 1780 514 998 905 923 777 540 665 281 392 306
KD009A 1790 243 339 428 501 526 549 569 424 388 432
KD009A 1800 493 372 411 434 649 700 625 782 912 1025
KD009A 1810 203 676 956 788 927 637 755 583 706 869
KD009A 1820 585 500 574 520 670 937 845 817 893 1366
KD009A 1830 1274 1322 1295 1434 1411 1339 1019 895 674 651
KD009A 1840 452 371 350 244 217 199 212 237 203 177
KD009A 1850 149 172 143 175 201 211 147 128 111 91
KD009A 1860 97 63 66 70 102 153 101 134 182 284
KD009A 1870 246 350 279 260 208 218 226 309 292 262
KD009A 1880 129 283 132 112 224 406 370 235 333 357
KD009A 1890 296 339 205 213 146 230 220 240 161 139
KD009A 1900 245 138 184 185 344 402 367 297 309 290
KD009A 1910 376 464 541 692 621 411 223 327 371 430
KD009A 1920 511 302 382 372 464 324 388 245 196 207
KD009A 1930 283 269 128 165 192 244 117 270 482 393
KD009A 1940 287 435 334 275 299 191 173 224 237 442
KD009A 1950 294 320 389 408 573 456 246 135 124 117
KD009A 1960 156 164 118 139 92 114 200 93 123 249
KD009A 1970 240 241 228 179 328 243 344 481 958 1141
KD009A 1980 784 893 935 922 453 418 398 1860 2347 2055
KD009A 1990 1859 1749 2168 2401 2155 2081 1183 1831 2418 1908
KD009A 2000 2888 2830 2327 2016 2081 2059 1590 1876 1643 1730
KD009A 2010 1521 -9999

KD009B 1746 596 692 858 988
KD009B 1750 893 562 433 314 295 294 647 520 467 1015
KD009B 1760 627 700 983 693 670 543 183 131 146 594
KD009B 1770 822 817 930 996 928 536 436 203 209 260
KD009B 1780 195 133 216 495 462 415 249 314 230 352
KD009B 1790 513 487 425 477 686 684 720 599 454 535
KD009B 1800 211 245 161 151 251 283 336 451 418 526
KD009B 1810 384 562 672 764 618 631 709 992 894 565
KD009B 1820 566 697 793 291 464 679 732 1276 1215 1396
KD009B 1830 1273 1188 1046 780 562 764 571 703 707 710
KD009B 1840 569 650 852 613 455 561 554 602 457 506
KD009B 1850 410 355 167 79 95 87 39 44 47 41
KD009B 1860 73 40 23 66 176 94 22 65 59 56
KD009B 1870 88 126 50 123 94 76 60 118 91 100
KD009B 1880 94 110 131 117 133 229 266 260 153 190
KD009B 1890 115 93 78 44 68 28 64 49 75 39
KD009B 1900 153 160 169 157 233 470 532 475 404 372
KD009B 1910 470 514 427 418 611 508 204 233 410 435
KD009B 1920 522 253 376 367 373 228 216 164 142 121
KD009B 1930 193 258 241 232 328 348 271 385 462 365
KD009B 1940 284 308 266 169 269 260 285 416 481 780

```
KD009B 1950  850 1231 1303  975  773  685  420  338  329  293
KD009B 1960  369  275  258  195  208  270  205  227  290  358
KD009B 1970  379  519  467  323  120  135  178  311  334  370
KD009B 1980  524  829  846 1099  631  483  308  507  664  890
KD009B 1990 1244 2082 2052 1312 1466 1487 1557 1377 2512 1806
KD009B 2000 1984 1322 1577  998  900  888  765 1219 1200 1520
KD009B 2010  321 -9999

KD010A 1727  709  955 1238
KD010A 1730 1027 1158  986  731  956  819  921  943  752  873
KD010A 1740  837  854  923  821 1063  762 1263  872  592  695
KD010A 1750  718  489  553  558  600  612  418  546  435  698
KD010A 1760  532  429  476  419  404  433  437  420  565  422
KD010A 1770  564  561  430  430  408  412  501  485  327  410
KD010A 1780  430  458  442  494  380  540  486  504  372  531
KD010A 1790  225  393  404  324  438  417  422  459  467  388
KD010A 1800  151  404  516  499  370  360  317  273  399  167
KD010A 1810  294  142  269  281  182  169   49  205  272  248
KD010A 1820  156  152  237  271  200  149  168  157  198  193
KD010A 1830  221  182  158  130  166  222  264  206  236  232
KD010A 1840  309  209  211  224  297  226  244  187  191  441
KD010A 1850  188  268  372  291  362  309  296  228  286  275
KD010A 1860  181  354  215  260  401  247  265  187  216  183
KD010A 1870  223   88  267  171  136  178  173  161  258  241
KD010A 1880  270  255  205  203  206  237  234  177  207  188
KD010A 1890  156  145  164  189  183  354  263  300  414  131
KD010A 1900  216  220  220  194  274  147  233  144  147  124
KD010A 1910  189  243  196  179  248  190   62  166  217  198
KD010A 1920  217   84  160  151  159  138  117  109  149   66
KD010A 1930  103   86   59  140  157  242  191  205  198  151
KD010A 1940  130  182  163  172  259  253  303  302  117  166
KD010A 1950  204  208  219  292  215  208  252  280  298  244
KD010A 1960  214  265  170   71  121  202  200  212  279  187
KD010A 1970  276  265  285  291  256  310  309  370  369  454
KD010A 1980  384  449  362  245  661  813  735  744  885  667
KD010A 1990  884  475  867  811 1233  834  766  611  730  517
KD010A 2000  680  751  678  739  674  566  572  670  491  643
KD010A 2010  546 -9999

KD010B 1711  564  513  569  587 1648 1386 1874 1526 1877
KD010B 1720 1126 1067 1256 1257 1281 1291  783  990 1591 1148
KD010B 1730 1172  790  794 1023 1124 1334 1252  939  990  644
KD010B 1740  685  826 1092 1218  586  836  502  334  417  440
KD010B 1750  450  474  379  404  293  347  947  646  540  531
KD010B 1760  326  288  250  342  323  375  372  403  464  394
KD010B 1770  388  367  371  385  534  453  411  552  586  609
KD010B 1780  587  612  441  618  621  527  467  616  532  538
KD010B 1790  521  490  605  583  503  665  673  620  598  760
KD010B 1800  772  781  524  585  623  592  610  414  552  463
KD010B 1810  696  313  348  278  297  204  410  406  467  306
```

KD010B	1820	312	466	440	251	204	223	168	196	197	175
KD010B	1830	232	210	198	216	242	247	292	267	437	363
KD010B	1840	319	324	351	485	408	440	437	485	639	309
KD010B	1850	382	512	401	586	515	473	282	375	459	360
KD010B	1860	572	489	519	756	680	601	459	452	441	270
KD010B	1870	228	185	247	240	418	389	487	456	518	398
KD010B	1880	209	723	508	701	469	511	449	452	664	678
KD010B	1890	317	415	446	536	730	829	666	776	824	375
KD010B	1900	918	751	690	729	713	845	716	409	429	400
KD010B	1910	674	648	556	608	664	692	383	342	392	424
KD010B	1920	380	337	348	470	461	452	323	282	256	158
KD010B	1930	158	207	179	221	220	280	369	406	467	359
KD010B	1940	254	317	442	428	589	553	788	898	1013	1275
KD010B	1950	1169	1064	786	531	366	294	529	662	512	525
KD010B	1960	408	396	382	456	326	357	429	708	750	786
KD010B	1970	788	922	1081	1490	642	880	912	865	1155	1264
KD010B	1980	1409	1317	1037	1662	1610	1342	1029	877	987	1148
KD010B	1990	1384	1090	1310	1220	1521	1305	1384	1199	1167	1110
KD010B	2000	1463	1759	1269	1212	1400	1400	1014	972	944	1155
KD010B	2010	1189	-9999								
KD011A	1686	1117	969	847	666						
KD011A	1690	1625	1249	1072	674	761	850	1405	1200	925	744
KD011A	1700	1302	1526	1733	1339	996	544	657	548	559	629
KD011A	1710	571	812	573	785	1035	1175	1034	1138	1094	1332
KD011A	1720	1125	1415	1122	1278	1199	1651	1470	1694	1585	1245
KD011A	1730	1204	1298	1253	1214	1485	1964	1629	1544	1680	1191
KD011A	1740	1143	905	914	875	937	964	956	911	880	1104
KD011A	1750	1124	958	648	401	387	559	612	743	751	757
KD011A	1760	935	920	452	364	302	621	524	626	694	467
KD011A	1770	423	316	406	401	497	873	675	761	772	965
KD011A	1780	884	911	1022	1073	671	655	885	871	788	1026
KD011A	1790	815	785	596	649	547	660	379	656	684	529
KD011A	1800	664	536	431	510	405	463	319	462	477	491
KD011A	1810	278	499	392	415	385	183	343	162	559	278
KD011A	1820	274	589	187	377	458	329	129	86	317	358
KD011A	1830	210	385	546	222	556	622	702	684	710	619
KD011A	1840	608	608	552	398	311	342	530	321	450	460
KD011A	1850	555	619	804	684	338	686	400	703	825	565
KD011A	1860	454	495	437	425	458	440	405	692	389	362
KD011A	1870	463	458	451	534	485	708	482	553	653	801
KD011A	1880	704	572	481	364	416	464	381	667	336	341
KD011A	1890	632	731	660	563	599	395	348	396	490	671
KD011A	1900	611	742	485	656	742	217	509	602	543	658
KD011A	1910	981	543	362	308	299	217	405	369	312	473
KD011A	1920	477	311	100	382	617	544	435	165	373	390
KD011A	1930	432	363	326	249	347	295	236	303	299	528
KD011A	1940	391	281	194	285	368	401	323	369	282	376
KD011A	1950	450	587	573	557	400	400	673	630	290	209
KD011A	1960	114	115	279	293	293	239	366	251	217	205

```
KD011A 1970  166  354  379  358  390  337  691  674  982  502
KD011A 1980  336  323  237  311  243  194  145  156  226  137
KD011A 1990   93  116  147  204  111  104  180  110   72   31
KD011A 2000  100   30   47   94  172  236  118  166  238  138
KD011A 2010   95 -9999

KD011B 1711  184  134  231  321  456  609  501  332  268
KD011B 1720  233  328  247  277  315  372  294  382  417  310
KD011B 1730  299  575  513  455  464  348  627  711  828  537
KD011B 1740  450  856 1242  700  714  516  451  503  452  408
KD011B 1750  212  213  273  373  156  135  100  379  294  323
KD011B 1760  446  179  232  219  245  323  444  429  485  613
KD011B 1770  496  525  428  581  593  778  365  507  464  495
KD011B 1780  448  574  443  626  628  566  478  630  299  864
KD011B 1790  896  416  608  515  306  262  269  376  187  689
KD011B 1800  834  329  152  251  384  364  189  164  271  112
KD011B 1810  272  242  195  152  231  166  278  395  320  124
KD011B 1820  163  306  224  113  202  322  183  188   64   91
KD011B 1830  116   97  144  118  145  244  186  167  264  243
KD011B 1840  287  462  495  420  663  419  376  604  953  478
KD011B 1850  593  760  460  388  430  481  282  652  417  574
KD011B 1860  944  440  364  537  470  401  307  225  419  266
KD011B 1870  350  355  506  330  864  573  392  398  451  439
KD011B 1880  117  536  343  266  377  442  461  280  531  550
KD011B 1890  404  592  480  719  595 1220  852  892  940  268
KD011B 1900  666  668  457  463 1043  759  406  365  240  214
KD011B 1910  265  404  304  532  713  458  613  988  704  563
KD011B 1920  581  119  299  337  356  323  421  338  566  564
KD011B 1930  479  681  515  517  422  440  454  932  554  533
KD011B 1940  479  704  417  555  529  582  300  341  501  795
KD011B 1950 1052  855  554  161  119  231  346  681  370  250
KD011B 1960  320  232  228  497  668  886  527  648  712  363
KD011B 1970  781  671  933  535  248  369  272  330  407  403
KD011B 1980  299  250  420  475  313  224  178   83  170  155
KD011B 1990  238  252  345  332  541  428  164  162  262  244
KD011B 2000  248  255  341  302  271  476  374  454  664  942
KD011B 2010  884 -9999

KD024A 1848 1456 2127
KD024A 1850 2742 2920 2463 2173 1667 1860 1771 1390 1890 1189
KD024A 1860 1552 1380 1295 1488 1376 1378 1475 1420 1578 1509
KD024A 1870 1679 1687 1582 1765 1696 1731 1398 1120 1316 1301
KD024A 1880 1453 1827 2035 1733 1425 1555 1279 1463 1366 1458
KD024A 1890 1488 1747 1875 1697 1805 1499 1703 1634 1736 1809
KD024A 1900 1873 2029 2493 2555 2069 2263 2346 2476 2207 2394
KD024A 1910 2268 2301 2556 3025 3253 2623 2568 2173 2888 2144
KD024A 1920 2204 1985 1754 2509 3027 2225 2627 3814 3561 4368
KD024A 1930 3228 2646 2959 2414 2560 2861 1751  864  868  887
KD024A 1940 1030  788  797  717  757  755 1021  720 1018  987
KD024A 1950  808  660  792  950  708  727  588  344  581  399
```

KD024A 1960 506 471 544 570 233 168 172 186 188 249
KD024A 1970 229 239 248 80 179 35 180 166 206 109
KD024A 1980 209 184 71 40 237 150 185 98 226 208
KD024A 1990 70 15 57 63 53 103 82 124 41 97
KD024A 2000 136 63 119 46 137 137 106 52 131 179
KD024A 2010 94 -9999

KD024B 1856 3150 2772 2610 2836
KD024B 1860 4338 3202 1655 2907 2554 1664 1606 1471 1566 1367
KD024B 1870 1545 2047 2996 1496 1581 1676 1398 1324 1158 1024
KD024B 1880 1169 1298 1328 1210 991 915 1145 966 1270 1012
KD024B 1890 998 1186 1305 1535 1435 1262 1088 1167 1122 1027
KD024B 1900 1465 1409 1262 1042 1139 736 731 621 843 626
KD024B 1910 615 609 582 744 679 525 563 739 401 590
KD024B 1920 795 570 589 550 461 654 733 624 938 920
KD024B 1930 1027 1060 2194 2552 4030 4513 4630 3451 4205 4022
KD024B 1940 3467 3585 3859 3614 3716 3449 2294 3188 2744 1978
KD024B 1950 1858 1027 650 723 755 853 633 573 857 427
KD024B 1960 332 408 372 563 718 815 838 676 580 959
KD024B 1970 689 756 670 694 408 598 833 812 1047 1231
KD024B 1980 718 750 580 552 691 700 542 687 489 346
KD024B 1990 560 706 605 522 1005 548 656 520 706 392
KD024B 2000 705 853 699 339 303 312 358 303 313 382
KD024B 2010 276 -9999

KD026A 1888 919 1075
KD026A 1890 1023 1134 1353 1401 1295 1446 1061 1219 1568 1311
KD026A 1900 1669 1609 1628 1691 1938 2057 1800 1694 1764 1840
KD026A 1910 1736 1499 1964 1968 2116 2007 1711 1506 1035 1409
KD026A 1920 1270 1175 866 944 1131 1165 1275 996 1445 1279
KD026A 1930 1337 1671 1449 1452 1993 1716 1507 1459 1492 1513
KD026A 1940 1807 1938 2412 1994 1788 1502 1948 2094 1798 1654
KD026A 1950 1752 1476 1462 1172 1863 2032 1487 1649 1835 1463
KD026A 1960 1579 1396 1595 1982 1740 1455 1652 2077 2252 1742
KD026A 1970 2123 1561 2122 1928 1486 1470 1654 1805 2040 1720
KD026A 1980 1770 2298 1935 2287 1805 1160 1266 1267 1667 1477
KD026A 1990 1671 1242 1800 1204 1458 1089 1486 1446 1715 1565
KD026A 2000 1426 1321 1408 1047 1336 1575 1816 1110 1363 1290
KD026A 2010 1855 -9999

KD026B 1873 1459 1497 1217 952 1021 967 989
KD026B 1880 821 1002 991 776 819 908 783 699 1143 1363
KD026B 1890 1048 1747 1969 1853 1713 1794 1230 1411 1464 1075
KD026B 1900 1066 1173 1321 1644 1895 1521 1458 685 705 685
KD026B 1910 689 716 678 838 955 1032 1168 1519 1110 1459
KD026B 1920 1217 1105 827 935 1142 1021 973 844 1028 1434
KD026B 1930 1292 1246 1263 850 1216 1209 860 1035 1178 1402
KD026B 1940 1610 905 798 712 1115 1042 1639 2205 1746 1619
KD026B 1950 1650 1551 1417 1199 1338 1468 1185 889 1367 990
KD026B 1960 1083 1103 1370 1323 1519 1151 1076 1013 1128 1142

```
KD026B  1970  1244   844  1103  1190  1011   957  1239  1280  1357  1450
KD026B  1980  1515  1991  1327  1846  1856   811   742   855  1352  1152
KD026B  1990  1653  1261  1124  1161  1392  1076   893   880  1392  1213
KD026B  2000  1188  1088  1238   877   977  1427  1300   886  1162  1198
KD026B  2010  1399 -9999

KD029A  1870  1277   892   923   386   554   539   798   761   621   389
KD029A  1880   545   481   386   429   432   415   361   576   440   544
KD029A  1890   639   585   543   579   762   427   613   901   725   882
KD029A  1900   717   742   718   719   745   855   743   795   786   762
KD029A  1910   681   787  1040   989   718   645   614   612   754   989
KD029A  1920  1184  1005   957   828   820   918   832   910   723   876
KD029A  1930   781   674   720   597   668   521   457   377   465   163
KD029A  1940   114   386   334   395   637   680   729   880   815   555
KD029A  1950   524   646   561   687   871   928   955   832   595   579
KD029A  1960   589   537   558   453   460   428   508   409   745   509
KD029A  1970   507   489   459   450   497   353   351   340   436   467
KD029A  1980   408   381   414   469   517   479   476   560   453   545
KD029A  1990   645   595   607   596   709   666   773   773   724   870
KD029A  2000   927  1002   966   882   920   680   996   705   935  1021
KD029A  2010  1116 -9999

KD-029B 1812   941   951   772   813   722   763   678   667
KD-029B 1820   699  1155  1633  1137  1124   851   943   744   611   512
KD-029B 1830   560   314   180   132   182   207   223   200   228   244
KD-029B 1840   233   254   219   207   200   207   192   180   158   166
KD-029B 1850   124   125   218   250   203   257   310   250   244   241
KD-029B 1860   204   152   146    81   167   247   186   133    53    79
KD-029B 1870   101    90    86    92    84   111   140   102    94   121
KD-029B 1880   134   156   132   157   136   148   158   137    95   117
KD-029B 1890   186   163   190   177   221   251   176   177   209   217
KD-029B 1900   292   269   232   217   203   180   209   155   159   156
KD-029B 1910   163   186   231   176   192   228   185   209   208   278
KD-029B 1920   242   245   197   210   214   252   186   191   240   213
KD-029B 1930   255   220   237   220   284   214   244   210   170   271
KD-029B 1940   208   198   229   257   222   183   224   245   304   243
KD-029B 1950   269   301   307   291   324   332   261   205   238   155
KD-029B 1960   163   154   126   201   152   170   145   121   204   175
KD-029B 1970   244   274   255   203   214   195   274   245   290   294
KD-029B 1980   342   458   365   312   555   386   402   583   509   497
KD-029B 1990   594   555   470   517   647   625   764   757   832   851
KD-029B 2000   941   974   995   796  1046   980  1082  1025   960   984
KD-029B 2010  1025 -9999

KD029C  1796  1732  1249   948   136
KD029C  1800   335   532   754  1295  1095   948  1182  1496  1288   998
KD029C  1810   878   510   538   589   595   566   521   541   396   373
KD029C  1820   350   339   355   291   270   395   461   388   462   485
KD029C  1830   547   489   817   629   569   558   681   724   789  1011
KD029C  1840  1033  1252  1247  1306  1441  1124   861  1318   776   688
```

KD029C 1850 593 599 714 899 1022 899 1177 1126 1133 2508
KD029C 1860 1228 1023 962 888 755 1218 1186 1061 1012 822
KD029C 1870 853 1201 1331 1205 1163 1114 1003 1249 803 1028
KD029C 1880 517 825 581 661 836 985 1011 793 964 1243
KD029C 1890 940 1585 1364 1061 1128 1025 1128 1413 1250 890
KD029C 1900 1256 1310 1131 1056 1197 1136 1256 1107 1060 1135
KD029C 1910 1149 973 1361 1320 1550 1113 1219 1175 1130 1308
KD029C 1920 1366 1490 1294 1372 1173 1327 1219 903 1163 701
KD029C 1930 670 643 647 870 881 1076 804 1022 1430 1360
KD029C 1940 920 1437 1110 915 903 608 1068 942 836 609
KD029C 1950 589 754 620 511 758 562 500 387 558 518
KD029C 1960 783 843 679 608 687 956 803 656 835 740
KD029C 1970 957 689 639 860 949 535 677 492 432 407
KD029C 1980 439 510 518 470 722 546 528 561 641 636
KD029C 1990 743 789 680 686 662 736 796 942 903 752
KD029C 2000 670 928 926 764 982 1042 1286 975 1048 1045
KD029C 2010 963 -9999

KD-033A 1812 2193 1926 1984 1718 2047 1805 1431 1460
KD-033A 1820 1429 2791 2557 1600 1885 2484 1945 1597 1674 1483
KD-033A 1830 1475 1873 1889 1943 2124 1556 2206 2307 2281 2644
KD-033A 1840 1961 1950 1931 2100 1795 2062 2156 1999 2492 1598
KD-033A 1850 1439 1638 1307 1171 1200 1130 1219 1188 1508 1520
KD-033A 1860 1945 1670 1436 1372 1378 1178 571 733 940 1006
KD-033A 1870 1338 2103 2769 2486 2939 2388 1970 2203 2216 2059
KD-033A 1880 1748 2168 2290 2653 2638 2503 2804 2332 2083 2150
KD-033A 1890 2180 2458 2408 2213 2314 2333 2234 2156 2161 1798
KD-033A 1900 2371 1859 1652 1860 1988 1894 1586 1755 1489 1840
KD-033A 1910 1910 1661 1883 1633 1532 1256 1157 1123 1224 1599
KD-033A 1920 1606 1833 1624 1621 1330 1339 1221 978 1224 1030
KD-033A 1930 1108 858 623 682 842 925 1054 1091 1134 1508
KD-033A 1940 1131 1585 1121 1066 1058 1417 1361 1139 1204 1210
KD-033A 1950 1153 1336 946 965 1094 1142 977 847 824 532
KD-033A 1960 552 508 448 377 820 753 734 880 678 691
KD-033A 1970 748 670 822 689 442 644 509 571 498 460
KD-033A 1980 458 418 386 308 459 468 361 451 501 323
KD-033A 1990 467 250 288 353 505 339 436 422 508 426
KD-033A 2000 763 722 580 658 483 379 666 567 791 831
KD-033A 2010 526 -9999

KD033B 1859 849
KD033B 1860 915 632 882 252 312 254 302 279 205 263
KD033B 1870 290 193 238 198 206 271 280 260 253 275
KD033B 1880 248 274 230 268 295 372 566 451 459 446
KD033B 1890 505 495 522 477 370 418 373 447 390 482
KD033B 1900 458 558 716 696 776 1012 858 594 530 650
KD033B 1910 785 845 839 790 731 760 826 742 730 829
KD033B 1920 596 956 938 891 1039 890 1023 827 786 1091
KD033B 1930 1118 1479 1420 1826 1132 1429 1134 963 724 712
KD033B 1940 948 768 1061 965 1112 855 855 1062 1044 1061

KD033B 1950 1083 888 892 759 695 1118 1360 1179 924 987
KD033B 1960 744 805 701 707 807 788 890 1064 1183 1019
KD033B 1970 992 521 509 798 956 671 884 769 811 478
KD033B 1980 836 759 1195 806 863 956 980 304 693 554
KD033B 1990 408 661 784 735 629 917 774 581 540 686
KD033B 2000 614 822 745 732 535 755 686 634 902 833
KD033B 2010 921 -9999

KD033C 1826 1813 1613 1858 1851
KD033C 1830 1825 1888 1886 1666 1877 1460 1531 1451 1385 1521
KD033C 1840 1239 1190 1051 942 1011 1022 975 742 788 477
KD033C 1850 661 794 666 545 576 499 571 570 549 489
KD033C 1860 562 509 502 623 485 412 267 228 217 309
KD033C 1870 472 486 691 835 888 869 777 979 887 800
KD033C 1880 517 529 566 782 919 942 935 867 959 825
KD033C 1890 958 1050 793 745 920 1029 805 1038 965 763
KD033C 1900 1214 1027 1063 935 815 815 1010 1061 905 897
KD033C 1910 940 897 907 961 794 624 610 619 563 961
KD033C 1920 887 966 778 878 676 799 881 1055 1068 986
KD033C 1930 907 897 978 937 692 725 551 593 600 913
KD033C 1940 841 1115 910 1050 1005 720 1056 1056 983 1073
KD033C 1950 1008 763 630 748 964 963 873 677 783 574
KD033C 1960 552 554 527 655 1158 1162 1089 1097 689 513
KD033C 1970 457 660 893 938 451 825 858 718 491 621
KD033C 1980 609 801 713 689 829 758 632 916 852 523
KD033C 1990 961 753 669 634 1077 759 650 736 803 634
KD033C 2000 850 626 732 533 732 820 779 867 910 1369
KD033C 2010 688 -9999

KD036B 1842 1215 1020 838 977 1143 1001 1038 795
KD036B 1850 983 1235 839 884 723 724 664 594 919 1325
KD036B 1860 1702 1462 1415 1168 1031 811 690 935 1116 942
KD036B 1870 857 1046 917 1160 1358 1186 1083 939 669 1021
KD036B 1880 1029 1165 1247 811 558 746 625 677 882 724
KD036B 1890 636 871 959 1221 961 779 569 721 734 680
KD036B 1900 788 888 673 922 793 687 802 740 774 682
KD036B 1910 906 820 690 973 965 867 1266 694 260 480
KD036B 1920 425 433 287 344 312 335 466 470 587 578
KD036B 1930 585 900 837 730 560 506 382 334 470 556
KD036B 1940 577 1196 972 916 1587 1043 1110 1887 1510 1757
KD036B 1950 2822 2916 2835 2231 2232 1798 1748 2915 2265 1176
KD036B 1960 1790 1134 1414 1171 1180 877 898 928 980 770
KD036B 1970 959 737 858 904 1305 1221 2799 3083 3487 722
KD036B 1980 2287 1537 1058 1989 1625 495 814 974 1278 75
KD036B 1990 762 283 315 1387 2848 4542 3790 1521 3101 3044
KD036B 2000 3129 2292 2094 1187 1407 1710 1669 821 1532 844
KD036B 2010 1253 -9999

KD-036D 1824 711 1016 869 769 854 931
KD-036D 1830 853 840 706 736 737 621 685 792 808 823

KD-036D	1840	881	1133	1118	971	1032	1381	1118	935	954	719
KD-036D	1850	837	1219	916	991	860	822	872	956	432	1004
KD-036D	1860	1214	1236	1137	1081	938	868	776	851	716	525
KD-036D	1870	441	473	607	563	844	708	440	378	325	576
KD-036D	1880	607	683	1035	611	449	469	701	751	815	536
KD-036D	1890	570	738	1134	1144	1156	865	737	783	776	663
KD-036D	1900	735	799	576	748	947	800	810	560	456	428
KD-036D	1910	535	677	664	835	609	775	719	483	271	332
KD-036D	1920	265	224	266	321	283	232	279	191	527	507
KD-036D	1930	655	783	756	805	717	737	577	506	751	983
KD-036D	1940	780	815	869	1019	1114	560	803	1156	1125	1122
KD-036D	1950	1376	1480	1606	1210	1272	1242	1078	1344	1567	1038
KD-036D	1960	2947	3149	5508	7424	6282	5388	6077	4051	3693	3889
KD-036D	1970	3228	2097	4277	3077	1898	2311	2768	3134	3896	2698
KD-036D	1980	5583	5086	3527	5899	5025	1785	2335	2261	3123	602
KD-036D	1990	2076	1887	5481	5045	4918	6173	6536	3868	5577	3772
KD-036D	2000	4432	4303	4286	3208	7098	8423	6465	2550	2685	3565
KD-036D	2010	3422	-9999								

KD084A	1684	864	963	653	467	154	236				
KD084A	1690	270	363	606	810	621	753	566	609	599	619
KD084A	1700	651	586	822	710	940	1043	892	769	1094	1541
KD084A	1710	1819	1244	1316	1157	1030	806	870	593	520	508
KD084A	1720	431	533	533	475	351	505	610	496	634	540
KD084A	1730	600	829	842	802	755	653	788	655	739	561
KD084A	1740	971	985	789	645	454	418	467	444	355	346
KD084A	1750	307	430	405	327	378	429	407	454	395	410
KD084A	1760	295	373	360	345	401	543	540	411	382	431
KD084A	1770	703	586	650	628	624	606	616	580	574	480
KD084A	1780	443	616	579	488	446	406	493	405	587	537
KD084A	1790	555	559	373	391	467	559	545	401	333	287
KD084A	1800	345	388	469	418	427	392	461	417	307	511
KD084A	1810	222	595	553	504	417	297	429	366	294	196
KD084A	1820	173	365	301	291	201	178	208	317	445	480
KD084A	1830	426	386	436	277	379	443	310	232	341	370
KD084A	1840	605	520	538	509	507	427	420	346	379	320
KD084A	1850	418	462	307	343	348	234	371	508	498	389
KD084A	1860	453	351	268	311	238	247	267	244	264	214
KD084A	1870	241	285	310	179	224	229	153	239	284	274
KD084A	1880	149	365	293	448	420	324	284	273	308	264
KD084A	1890	359	360	367	371	450	453	484	447	557	319
KD084A	1900	407	609	751	790	889	770	734	669	693	740
KD084A	1910	819	687	697	725	739	575	469	586	478	437
KD084A	1920	538	615	471	561	570	488	467	529	594	535
KD084A	1930	795	583	625	649	979	897	396	298	307	333
KD084A	1940	308	600	458	519	741	690	822	631	991	922
KD084A	1950	1135	1224	880	810	841	778	756	991	1132	767
KD084A	1960	884	862	876	935	972	1326	1203	1294	1200	1029
KD084A	1970	1214	824	916	679	650	836	860	817	846	837
KD084A	1980	794	946	1027	1060	684	613	593	554	703	638

KD084A 1990 860 946 849 766 1121 1242 884 1102 1159 1161
KD084A 2000 1275 1375 1299 991 1560 1976 1380 1198 1415 1419
KD084A 2010 1425 -9999

KD084B 1671 1026 963 802 990 1528 845 1353 947 1133
KD084B 1680 572 589 649 712 1971 1061 898 1233 1027 550
KD084B 1690 543 730 840 671 1031 980 596 751 696 1378
KD084B 1700 1582 1265 1010 1148 1698 1225 1034 1220 1651 2117
KD084B 1710 1632 1227 1235 1830 2458 2121 1642 983 871 970
KD084B 1720 816 949 771 693 786 646 828 439 527 702
KD084B 1730 1086 1071 762 684 853 873 770 809 699 739
KD084B 1740 720 719 850 993 895 668 872 904 789 794
KD084B 1750 671 783 748 731 870 959 893 732 620 691
KD084B 1760 605 686 649 662 402 455 385 355 367 350
KD084B 1770 387 328 399 410 332 351 405 527 571 475
KD084B 1780 388 407 438 324 293 300 302 290 337 286
KD084B 1790 418 404 436 511 607 547 332 383 431 357
KD084B 1800 420 388 534 412 427 411 419 420 268 220
KD084B 1810 176 413 447 373 321 199 314 295 275 280
KD084B 1820 153 258 264 317 211 252 258 328 463 443
KD084B 1830 443 440 496 405 400 394 324 327 432 388
KD084B 1840 469 399 452 375 460 352 265 242 345 214
KD084B 1850 314 315 233 238 271 265 76 54 46 33
KD084B 1860 138 210 394 546 489 421 442 375 322 273
KD084B 1870 327 494 446 387 369 271 210 206 259 331
KD084B 1880 167 283 440 408 364 336 258 281 306 274
KD084B 1890 337 394 340 561 493 573 511 601 522 504
KD084B 1900 634 497 490 574 624 680 555 492 391 567
KD084B 1910 532 608 750 670 725 538 326 529 302 197
KD084B 1920 621 612 536 486 637 599 609 630 689 690
KD084B 1930 721 600 519 925 884 796 720 546 511 674
KD084B 1940 694 828 699 846 815 681 887 1100 1076 962
KD084B 1950 1450 1763 936 706 647 545 596 667 903 606
KD084B 1960 729 842 978 1081 958 1114 1040 1297 1481 1384
KD084B 1970 1092 955 909 609 568 785 665 556 699 751
KD084B 1980 777 1059 853 1129 523 546 476 532 495 410
KD084B 1990 651 539 700 607 1047 917 702 979 1072 848
KD084B 2000 765 798 816 709 971 1333 1031 932 1141 1108
KD084B 2010 1361 -9999

KD085A 1742 733 719 763 827 990 956 1198 1290
KD085A 1750 1203 1081 925 939 734 756 762 866 528 364
KD085A 1760 374 488 357 520 459 568 657 494 564 456
KD085A 1770 572 513 522 497 413 605 477 460 472 513
KD085A 1780 476 596 639 559 500 461 310 517 576 529
KD085A 1790 382 573 265 407 460 295 463 549 522 652
KD085A 1800 655 740 721 548 516 626 336 459 490 545
KD085A 1810 533 405 397 323 429 151 323 334 278 730
KD085A 1820 523 628 610 591 383 408 453 465 350 327
KD085A 1830 419 536 499 561 519 472 442 428 461 551

KD085A	1840	444	464	481	325	374	427	406	342	439	317
KD085A	1850	494	487	407	490	413	460	563	542	503	468
KD085A	1860	422	355	317	448	321	578	379	332	411	392
KD085A	1870	395	283	440	600	434	400	451	461	394	491
KD085A	1880	426	254	414	291	392	111	359	250	319	419
KD085A	1890	420	418	246	349	290	272	319	181	258	201
KD085A	1900	353	301	376	442	174	411	360	410	313	660
KD085A	1910	653	470	506	302	262	486	444	390	222	401
KD085A	1920	377	205	277	617	520	500	295	477	420	583
KD085A	1930	400	479	356	400	260	467	355	244	258	353
KD085A	1940	289	202	250	400	332	362	369	349	304	382
KD085A	1950	347	346	438	418	472	551	505	447	526	436
KD085A	1960	436	216	273	374	216	275	177	273	229	106
KD085A	1970	175	247	196	144	116	183	143	134	136	40
KD085A	1980	135	84	55	68	77	77	68	109	67	86
KD085A	1990	68	84	105	171	123	274	389	316	495	736
KD085A	2000	392	593	602	545	488	609	534	373	413	221
KD085A	2010	270	-9999								

KD085B	1672	542	605	511	618	1366	535	646	686		
KD085B	1680	643	607	650	411	218	627	607	529	580	538
KD085B	1690	659	225	609	883	464	432	745	277	327	576
KD085B	1700	758	473	473	402	206	544	597	560	397	301
KD085B	1710	249	322	377	459	147	189	197	101	120	143
KD085B	1720	144	70	74	59	50	70	100	59	156	168
KD085B	1730	206	182	277	172	218	257	274	274	282	220
KD085B	1740	286	353	243	132	236	220	228	337	376	268
KD085B	1750	335	253	319	312	362	527	330	449	468	406
KD085B	1760	436	348	533	677	934	901	712	593	551	482
KD085B	1770	496	517	346	309	360	319	295	422	348	356
KD085B	1780	327	286	333	214	305	355	316	221	293	402
KD085B	1790	365	295	274	307	219	257	332	329	208	229
KD085B	1800	143	343	311	298	214	402	194	332	261	172
KD085B	1810	260	298	272	324	430	425	354	230	238	322
KD085B	1820	167	205	270	318	318	263	248	242	317	124
KD085B	1830	211	266	197	399	253	358	316	313	230	219
KD085B	1840	395	377	295	349	254	215	192	304	284	245
KD085B	1850	232	203	220	246	250	244	223	179	185	209
KD085B	1860	214	203	275	216	304	300	247	351	258	285
KD085B	1870	408	366	286	315	286	264	227	269	159	307
KD085B	1880	145	172	236	224	251	173	208	306	241	319
KD085B	1890	176	242	201	210	284	262	199	202	173	242
KD085B	1900	64	291	130	173	203	276	241	126	229	182
KD085B	1910	145	183	87	143	133	302	156	151	150	75
KD085B	1920	156	159	231	148	208	276	257	252	234	262
KD085B	1930	343	293	222	141	261	235	124	119	291	285
KD085B	1940	429	191	274	248	325	275	306	222	256	168
KD085B	1950	244	208	146	151	172	246	195	229	294	189
KD085B	1960	276	186	169	163	178	167	150	201	174	225
KD085B	1970	243	195	173	195	145	178	112	128	167	65

KD085B 1980 100 53 57 75 52 57 65 34 44 73
KD085B 1990 149 114 116 61 51 44 20 19 27 32
KD085B 2000 48 56 52 59 82 58 53 83 63 56
KD085B 2010 64 -9999

KD086A 1724 1534 1445 1762 1676 2099 1661
KD086A 1730 1458 1715 1462 1603 1376 1464 1807 1794 1437 1554
KD086A 1740 2244 2376 2557 2261 1236 1227 1577 1254 1272 1384
KD086A 1750 1241 1125 917 1139 1184 1229 1254 1048 1353 1004
KD086A 1760 1009 1190 1115 1209 1216 1266 1302 1435 1605 1547
KD086A 1770 1447 1209 1711 1449 1308 1301 1264 1130 1187 1064
KD086A 1780 1197 1023 935 1140 1189 1029 1151 1103 1264 1070
KD086A 1790 897 980 1269 1178 1590 1363 1522 1374 1044 814
KD086A 1800 712 998 1433 1563 1192 1155 1144 833 574 887
KD086A 1810 294 711 710 614 645 456 717 670 504 379
KD086A 1820 267 775 767 558 629 717 815 918 1346 1129
KD086A 1830 1049 1119 1185 1059 1060 803 896 1262 1321 1145
KD086A 1840 874 1068 1376 1213 994 1220 1245 1253 1053 785
KD086A 1850 920 980 714 1140 1205 1009 937 1001 939 745
KD086A 1860 1071 709 807 873 713 497 570 617 745 542
KD086A 1870 478 555 641 558 520 425 251 285 305 383
KD086A 1880 80 635 480 509 443 500 559 403 536 469
KD086A 1890 477 615 706 958 911 884 461 799 752 410
KD086A 1900 891 798 774 699 724 639 661 627 534 449
KD086A 1910 615 631 640 559 636 635 569 805 930 894
KD086A 1920 749 754 691 626 596 561 605 465 512 545
KD086A 1930 485 1167 1288 1279 1299 781 584 938 750 941
KD086A 1940 832 628 475 382 337 395 356 532 495 564
KD086A 1950 649 588 534 413 372 431 692 1381 1240 836
KD086A 1960 732 793 781 1075 1109 1167 929 927 737 621
KD086A 1970 1012 996 1298 1367 925 997 862 1203 1561 1725
KD086A 1980 1276 1127 861 1210 1071 607 509 878 1086 998
KD086A 1990 1137 669 543 573 989 1139 1071 635 2043 1847
KD086A 2000 2285 2414 2081 1447 1343 1775 1429 1066 718 1052
KD086A 2010 1123 -9999

KD086B 1745 1800 3120 2577 2909 2712
KD086B 1750 2447 2709 2887 3988 1798 1561 1633 765 1309 886
KD086B 1760 1098 1388 1265 1167 1033 1163 1151 1309 1428 1278
KD086B 1770 1308 1298 1479 1409 1112 983 1048 1176 1081 1340
KD086B 1780 1400 971 951 994 1069 1148 1214 860 991 904
KD086B 1790 961 1108 1073 879 1065 1097 1201 1124 1079 798
KD086B 1800 606 666 765 690 612 848 881 581 390 713
KD086B 1810 230 536 536 417 482 450 636 484 314 221
KD086B 1820 142 541 610 458 496 663 611 583 832 611
KD086B 1830 788 746 737 724 895 536 453 449 528 569
KD086B 1840 382 530 650 758 681 575 515 700 712 494
KD086B 1850 543 595 425 558 622 597 410 536 642 595
KD086B 1860 747 553 516 672 513 451 402 411 511 389
KD086B 1870 380 341 481 498 571 409 199 263 271 349

KD086B	1880	89	515	470	453	345	434	471	476	462	310
KD086B	1890	395	545	664	732	683	526	314	415	458	332
KD086B	1900	624	561	462	457	472	412	304	422	410	530
KD086B	1910	368	418	500	359	475	347	264	355	410	265
KD086B	1920	285	258	306	284	311	316	339	307	440	390
KD086B	1930	375	350	397	334	531	464	330	381	554	469
KD086B	1940	462	536	520	501	656	712	578	1028	688	746
KD086B	1950	627	538	386	307	318	500	721	1297	586	315
KD086B	1960	276	206	210	274	399	632	817	835	922	1234
KD086B	1970	1803	1707	2355	1511	1565	1580	1522	1875	2393	3459
KD086B	1980	2781	3244	1563	1848	2385	1026	978	1039	1299	1544
KD086B	1990	2089	987	1204	2477	1830	1910	1734	676	1252	1647
KD086B	2000	1973	1866	2166	1482	1098	1504	1145	715	683	1112
KD086B	2010	1616	-9999								
KD087A	1754	89	86	137	167	118	71				
KD087A	1760	117	136	151	174	251	247	227	309	369	518
KD087A	1770	530	372	634	157	656	739	592	609	751	522
KD087A	1780	467	470	423	578	614	269	647	538	740	664
KD087A	1790	559	586	635	961	1031	735	705	653	385	281
KD087A	1800	381	291	652	710	798	530	347	302	579	387
KD087A	1810	417	322	294	543	400	495	203	300	844	274
KD087A	1820	664	519	282	283	207	122	128	114	162	164
KD087A	1830	178	208	156	116	183	228	227	273	296	194
KD087A	1840	559	224	138	209	571	495	355	344	265	850
KD087A	1850	478	593	445	142	111	123	118	217	427	486
KD087A	1860	471	477	521	526	455	443	295	254	237	171
KD087A	1870	74	76	133	175	123	233	307	354	317	230
KD087A	1880	220	471	567	418	379	257	164	95	288	273
KD087A	1890	246	267	351	419	541	458	453	451	385	432
KD087A	1900	563	508	331	426	454	409	383	401	378	472
KD087A	1910	436	492	397	458	506	529	254	779	852	620
KD087A	1920	650	537	417	532	570	559	565	419	668	595
KD087A	1930	726	687	390	566	844	758	525	653	406	557
KD087A	1940	490	516	450	833	710	711	1023	990	726	642
KD087A	1950	733	794	1004	576	617	667	672	557	686	682
KD087A	1960	557	577	706	850	848	741	885	592	988	634
KD087A	1970	674	488	546	468	325	409	425	489	547	526
KD087A	1980	596	625	881	1201	749	457	303	289	340	386
KD087A	1990	478	658	640	855	1177	1347	1575	2058	2338	2127
KD087A	2000	2225	2211	1971	1441	1451	1365	1147	1214	1115	1003
KD087A	2010	927	-9999								
KD087B	1779	555									
KD087B	1780	506	506	525	802	481	483	331	415	458	514
KD087B	1790	377	369	143	269	386	246	382	368	333	313
KD087B	1800	301	181	143	153	140	167	25	149	211	290
KD087B	1810	285	208	241	66	93	58	78	66	73	48
KD087B	1820	88	121	92	39	63	28	42	71	226	150
KD087B	1830	111	96	81	102	171	186	159	148	115	131

KD087B	1840	108	110	68	121	110	131	138	156	122	155
KD087B	1850	34	59	125	108	109	141	118	181	310	243
KD087B	1860	105	182	138	229	182	170	93	70	145	132
KD087B	1870	106	115	109	169	113	182	161	104	128	154
KD087B	1880	375	162	118	174	179	198	170	56	179	180
KD087B	1890	255	300	234	325	305	445	424	404	462	415
KD087B	1900	717	605	653	788	687	656	651	609	682	676
KD087B	1910	738	542	881	686	965	627	477	817	784	740
KD087B	1920	802	734	642	651	598	577	662	657	783	645
KD087B	1930	779	931	752	906	1112	911	1051	1116	992	692
KD087B	1940	768	1144	976	932	876	977	1284	1530	1345	430
KD087B	1950	691	963	1010	984	1001	858	563	733	888	804
KD087B	1960	661	818	881	1186	1159	753	1141	974	836	816
KD087B	1970	819	581	615	379	379	373	378	546	949	863
KD087B	1980	855	881	856	948	850	728	696	832	1009	1201
KD087B	1990	1323	918	375	478	463	461	566	675	838	739
KD087B	2000	647	705	767	695	897	1001	954	1021	801	870
KD087B	2010	853	-9999								

KD089A	1677	489	287	261							
KD089A	1680	352	654	676	800	646	937	800	815	545	504
KD089A	1690	515	527	626	654	703	588	390	585	590	703
KD089A	1700	738	538	587	477	552	988	867	1168	929	1014
KD089A	1710	679	1020	1063	1054	1267	1067	711	1018	1177	1164
KD089A	1720	1150	1057	948	1313	1468	1161	1091	1485	1156	1258
KD089A	1730	901	700	976	1070	983	951	871	917	756	757
KD089A	1740	910	1148	1223	930	1609	874	875	1254	2226	2027
KD089A	1750	1581	1626	1550	1258	1010	862	997	765	678	443
KD089A	1760	377	346	714	827	804	771	821	792	755	712
KD089A	1770	589	441	603	675	937	763	827	1053	1256	983
KD089A	1780	829	816	537	678	591	710	656	666	514	660
KD089A	1790	802	836	930	699	1036	1133	1033	1377	1464	1592
KD089A	1800	1318	796	865	1277	1459	1260	1491	954	960	595
KD089A	1810	840	176	881	993	632	1094	752	1192	1160	1156
KD089A	1820	703	375	799	792	833	624	967	644	664	1245
KD089A	1830	720	702	612	639	688	994	765	721	1005	858
KD089A	1840	825	850	1447	1502	1153	1049	1168	1412	1505	1699
KD089A	1850	911	1221	1212	628	679	785	693	555	642	792
KD089A	1860	847	1683	1662	1149	835	890	813	742	610	957
KD089A	1870	631	429	452	595	692	786	613	323	363	425
KD089A	1880	538	893	884	1370	930	612	496	409	626	405
KD089A	1890	254	420	688	945	890	971	469	574	569	162
KD089A	1900	479	719	635	421	691	658	561	275	223	212
KD089A	1910	429	365	356	476	672	409	254	435	547	583
KD089A	1920	516	432	450	386	409	304	344	303	278	339
KD089A	1930	431	477	564	716	694	584	534	498	309	382
KD089A	1940	438	364	349	333	412	314	413	454	346	1290
KD089A	1950	1626	2010	1410	505	358	263	316	412	418	455
KD089A	1960	607	420	395	472	558	910	735	405	500	409
KD089A	1970	710	553	345	255	192	358	346	371	467	742

KD089A 1980 484 368 326 214 182 247 197 294 391 436
KD089A 1990 563 517 724 1439 1658 1589 1214 1160 2860 2444
KD089A 2000 2341 2302 2179 1705 2618 3117 2395 1767 1184 869
KD089A 2010 787 -9999

KD089B 1721 912 884 1035 782 663 463 622 724 870
KD089B 1730 1017 782 604 827 722 720 636 755 720 604
KD089B 1740 916 795 901 626 459 779 617 510 834 968
KD089B 1750 835 697 493 619 610 481 326 348 581 466
KD089B 1760 788 551 493 632 712 805 425 404 361 366
KD089B 1770 225 312 414 354 436 473 599 561 641 626
KD089B 1780 745 935 650 432 517 337 238 182 208 139
KD089B 1790 329 293 160 220 270 391 470 475 665 763
KD089B 1800 1088 769 325 313 644 530 538 482 351 297
KD089B 1810 95 291 362 393 641 787 423 865 539 577
KD089B 1820 316 89 692 529 363 537 1507 652 824 759
KD089B 1830 629 488 530 796 612 1014 879 689 738 594
KD089B 1840 530 764 965 725 661 596 694 631 582 751
KD089B 1850 383 458 497 288 362 425 473 293 348 364
KD089B 1860 316 671 618 504 569 520 540 373 434 516
KD089B 1870 342 295 237 347 288 551 450 249 233 250
KD089B 1880 214 497 373 549 475 420 381 253 483 272
KD089B 1890 323 385 350 542 450 708 375 478 549 283
KD089B 1900 588 432 352 279 445 426 428 235 177 158
KD089B 1910 347 354 320 282 345 362 189 593 555 400
KD089B 1920 365 255 312 348 350 315 291 232 339 352
KD089B 1930 396 263 493 691 482 488 555 620 499 400
KD089B 1940 546 437 354 292 299 331 379 394 674 1124
KD089B 1950 1197 1052 704 426 409 285 471 406 303 231
KD089B 1960 141 147 177 183 188 131 188 145 198 215
KD089B 1970 238 309 388 233 176 314 213 212 184 315
KD089B 1980 299 285 321 302 412 391 243 265 310 381
KD089B 1990 453 340 343 627 850 653 548 442 1062 936
KD089B 2000 769 513 646 354 463 587 642 372 216 355
KD089B 2010 602 -9999

KD090A 1793 706 747 919 1129 728 575 775
KD090A 1800 745 760 921 858 983 900 561 806 544 763
KD090A 1810 360 540 562 505 570 558 799 775 756 657
KD090A 1820 518 988 700 777 335 682 794 868 1021 966
KD090A 1830 828 962 735 734 752 581 747 826 634 643
KD090A 1840 570 472 483 711 666 658 471 546 809 639
KD090A 1850 871 985 568 785 696 743 930 805 984 772
KD090A 1860 1098 680 737 757 809 851 961 963 995 574
KD090A 1870 575 662 789 762 699 569 476 491 589 744
KD090A 1880 338 948 638 633 717 759 758 822 750 610
KD090A 1890 798 909 909 884 845 933 774 982 784 492
KD090A 1900 842 832 680 719 738 1131 919 746 732 875
KD090A 1910 1394 1064 1117 847 863 891 734 871 860 767
KD090A 1920 759 691 575 635 997 800 853 1073 693 553

KD090A	1930	647	641	672	568	666	721	1246	929	679	475
KD090A	1940	341	449	381	418	399	416	957	1112	1193	910
KD090A	1950	832	706	809	497	549	833	741	539	845	1032
KD090A	1960	643	807	1070	1504	1087	1014	786	1009	1089	981
KD090A	1970	963	734	768	545	935	1062	794	884	520	845
KD090A	1980	1038	511	396	370	364	427	408	542	1322	1309
KD090A	1990	2952	2370	2686	848	1638	2293	2785	2393	3119	2923
KD090A	2000	4120	3412	3537	2704	2219	1865	1612	1807	2039	1841
KD090A	2010	2289	-9999								
KD090B	1658	604	622								
KD090B	1660	317	392	265	263	360	390	211	131	145	140
KD090B	1670	350	375	441	354	267	414	360	302	368	422
KD090B	1680	385	442	630	604	470	691	736	866	640	664
KD090B	1690	886	773	1078	1013	817	838	638	585	730	650
KD090B	1700	792	494	626	533	596	537	511	473	543	401
KD090B	1710	400	419	445	580	585	390	643	494	526	459
KD090B	1720	448	507	541	419	480	546	742	696	742	572
KD090B	1730	475	643	573	550	488	418	569	314	480	427
KD090B	1740	527	461	349	439	428	240	386	406	434	415
KD090B	1750	326	399	349	378	388	376	386	416	368	377
KD090B	1760	391	521	507	466	486	493	487	445	404	484
KD090B	1770	513	447	442	487	357	371	458	466	468	392
KD090B	1780	369	300	408	410	431	365	368	265	302	394
KD090B	1790	333	255	268	377	348	340	297	229	92	115
KD090B	1800	106	54	193	206	234	303	264	288	182	264
KD090B	1810	100	328	230	167	187	134	271	217	175	195
KD090B	1820	74	122	202	180	181	241	263	315	452	426
KD090B	1830	449	438	464	548	503	406	374	353	318	259
KD090B	1840	294	310	317	395	363	321	326	310	449	251
KD090B	1850	334	302	286	361	355	276	310	310	206	218
KD090B	1860	372	248	347	352	411	343	312	306	249	227
KD090B	1870	186	167	230	222	402	354	236	213	211	318
KD090B	1880	115	451	356	350	300	401	339	318	325	269
KD090B	1890	286	268	238	269	257	299	216	293	312	192
KD090B	1900	332	342	353	297	346	274	358	242	189	165
KD090B	1910	336	308	162	281	227	175	82	290	400	463
KD090B	1920	322	201	245	256	274	287	231	239	193	237
KD090B	1930	216	208	194	240	276	259	132	197	220	206
KD090B	1940	164	176	171	171	211	236	257	313	251	234
KD090B	1950	254	254	211	189	195	189	618	382	473	424
KD090B	1960	411	329	305	323	413	377	454	326	254	219
KD090B	1970	481	682	406	247	290	248	270	298	349	420
KD090B	1980	416	429	464	467	489	379	377	446	544	419
KD090B	1990	713	341	395	356	506	678	860	649	963	752
KD090B	2000	899	617	800	543	533	548	676	811	683	703
KD090B	2010	510	-9999								
KD097A	1680	1242	1309	696	520	746	1215	726	726	705	610
KD097A	1690	552	576	612	483	524	649	787	940	791	968

KD097A	1700	840	1122	409	132	380	511	823	510	765	862
KD097A	1710	809	478	673	595	750	691	944	728	794	666
KD097A	1720	681	571	527	666	610	735	858	868	804	931
KD097A	1730	841	873	1006	832	808	1061	1049	1083	979	960
KD097A	1740	1006	900	894	826	633	788	1232	1117	972	873
KD097A	1750	1254	1086	834	986	868	1048	916	689	420	288
KD097A	1760	273	195	177	347	298	283	271	293	297	343
KD097A	1770	361	382	431	417	411	382	462	630	656	531
KD097A	1780	617	551	517	407	594	459	466	394	329	332
KD097A	1790	389	229	380	405	274	462	393	376	426	394
KD097A	1800	262	290	361	284	284	244	402	636	604	454
KD097A	1810	399	491	507	692	481	524	356	416	267	450
KD097A	1820	401	378	262	205	426	459	290	266	305	220
KD097A	1830	304	329	337	356	305	357	433	396	384	371
KD097A	1840	391	315	637	428	448	462	486	511	476	473
KD097A	1850	301	571	352	366	499	348	346	330	336	329
KD097A	1860	326	287	294	501	318	346	488	429	295	313
KD097A	1870	287	327	333	271	260	332	279	297	217	182
KD097A	1880	152	229	236	51	473	445	428	275	264	252
KD097A	1890	151	323	254	186	263	319	275	361	453	386
KD097A	1900	354	372	209	342	380	338	281	254	245	197
KD097A	1910	193	189	174	305	337	287	190	192	165	57
KD097A	1920	159	207	195	211	125	160	151	130	107	74
KD097A	1930	86	53	137	114	116	91	138	107	122	90
KD097A	1940	111	127	132	154	174	159	139	171	178	276
KD097A	1950	219	212	154	125	114	118	166	196	209	210
KD097A	1960	229	201	217	268	202	281	284	279	316	280
KD097A	1970	314	199	223	290	203	171	188	179	205	212
KD097A	1980	193	201	165	166	237	219	217	193	210	226
KD097A	1990	311	324	342	272	261	177	154	98	229	326
KD097A	2000	313	275	231	194	285	332	340	337	353	371
KD097A	2010	300	-9999								

KD097B	1699	836									
KD097B	1700	655	614	378	484	550	394	693	617	448	496
KD097B	1710	555	711	397	251	343	322	312	349	384	265
KD097B	1720	353	349	371	316	339	241	237	550	780	1026
KD097B	1730	1072	409	1133	819	521	598	1025	777	539	265
KD097B	1740	289	271	421	332	361	232	223	169	266	252
KD097B	1750	225	305	383	424	414	409	319	500	411	335
KD097B	1760	268	278	234	479	411	337	286	252	428	369
KD097B	1770	369	315	411	550	417	416	303	259	530	514
KD097B	1780	432	289	375	306	400	421	544	217	152	156
KD097B	1790	215	221	202	200	235	217	231	191	175	197
KD097B	1800	193	203	210	190	236	246	187	273	237	270
KD097B	1810	274	682	386	346	286	275	197	256	109	98
KD097B	1820	106	144	194	216	154	309	326	259	285	239
KD097B	1830	197	182	237	223	213	266	308	450	273	306
KD097B	1840	207	220	174	253	222	145	107	102	289	195
KD097B	1850	152	95	103	191	255	268	211	181	194	210

KD097B	1860	219	227	218	244	272	275	247	226	274	223
KD097B	1870	268	266	259	215	176	269	174	191	226	244
KD097B	1880	201	196	139	166	201	261	253	356	250	234
KD097B	1890	283	245	161	202	157	198	211	156	163	258
KD097B	1900	209	162	165	125	138	156	191	83	254	280
KD097B	1910	288	218	236	179	121	188	123	99	119	141
KD097B	1920	160	197	266	150	186	221	135	218	271	171
KD097B	1930	162	142	141	165	138	149	153	182	153	141
KD097B	1940	119	130	105	105	128	152	168	130	122	87
KD097B	1950	94	103	53	105	132	124	109	90	57	94
KD097B	1960	121	101	118	100	121	120	113	109	175	175
KD097B	1970	118	128	141	59	59	86	93	36	84	123
KD097B	1980	73	101	70	94	46	80	80	69	37	79
KD097B	1990	78	90	77	86	44	85	112	117	109	152
KD097B	2000	95	154	129	75	164	200	187	155	138	151
KD097B	2010	196	-9999								
KD146A	1880	315	619	552	617	561	456	496	315	363	306
KD146A	1890	307	407	355	265	370	486	330	453	388	297
KD146A	1900	732	482	514	422	529	340	345	413	355	426
KD146A	1910	413	398	360	395	522	532	387	353	541	495
KD146A	1920	534	377	416	437	433	410	510	436	533	396
KD146A	1930	574	551	459	426	456	407	261	336	346	348
KD146A	1940	373	416	376	352	396	359	297	363	361	440
KD146A	1950	385	382	375	306	207	327	324	438	448	363
KD146A	1960	442	311	251	370	474	633	475	408	452	356
KD146A	1970	557	623	660	710	347	508	591	580	536	675
KD146A	1980	815	843	695	885	487	637	387	516	569	350
KD146A	1990	479	362	373	390	553	430	348	353	339	216
KD146A	2000	334	248	269	207	323	281	175	60	116	181
KD146A	2010	49	-9999								
KD146B	1780	1415	1539	1787	1967	2524	2152	1909	1839	1574	1815
KD146B	1790	2197	1529	1714	1399	902	670	1114	1409	1247	1106
KD146B	1800	880	878	713	1397	1105	1238	1355	1214	1164	960
KD146B	1810	759	611	580	806	774	1063	793	644	941	697
KD146B	1820	992	777	791	507	245	386	360	427	403	400
KD146B	1830	455	468	418	529	555	536	530	719	804	778
KD146B	1840	588	540	655	745	650	641	669	808	860	595
KD146B	1850	570	727	940	829	711	676	598	720	665	831
KD146B	1860	1103	1111	990	1019	824	855	812	830	633	467
KD146B	1870	506	537	545	647	578	670	545	673	495	498
KD146B	1880	359	500	715	826	647	601	527	486	491	415
KD146B	1890	545	739	572	544	861	769	561	602	548	447
KD146B	1900	875	567	527	494	644	564	668	624	530	782
KD146B	1910	840	918	1097	822	1110	612	573	1025	1371	1361
KD146B	1920	1619	1576	1622	1454	1348	1223	1364	1047	1204	1133
KD146B	1930	1247	938	1108	1204	1610	1350	936	1151	1195	900
KD146B	1940	1378	1495	1010	1291	1055	1436	1367	1532	1353	1378
KD146B	1950	1069	849	943	1026	1040	1248	1114	1304	1529	1150

KD146B 1960 1446 1387 955 838 897 1160 945 1220 1021 668
KD146B 1970 803 761 812 672 473 695 712 595 445 523
KD146B 1980 487 449 423 327 326 426 322 294 302 267
KD146B 1990 301 271 307 288 356 331 335 332 276 205
KD146B 2000 225 161 169 128 105 54 118 86 93 137
KD146B 2010 128 -9999

KD147A 1742 3074 2393 2285 2057 1797 1233 1298 1670
KD147A 1750 1706 1284 1042 1084 1524 1515 1038 948 681 818
KD147A 1760 1250 958 719 364 551 576 503 428 459 434
KD147A 1770 813 1075 1300 990 1084 1408 1499 1374 1155 773
KD147A 1780 729 833 936 738 1014 1167 861 1140 909 1086
KD147A 1790 1211 1586 2057 1560 1596 1341 1227 1100 952 744
KD147A 1800 913 1055 998 1119 1035 1189 996 864 1139 872
KD147A 1810 866 978 1057 1043 1180 1439 1341 1045 924 699
KD147A 1820 825 512 350 515 619 704 756 882 799 670
KD147A 1830 626 764 797 727 675 815 844 832 617 680
KD147A 1840 924 818 862 713 863 795 681 757 526 617
KD147A 1850 783 723 644 695 782 756 791 867 917 1444
KD147A 1860 1248 1263 1063 773 521 554 718 675 572 493
KD147A 1870 613 619 574 521 500 439 479 532 482 498
KD147A 1880 619 552 500 454 530 476 446 569 497 464
KD147A 1890 616 843 995 872 949 744 646 650 638 798
KD147A 1900 749 607 613 878 1120 743 573 488 386 506
KD147A 1910 470 682 735 525 550 642 715 537 607 641
KD147A 1920 683 456 463 566 576 547 476 705 607 512
KD147A 1930 570 637 791 715 552 528 354 584 589 611
KD147A 1940 596 478 454 448 498 607 815 785 839 896
KD147A 1950 778 524 421 510 562 583 534 423 301 391
KD147A 1960 339 400 453 441 689 786 586 647 683 840
KD147A 1970 633 857 1213 963 1807 1747 1345 1442 1626 1565
KD147A 1980 1706 2352 2803 1720 2271 3495 3190 2807 3260 2412
KD147A 1990 1568 1957 1721 2267 2035 1804 1525 2511 1802 2684
KD147A 2000 2235 2975 1649 645 2224 3171 2266 1336 1269 1355
KD147A 2010 1488 -9999

KD147B 1836 672 553 463 397
KD147B 1840 514 677 671 556 799 853 730 443 463 378
KD147B 1850 432 547 657 591 465 500 504 349 461 396
KD147B 1860 428 477 441 453 480 382 341 424 409 455
KD147B 1870 373 401 366 397 386 398 330 271 336 500
KD147B 1880 622 618 519 376 324 357 386 480 600 567
KD147B 1890 477 414 451 528 395 464 663 544 783 1375
KD147B 1900 1638 1727 500 127 262 539 170 186 186 356
KD147B 1910 327 325 337 190 390 434 360 410 626 710
KD147B 1920 863 624 618 570 505 454 572 644 537 663
KD147B 1930 790 668 528 565 735 808 621 853 1101 1243
KD147B 1940 913 641 642 571 640 780 691 782 665 716
KD147B 1950 326 258 217 213 234 203 290 279 219 190
KD147B 1960 258 317 289 332 311 206 279 279 270 406

KD147B	1970	414	387	218	237	230	169	202	266	241	265
KD147B	1980	184	162	212	206	236	278	160	208	233	221
KD147B	1990	222	280	284	290	247	297	293	253	194	198
KD147B	2000	212	217	165	269	254	294	257	217	189	190
KD147B	2010	179	-9999								

KD147C	1800	986	1466	1515	1356	1210	1820	1941	1789	1567	1218
KD147C	1810	1416	1643	2130	2071	728	1041	1164	1210	1091	1086
KD147C	1820	1017	914	882	820	869	967	1300	1022	1329	1273
KD147C	1830	1080	1620	1121	1446	1119	1055	791	875	976	1078
KD147C	1840	1309	1117	1102	804	712	772	963	863	779	1094
KD147C	1850	723	749	760	797	817	674	688	830	343	563
KD147C	1860	420	664	439	385	337	599	670	778	945	1115
KD147C	1870	958	1034	981	1187	1032	848	883	1111	1015	1020
KD147C	1880	1050	1237	1081	1067	839	946	930	800	898	699
KD147C	1890	575	870	839	989	1034	935	881	1082	1173	1163
KD147C	1900	1260	1002	869	916	980	841	847	737	707	743
KD147C	1910	492	655	856	970	863	912	625	597	619	482
KD147C	1920	585	660	762	683	598	620	589	545	636	780
KD147C	1930	669	758	856	919	789	757	679	693	772	620
KD147C	1940	878	779	666	699	762	666	656	604	519	552
KD147C	1950	660	635	853	879	852	655	718	729	603	518
KD147C	1960	546	529	397	422	467	431	434	317	454	533
KD147C	1970	599	565	621	698	680	579	555	480	573	610
KD147C	1980	729	688	573	655	716	634	769	1103	995	975
KD147C	1990	1102	885	872	784	992	1039	1056	1006	971	686
KD147C	2000	717	561	672	850	1164	1416	1558	1350	789	418
KD147C	2010	207	-9999								

KD148A	1760	1102	1416	1557	1646	1628	1685	1272	751	995	1074
KD148A	1770	1018	970	796	828	811	568	636	762	949	572
KD148A	1780	634	498	520	648	754	738	645	471	694	790
KD148A	1790	687	763	755	920	725	909	989	768	965	743
KD148A	1800	624	583	657	603	1040	1032	802	810	695	1020
KD148A	1810	699	696	660	768	1212	1027	1061	885	709	615
KD148A	1820	523	840	410	337	284	363	318	409	581	664
KD148A	1830	528	561	702	659	694	549	485	533	618	441
KD148A	1840	370	551	515	508	529	646	568	428	711	488
KD148A	1850	482	587	497	597	706	593	756	768	949	746
KD148A	1860	928	1047	1092	853	624	429	409	523	561	487
KD148A	1870	579	589	576	850	958	771	470	474	558	749
KD148A	1880	537	775	413	624	540	636	676	419	525	489
KD148A	1890	419	467	521	562	601	742	441	548	795	553
KD148A	1900	1342	1184	744	641	1218	1869	1145	721	492	679
KD148A	1910	711	790	597	657	844	771	582	738	487	690
KD148A	1920	833	830	814	1065	1046	975	1002	826	1201	847
KD148A	1930	940	1144	859	668	756	796	553	562	682	1060
KD148A	1940	775	765	501	646	615	679	638	950	1168	2423
KD148A	1950	2578	1998	1170	792	871	926	898	961	946	682
KD148A	1960	527	611	755	785	1036	1349	1024	641	578	457

KD148A 1970 519 756 1006 607 294 323 370 323 460 610
KD148A 1980 459 396 283 248 217 188 195 227 446 636
KD148A 1990 769 317 408 497 835 505 402 492 854 677
KD148A 2000 749 571 1044 768 541 502 375 261 173 276
KD148A 2010 283 -9999

KD148B 1747 529 651 545
KD148B 1750 690 652 462 447 211 199 344 238 160 184
KD148B 1760 149 120 108 103 319 487 605 766 817 1010
KD148B 1770 1385 2239 1581 1735 1715 928 935 1865 1694 978
KD148B 1780 912 720 1183 1141 1014 869 812 652 694 651
KD148B 1790 911 1015 1346 1185 1239 1315 1049 703 903 1139
KD148B 1800 1099 1117 996 769 1271 1317 951 814 559 1038
KD148B 1810 681 715 813 879 1069 939 1207 1034 713 455
KD148B 1820 407 704 375 314 483 1008 1017 1002 1610 1314
KD148B 1830 874 725 800 815 843 667 769 1206 1308 1109
KD148B 1840 680 916 872 729 1220 1466 1284 1430 1637 923
KD148B 1850 1055 1429 817 1010 1124 1263 940 1573 1521 1432
KD148B 1860 1906 1695 1488 1414 1223 1197 834 674 677 641
KD148B 1870 735 761 970 1269 1557 1261 712 796 787 649
KD148B 1880 420 680 590 801 758 1451 1480 1082 1414 1056
KD148B 1890 759 1003 1410 1184 1223 1522 869 993 1502 975
KD148B 1900 1944 1533 1129 796 1192 1120 1109 637 537 722
KD148B 1910 816 801 678 1147 1763 1781 997 661 821 985
KD148B 1920 984 935 1878 1826 1662 1407 1404 787 1501 1207
KD148B 1930 1144 2137 2133 1555 1976 1149 796 967 1144 1245
KD148B 1940 1124 1178 653 529 553 756 548 516 454 489
KD148B 1950 742 1180 1011 534 671 763 818 1069 1463 735
KD148B 1960 924 901 854 1066 1564 1970 1558 1242 544 265
KD148B 1970 329 370 338 392 193 280 443 541 621 639
KD148B 1980 569 823 847 1497 1542 820 465 699 1347 1764
KD148B 1990 1752 633 722 1324 2383 2775 2324 2143 2496 1864
KD148B 2000 1985 1823 1560 1053 1339 1661 1141 381 307 658
KD148B 2010 466 -9999

KD149A 1816 1082 860 777 762
KD149A 1820 617 1066 831 446 651 839 637 880 925 1157
KD149A 1830 1166 1343 1416 1460 1546 1414 1627 1681 1699 1376
KD149A 1840 1399 1261 1351 1729 1084 1213 1580 1266 1352 1167
KD149A 1850 1280 1757 1561 1477 1427 1497 1134 1512 1504 1427
KD149A 1860 2159 1944 1779 1768 1604 1445 1335 1315 1440 918
KD149A 1870 893 1298 1591 1495 1741 1485 1291 1566 1548 1309
KD149A 1880 802 1213 1640 1789 1421 1406 925 853 1031 1009
KD149A 1890 1198 1423 1336 1282 1351 1463 743 1276 1381 1004
KD149A 1900 1577 1212 1112 1185 1779 1844 1366 1003 1185 1251
KD149A 1910 1284 1255 1410 1210 1244 964 1088 1641 1977 1665
KD149A 1920 1588 1471 1170 1287 1247 1055 943 933 1271 932
KD149A 1930 799 798 793 798 1274 1328 1185 870 781 911
KD149A 1940 753 809 820 1102 1225 907 1025 1282 1231 471
KD149A 1950 1373 1689 1053 815 892 918 979 1094 1051 732

```
KD149A 1960  707  634  646 1021  953  926  759  673  585  682
KD149A 1970  705  499  674  637  459  710  922  674  695  712
KD149A 1980  638  676  624  649  625  535  539  571  749  835
KD149A 1990  905  741  846  790 1031  959 1348 1357 1432 1136
KD149A 2000 1372 1168 1229  902 1018 1170 1097 1383 1293 1514
KD149A 2010 1221 -9999

KD149B 1799 1159
KD149B 1800  974  893  931 1150 1106 1016  902 1018  758  981
KD149B 1810  415  659 1006 1109 1025  566 1066 1038  881  736
KD149B 1820  573  973  794  750  788  826  766  837 1015  988
KD149B 1830 1169  789 1261 1066 1004  673 1190  972 1063 1044
KD149B 1840 1053 1033  807 1205 1190  996 1166 1189 1204  886
KD149B 1850  847 1247 1279 1134 1275  942  925  775  956  859
KD149B 1860 1494 1299 1513 1154 1135  718  601  752  721  575
KD149B 1870  701  779  983 1161 1485 1045  879  929  868  691
KD149B 1880  645 1353 1511 1270 1028 1273 1222  971 1143  934
KD149B 1890 1144 1371 1757 1516 1479 1619 1023 1399 1276  701
KD149B 1900 1376 1244 1025  975 1345 1453 1156  958 1100 1112
KD149B 1910 1671 1335 1763 1377 1460 1087 1272 1372 1654 1294
KD149B 1920 1300 1029 1153 1067 1033  894  799  574  871  774
KD149B 1930  781 1004 1124 1297 1152  694  509  804 1081 1029
KD149B 1940  834 1139 1069 1075 1237 1133 1256 1560 1261 1301
KD149B 1950 1702 1776 1122  853  897 1089  806 1131 1137  653
KD149B 1960  642  715  769 1044 1002 1304  971  644  789  750
KD149B 1970  916  580  522  787  491  786  848  924  769  705
KD149B 1980  777  791  838 1076 1012  714  666  625  733  922
KD149B 1990 1102  646  645  697 1138 1215 1276 1065 1220  977
KD149B 2000 1349 1204 1446 1273 1724 2915 2428 2568 2546 3604
KD149B 2010 2662 -9999

KD150A 1733  552  332  200  171  182  235  200
KD150A 1740  193  190  312  147  155  124  243  200  169  136
KD150A 1750  215  268  529  478  371  415  382  260  239  185
KD150A 1760  427  395  185  180  283  204  307  205  259  237
KD150A 1770  260  206  181  229  170  317  443  285  343  209
KD150A 1780  121  278  290  250  292  290  204  233  422  270
KD150A 1790  331  267  361  290  316  632  210  209  142  197
KD150A 1800  180  229  237  204  226   77  114  138  214  102
KD150A 1810   69  176  262   54  105  111  209   66  136   91
KD150A 1820   97  182  120  116  135  169   70  102  204  309
KD150A 1830  239  249  453  456  372  205  244  300  228  425
KD150A 1840  151  290  210  280  376  358  450  270  681  485
KD150A 1850  389  478  485  401  448  321   73  203  337  471
KD150A 1860  515  468  477  590  714  607  537  580  584  453
KD150A 1870  319  325  349  405  590  561  476  802  605  425
KD150A 1880  452 1025 1040  812  702  709  555  606  953  582
KD150A 1890  515  670  668  948  984 1058  694  681  867  605
KD150A 1900  869  775  727  720  894  760  486  577  727  586
KD150A 1910  738  535  613  788  881  938  741  862  875  872
```

KD150A 1920 985 861 810 899 942 905 813 845 1047 856
KD150A 1930 977 978 980 956 1143 991 1019 1124 1093 851
KD150A 1940 888 1054 972 1034 974 737 917 1111 997 1026
KD150A 1950 1190 1008 881 898 1088 985 937 1315 1286 961
KD150A 1960 783 983 1030 1688 1573 1398 1550 1309 1312 1170
KD150A 1970 1177 943 935 1127 978 872 1039 959 1327 1582
KD150A 1980 1528 1476 1125 1436 1144 1045 1336 1121 1300 1225
KD150A 1990 1447 1091 1314 1817 2038 1639 1826 1644 1522 1025
KD150A 2000 1241 1596 1630 1175 886 1272 1047 1912 1782 1521
KD150A 2010 2297 -9999

KD150B 1732 409 626 718 424 308 522 494 346
KD150B 1740 377 300 459 293 306 436 441 432 797 491
KD150B 1750 497 434 314 334 587 421 514 579 300 290
KD150B 1760 389 439 628 339 305 488 431 544 560 404
KD150B 1770 510 560 432 239 317 209 163 472 486 428
KD150B 1780 416 340 220 700 568 912 697 820 421 477
KD150B 1790 599 851 453 432 326 425 628 683 687 840
KD150B 1800 641 346 460 530 420 246 177 166 323 420
KD150B 1810 274 167 275 421 288 371 465 618 484 448
KD150B 1820 369 257 233 257 399 404 237 231 412 465
KD150B 1830 483 526 677 662 562 617 667 720 556 963
KD150B 1840 455 847 826 859 820 885 829 1279 1509 1427
KD150B 1850 1307 1515 1069 1017 654 392 171 469 566 650
KD150B 1860 1294 1560 1568 1841 1394 1277 1508 1374 1293 722
KD150B 1870 549 763 839 1117 970 1182 1065 958 817 799
KD150B 1880 1029 1625 1707 1478 1008 992 871 1597 2549 1507
KD150B 1890 501 791 1439 1549 1897 1573 992 1390 1491 1065
KD150B 1900 1625 1140 1087 957 1036 733 563 637 771 762
KD150B 1910 1124 872 1083 1325 1286 1105 1135 1320 1226 904
KD150B 1920 837 762 1001 782 968 690 805 625 723 614
KD150B 1930 846 706 1028 856 1348 1185 1052 987 1132 912
KD150B 1940 894 1248 940 919 878 848 1023 1302 1022 1104
KD150B 1950 1104 932 855 713 782 972 871 897 1087 587
KD150B 1960 616 624 678 1215 790 687 785 955 702 506
KD150B 1970 611 407 319 372 192 244 208 275 307 325
KD150B 1980 280 382 319 436 315 330 315 397 415 291
KD150B 1990 317 240 206 168 257 273 237 177 243 226
KD150B 2000 265 283 328 243 203 325 308 166 214 241
KD150B 2010 181 -9999

KD151A 1696 1068 1002 815 707
KD151A 1700 946 800 1069 845 943 1029 1228 896 1107 1004
KD151A 1710 1445 1188 1292 1251 1110 1090 1304 1049 1048 1056
KD151A 1720 1419 1370 1432 1136 1013 1056 1357 1101 1913 1479
KD151A 1730 1237 1364 1337 1230 1353 1262 1008 572 718 614
KD151A 1740 733 842 1145 1251 726 691 825 861 665 502
KD151A 1750 404 848 676 884 616 690 821 794 743 657
KD151A 1760 588 520 447 449 506 395 448 920 742 670
KD151A 1770 786 1198 1517 1660 885 1098 952 828 898 1478

```
KD151A 1780 1252 1104  600  890  946 1051 1257  760 1198 1520
KD151A 1790 1503 1409 1526 1718 1311 1356 1239  670 1025  962
KD151A 1800  823  978  971  721  840 1432 1237 1030  834 1061
KD151A 1810  612  685  773  789  718  882 1301 1433 1158 1383
KD151A 1820  959 1016  841  933  932 1279 1275 1123 1022 1211
KD151A 1830  952 1304 1503 2003 1750 1013  913 1647 1901 1699
KD151A 1840 1356 1620 1156 1078  913 1096  978 1023  740  526
KD151A 1850  689  865  642 1060  914  967  835  986 1457 1278
KD151A 1860 1674 1300 1177 1367  830  707  466  749  860  834
KD151A 1870 1072  927  894  892 1048 1016  848 1183 1439 1494
KD151A 1880 1276 1964 1212 1161  929 1610 1093  920 1001 1298
KD151A 1890 2170 2289 2591 2219 2091 1637  944 1253 1438 1069
KD151A 1900 1852 1681 1141 1176 1604 1935 1548  970 1199  935
KD151A 1910 1016  741  716  981 1205  982 1183  880  847 1104
KD151A 1920 1112 1249  987  961  486  716  701  819  945  849
KD151A 1930  762  957 1226 1202 1114 1609 1850 1354 1369 1499
KD151A 1940 1001 1361 1354 1165 1133  827  896  927  402  273
KD151A 1950  441  483  351  261  377  408  600  442  432  200
KD151A 1960  243  185  231  450  679  736  666  603  517  498
KD151A 1970  421  656 1460 1233  714  617  448  354  595 1255
KD151A 1980 1190  794  899  662  466  356  238  315  363  537
KD151A 1990  743  405  387  393  459  541  514  532  527  203
KD151A 2000  355  530 1019  690  673  702  502  226  523  588
KD151A 2010  176 -9999

KD151B 1717  856  759  841
KD151B 1720  692  969  586  637  672  695  552  865  802  541
KD151B 1730  832  491  530  475  611  548  587  621  702  987
KD151B 1740  789  810  603  441  366  483  344  549  399  347
KD151B 1750  449  323  458  367  418  413  459  370  404  443
KD151B 1760  486  431  291  497  480  412  495  814  499  500
KD151B 1770  498  723  823  966  594  590  756  458  673  951
KD151B 1780  897  897  469  454  512  697  796  694  552  894
KD151B 1790 1047  704  854  756 1109  952  900  511  688  961
KD151B 1800  780  568  639  468  601  878  645  577  492  526
KD151B 1810  338  499  386  328  344  502  561  735  489  734
KD151B 1820  905 1119 1090  926  975 1585 2065 1728 1279 1404
KD151B 1830 1053 1351 2189 2539 2452 1863 1641 2129 2301 1638
KD151B 1840  824 1498 1139 1021  820  779  930  892  678  467
KD151B 1850  500  525  410  606  575  514  518  506  679  886
KD151B 1860 1205 1061 1109  871  473  403  376  398  307  186
KD151B 1870  276  278  286  358  397  396  352  274  333  567
KD151B 1880  424  674  530  507  431  395  450  406  434  399
KD151B 1890  383  568 1698 1919 1695 1208  680  824 1009  777
KD151B 1900 1333 1597  827  764 1167 1049  782  662  661  631
KD151B 1910  763  512  532  743  692  461  546  556  302  422
KD151B 1920  314  379  415  424  381  373  385  420  427  400
KD151B 1930  239  248  349  485  345  512  427  354  483  506
KD151B 1940  421  409  374  560  765  806  729  679  796 1060
KD151B 1950 1345 1117  761  406  477  994 1672 2092 1585  862
```

KD151B	1960	840	647	833	1180	1024	1058	992	600	523	591
KD151B	1970	321	274	316	251	295	318	338	299	338	358
KD151B	1980	285	298	398	360	486	339	296	432	358	511
KD151B	1990	534	336	351	331	464	370	440	409	414	433
KD151B	2000	424	505	692	456	405	446	385	189	174	257
KD151B	2010	93	-9999								
KD153B	1716	454	580	528	668						
KD153B	1720	615	678	606	862	514	411	536	473	783	960
KD153B	1730	1258	569	890	652	612	609	635	765	805	724
KD153B	1740	1032	1157	975	980	782	1030	690	890	813	809
KD153B	1750	746	467	408	643	668	832	724	769	727	605
KD153B	1760	636	506	660	631	504	519	544	439	455	501
KD153B	1770	583	543	694	670	676	678	743	824	713	698
KD153B	1780	837	776	792	951	1014	1265	1155	911	718	766
KD153B	1790	771	794	728	685	568	815	716	799	918	704
KD153B	1800	828	873	717	731	437	500	606	547	403	606
KD153B	1810	620	625	743	561	749	755	821	397	715	623
KD153B	1820	488	795	598	891	608	421	498	506	583	404
KD153B	1830	454	341	539	565	546	591	595	507	373	484
KD153B	1840	515	576	403	417	510	554	658	447	489	506
KD153B	1850	373	424	572	486	625	559	400	360	500	504
KD153B	1860	453	442	445	489	535	472	471	464	514	553
KD153B	1870	609	635	453	491	444	492	361	214	261	376
KD153B	1880	270	232	260	196	340	396	401	366	412	435
KD153B	1890	419	327	433	341	258	265	293	235	321	219
KD153B	1900	221	253	273	197	290	331	200	365	276	372
KD153B	1910	213	335	412	140	155	158	196	169	211	282
KD153B	1920	345	229	191	207	164	182	238	163	172	146
KD153B	1930	180	157	161	125	184	132	166	178	169	150
KD153B	1940	183	160	139	169	174	190	211	221	142	145
KD153B	1950	199	164	152	179	162	165	156	177	163	129
KD153B	1960	133	187	173	315	268	231	226	160	136	172
KD153B	1970	163	192	189	145	182	173	91	62	103	184
KD153B	1980	90	136	101	123	134	123	80	105	135	122
KD153B	1990	157	131	126	162	124	100	64	119	124	132
KD153B	2000	64	155	137	71	125	114	116	128	159	106
KD153B	2010	101	-9999								
KD154A	1734	400	617	621	304	225	308				
KD154A	1740	368	241	241	399	214	586	823	376	437	1015
KD154A	1750	420	191	208	292	254	313	727	300	128	100
KD154A	1760	129	82	99	139	89	131	145	78	71	92
KD154A	1770	225	268	142	287	294	264	235	495	549	213
KD154A	1780	335	148	335	332	436	281	310	143	390	363
KD154A	1790	215	360	345	377	421	397	130	278	286	193
KD154A	1800	220	138	281	286	565	418	363	343	202	189
KD154A	1810	94	275	259	273	296	179	276	277	292	146
KD154A	1820	258	358	312	226	284	445	350	439	493	671
KD154A	1830	593	505	622	665	560	422	491	582	701	490

KD154A	1840	501	759	422	562	658	757	747	588	549	496
KD154A	1850	574	643	500	660	675	781	813	801	785	795
KD154A	1860	966	787	856	995	721	718	733	734	546	541
KD154A	1870	481	590	428	618	765	779	599	730	735	1238
KD154A	1880	882	1092	1028	1061	811	820	505	673	691	585
KD154A	1890	620	415	571	837	853	846	785	919	651	515
KD154A	1900	1055	949	1057	1060	936	948	898	656	973	878
KD154A	1910	1022	968	935	918	1014	862	671	674	728	721
KD154A	1920	739	654	672	810	560	716	606	572	663	524
KD154A	1930	851	474	601	868	728	780	690	760	688	713
KD154A	1940	742	887	589	942	1213	1002	883	1082	1216	995
KD154A	1950	951	758	532	572	501	689	693	807	868	559
KD154A	1960	630	478	509	532	438	526	463	494	492	354
KD154A	1970	445	506	478	458	329	469	511	493	511	542
KD154A	1980	604	564	458	544	435	523	488	702	652	512
KD154A	1990	496	427	459	436	842	532	538	502	861	962
KD154A	2000	1270	1113	1208	890	643	954	1350	738	819	1183
KD154A	2010	1166	-9999								

KD154B	1692	592	305	346	659	808	491	460	403		
KD154B	1700	466	372	438	933	572	373	204	113	219	199
KD154B	1710	161	680	971	619	883	464	342	197	509	282
KD154B	1720	435	631	741	1264	808	771	310	288	481	317
KD154B	1730	154	183	165	564	590	489	213	474	302	224
KD154B	1740	292	315	275	165	87	195	155	184	412	443
KD154B	1750	475	700	435	280	372	114	113	231	226	244
KD154B	1760	351	319	299	306	271	238	276	295	180	153
KD154B	1770	153	301	233	219	268	216	203	209	189	425
KD154B	1780	207	133	246	308	521	408	383	137	271	217
KD154B	1790	248	400	364	452	383	421	200	417	493	350
KD154B	1800	262	316	497	384	387	447	305	276	272	542
KD154B	1810	424	718	532	324	373	211	381	327	349	212
KD154B	1820	194	233	327	267	230	236	378	260	167	217
KD154B	1830	214	245	341	308	261	299	287	165	306	232
KD154B	1840	248	279	270	362	353	361	314	250	297	219
KD154B	1850	263	332	281	435	369	400	467	472	442	379
KD154B	1860	507	499	582	677	656	573	589	504	513	534
KD154B	1870	284	364	350	361	211	225	223	195	304	505
KD154B	1880	339	526	452	501	555	574	581	420	600	439
KD154B	1890	581	573	422	610	397	470	369	509	357	276
KD154B	1900	523	307	297	292	357	290	330	315	345	340
KD154B	1910	353	368	327	376	382	335	350	325	257	312
KD154B	1920	352	218	327	330	233	297	373	377	457	243
KD154B	1930	421	193	254	302	246	281	293	293	240	233
KD154B	1940	370	356	279	304	393	367	373	480	591	628
KD154B	1950	590	1179	732	1515	1413	1515	1256	1538	1165	660
KD154B	1960	914	500	560	606	313	603	715	846	602	442
KD154B	1970	742	653	499	669	291	404	1054	805	592	501
KD154B	1980	458	505	317	413	416	379	263	651	382	217
KD154B	1990	299	168	220	324	365	269	917	611	1505	1283

```
KD154B  2000  1247   777   564   262   247  1433  1519   290   217   261
KD154B  2010   211 -9999

KD-155A 1818  1364   990
KD-155A 1820   785  1436  1837  1208  1016   858   776   728   799  1177
KD-155A 1830  1310  1171  1096  1097  1373  1576  1397  1315  1439  1617
KD-155A 1840  1461  1090  1273  1324  1017  1026  1688  1327  1037   928
KD-155A 1850   831   874   927   765   969  1036  1194  1202  1105  1171
KD-155A 1860   990  1075  1051  1167  1080   805   741   851   911   980
KD-155A 1870   906  1023   825  1441  1280  1213  1046   830   932  1222
KD-155A 1880   944   651   968   740   832   950   920   846   711   786
KD-155A 1890  1228   736   465   765   844   800   922   948  1131  1158
KD-155A 1900   879   886   996   996   990  1507  1605   943   690   592
KD-155A 1910   655   816   599   804   812   899   811   729   738   656
KD-155A 1920   746   827   933   696   699   795   821   791   648   798
KD-155A 1930   848   857  1644  1850  1521  1261  1395  1494   950   719
KD-155A 1940   706   547   450   467   354   267   277   305   332   266
KD-155A 1950   216   249   386   310   109   196   172   226   236   219
KD-155A 1960   215   361   363   410   356   279   393   568   484   461
KD-155A 1970   477   481   438   499   383   310   268   185   168   275
KD-155A 1980   318   301   228   359   330   453   326   263   309   215
KD-155A 1990   400   264   227   174   464   308   198   259   241   309
KD-155A 2000   271   290   550   658   496   513   687   778   497   638
KD-155A 2010   530 -9999

KD155B  1821  1741  1712   992  1512  1304   693   583   520   536
KD155B  1830   918   867  1278  1492  1157  1300  1138   902  1256   864
KD155B  1840   925   717   843  1272  1137   931  1237  1287  1199  1171
KD155B  1850   797  1003   897   701  1058   891  1126  1056   894   995
KD155B  1860   952   886   815  1189  1150   743   693   652   817   700
KD155B  1870   512   538   633   690   714   704   708   680   747   789
KD155B  1880   619   374   807   703   642   620   692   717   529   658
KD155B  1890   415   295   728   553   591  1284   723   883   824   673
KD155B  1900   802   965   996   969  1490  1487   789   616   433   532
KD155B  1910   700   627   703   909  1164   759   702   649   675   768
KD155B  1920   562   550   478   465   486   502   463   345   730   519
KD155B  1930   585   510   541   602   645   383   629   565   582   559
KD155B  1940   555   552   366   452   370   242   440   412   456   502
KD155B  1950   776   904   674   374   386   369   448   686   401   658
KD155B  1960   549   461   587   591   525   549   744   516  1016   654
KD155B  1970   536   393   583   705   517   567   603   483   312   521
KD155B  1980   363   320   536   424   847   466   582   795   755   610
KD155B  1990   628   345   289   357   212   230   223   383   833  1132
KD155B  2000   856   904   629   595   908  1018   914   812   758   796
KD155B  2010   628 -9999

KD156A  1728  2793  2402
KD156A  1730  2382  1639  1638  1640  1813  2216  2299  3223  3073  2175
KD156A  1740  2430  1976  2076  1885  1718  1759  1432  1865  2312  2360
KD156A  1750  3027  2663  2322  1424  1357  1390  1504  1670  1621  1016
```

KD156A	1760	897	1242	1051	1452	1402	1657	1346	1387	947	1069
KD156A	1770	1183	1055	1253	1507	1304	1472	1350	1487	1593	1231
KD156A	1780	1202	982	1018	1136	1459	1245	1167	816	938	1295
KD156A	1790	1178	1184	1111	1617	1437	1324	1576	1699	1848	1441
KD156A	1800	1461	1351	1059	1113	1465	1609	1206	1156	946	675
KD156A	1810	532	586	459	615	531	510	533	553	642	732
KD156A	1820	609	634	672	436	460	812	883	776	850	929
KD156A	1830	890	1159	1107	1112	1056	1024	1148	1200	920	1164
KD156A	1840	978	1151	869	914	975	1003	1124	747	969	953
KD156A	1850	1065	1137	913	1084	1134	1285	1171	1198	1343	893
KD156A	1860	1146	1031	919	1023	808	783	888	753	749	705
KD156A	1870	897	924	857	838	781	655	454	710	573	693
KD156A	1880	223	533	588	511	545	562	620	453	689	709
KD156A	1890	772	961	856	828	690	611	605	644	793	509
KD156A	1900	745	1101	826	939	1061	1053	1043	901	935	847
KD156A	1910	621	858	788	1021	1189	924	822	567	615	629
KD156A	1920	650	501	565	612	574	526	546	563	645	566
KD156A	1930	642	690	670	583	376	547	517	560	611	578
KD156A	1940	574	703	770	786	744	697	613	534	718	596
KD156A	1950	782	774	755	784	522	722	455	558	773	645
KD156A	1960	804	612	766	948	914	1262	956	838	825	853
KD156A	1970	1057	886	587	939	409	435	518	627	508	567
KD156A	1980	712	587	623	666	681	485	509	595	794	608
KD156A	1990	884	431	487	724	889	582	582	531	986	884
KD156A	2000	829	985	975	902	924	867	698	631	758	806
KD156A	2010	800	-9999								

KD-156B	1721	3711	3506	3633	3744	4209	2929	3323	3123	3607	
KD-156B	1730	3168	2804	1779	1448	1040	757	1009	1199	1715	2068
KD-156B	1740	1427	1396	1417	1922	1483	1475	1472	1261	1740	1891
KD-156B	1750	1765	2212	2178	2070	1401	1292	1090	1180	1379	1386
KD-156B	1760	834	1091	1041	1017	1344	1461	1806	1734	1681	1290
KD-156B	1770	1068	1309	1274	1297	1583	1371	1399	1433	1425	1464
KD-156B	1780	1274	1069	1165	1259	1578	1585	1733	1582	1117	1298
KD-156B	1790	2173	1617	1712	1565	1886	1380	1716	1748	1614	1677
KD-156B	1800	1409	1439	1485	1185	955	1543	1494	1468	1384	996
KD-156B	1810	819	500	799	543	483	1190	776	687	587	790
KD-156B	1820	544	815	836	496	485	566	652	713	636	671
KD-156B	1830	790	856	898	925	1076	1132	1143	1342	1075	1212
KD-156B	1840	962	1181	1028	866	1052	1422	1577	1099	1182	933
KD-156B	1850	1002	1256	1038	985	899	1278	1327	1145	1565	1271
KD-156B	1860	1435	1373	988	1147	967	893	991	833	822	542
KD-156B	1870	642	559	646	731	984	993	706	1020	888	987
KD-156B	1880	312	945	831	785	887	988	1075	1088	1102	953
KD-156B	1890	987	1129	1161	1052	846	803	783	760	949	796
KD-156B	1900	931	1005	837	955	1067	1066	1120	1051	998	842
KD-156B	1910	659	740	753	787	826	996	805	683	645	647
KD-156B	1920	626	658	622	673	591	668	701	706	692	645
KD-156B	1930	743	1155	1213	1249	1166	1310	935	850	903	884
KD-156B	1940	857	975	1033	944	993	1048	1040	814	1117	1079

KD-156B	1950	1120	971	967	1026	1013	929	1020	838	740	479
KD-156B	1960	502	434	518	654	812	862	586	514	547	601
KD-156B	1970	795	446	442	417	291	349	374	538	393	514
KD-156B	1980	567	617	442	336	355	294	332	464	643	630
KD-156B	1990	836	477	428	861	759	581	656	627	647	642
KD-156B	2000	637	726	622	391	369	467	500	607	721	925
KD-156B	2010	794	-9999								

KD157A	1672	2158	1406	2009	2112	1346	1506	1699	1265		
KD157A	1680	1061	1162	1651	931	964	751	985	1009	1133	876
KD157A	1690	806	742	707	978	1082	966	1061	1170	1390	1183
KD157A	1700	1008	1283	883	1131	980	1111	1171	1454	1197	1159
KD157A	1710	1365	1356	1349	1199	1151	1070	851	1040	821	998
KD157A	1720	1156	1041	785	838	739	568	764	1197	1098	1354
KD157A	1730	935	798	859	688	875	683	740	684	422	525
KD157A	1740	405	505	373	322	424	258	226	255	249	300
KD157A	1750	256	166	206	118	169	86	84	209	107	185
KD157A	1760	182	174	196	223	328	191	202	156	135	191
KD157A	1770	185	236	298	354	558	488	386	397	390	410
KD157A	1780	437	497	453	434	464	484	507	540	438	390
KD157A	1790	493	424	321	350	621	547	624	584	648	522
KD157A	1800	612	501	515	656	735	655	697	553	564	330
KD157A	1810	520	405	483	500	523	370	600	536	488	397
KD157A	1820	245	402	347	369	214	261	296	384	495	303
KD157A	1830	248	250	199	181	293	373	334	446	434	337
KD157A	1840	352	353	330	391	394	353	219	257	390	266
KD157A	1850	397	336	228	393	353	237	274	334	430	453
KD157A	1860	831	364	336	333	349	265	235	249	268	224
KD157A	1870	193	219	427	449	501	400	254	166	235	399
KD157A	1880	112	365	360	386	329	306	221	255	389	260
KD157A	1890	319	393	354	371	294	443	372	591	512	240
KD157A	1900	591	600	500	462	469	424	419	303	299	369
KD157A	1910	429	388	327	371	328	344	163	317	283	284
KD157A	1920	327	324	384	386	337	363	387	290	352	271
KD157A	1930	299	270	323	360	314	519	422	506	292	388
KD157A	1940	277	358	317	305	212	310	343	423	405	654
KD157A	1950	431	340	238	188	184	146	231	246	255	309
KD157A	1960	269	253	210	291	308	293	328	233	220	312
KD157A	1970	484	387	431	476	758	638	523	453	674	721
KD157A	1980	790	366	613	531	733	659	404	502	297	257
KD157A	1990	273	124	241	339	506	336	265	236	254	296
KD157A	2000	202	242	249	207	175	162	98	85	99	220
KD157A	2010	178	-9999								

KD157B	1669	780									
KD157B	1670	751	1277	638	1412	1128	1604	1246	1947	2533	2127
KD157B	1680	2313	1842	1438	1351	944	1395	1148	1035	596	838
KD157B	1690	906	634	845	815	993	1052	1330	1511	1405	1043
KD157B	1700	1161	1294	1346	1191	1244	798	1182	1115	1466	1654
KD157B	1710	1887	1645	1555	1439	1604	1410	1253	1156	1013	980

KD157B	1720	1057	1090	1139	1129	1139	818	887	834	750	866
KD157B	1730	1036	949	975	827	734	1038	879	883	770	883
KD157B	1740	746	623	609	505	764	427	321	405	433	401
KD157B	1750	740	643	639	661	470	613	437	375	243	206
KD157B	1760	324	239	300	256	215	234	196	318	216	318
KD157B	1770	271	264	285	242	271	293	275	352	278	341
KD157B	1780	378	286	361	363	418	296	382	359	540	544
KD157B	1790	602	512	541	490	465	433	387	420	472	515
KD157B	1800	478	639	420	534	476	552	650	606	587	591
KD157B	1810	391	371	180	389	398	369	284	266	146	464
KD157B	1820	366	234	166	206	495	324	181	103	195	148
KD157B	1830	178	245	139	164	202	170	109	165	129	135
KD157B	1840	135	187	196	237	295	291	456	442	369	317
KD157B	1850	447	508	319	457	357	249	404	415	330	437
KD157B	1860	422	371	414	779	476	356	500	361	254	245
KD157B	1870	238	313	166	237	155	137	136	94	271	460
KD157B	1880	116	379	334	321	288	262	255	175	295	175
KD157B	1890	269	239	177	302	176	454	371	423	389	190
KD157B	1900	357	401	335	267	325	354	312	268	211	282
KD157B	1910	379	351	267	344	354	521	99	273	302	180
KD157B	1920	330	204	321	259	266	270	195	153	210	186
KD157B	1930	172	172	254	375	210	287	179	259	225	189
KD157B	1940	204	213	333	406	219	329	383	399	440	668
KD157B	1950	430	312	196	200	142	173	425	398	393	350
KD157B	1960	195	186	234	302	265	274	308	244	215	249
KD157B	1970	241	216	174	332	262	459	654	397	584	728
KD157B	1980	579	433	196	197	662	406	298	641	1405	957
KD157B	1990	668	187	540	368	631	414	913	1268	1258	685
KD157B	2000	655	409	1261	580	482	465	452	228	385	346
KD157B	2010	122	-9999								
KD-158A	1660	1052	1509	1163	2253	1983	1806	1429	1354	1378	2048
KD-158A	1670	1472	1788	1625	1393	1543	1351	1155	1201	1287	1255
KD-158A	1680	997	1633	963	778	550	818	883	960	809	868
KD-158A	1690	964	897	843	997	901	910	877	864	710	536
KD-158A	1700	637	601	630	585	698	704	972	826	1065	1164
KD-158A	1710	1197	1257	1320	1192	1017	1250	1264	1135	1339	1179
KD-158A	1720	1203	883	1102	1057	966	1187	1251	1069	1157	1014
KD-158A	1730	915	605	802	777	643	721	738	486	638	585
KD-158A	1740	740	721	960	766	522	469	642	512	605	453
KD-158A	1750	411	438	420	519	461	402	468	419	416	273
KD-158A	1760	201	317	361	388	414	453	446	472	326	333
KD-158A	1770	364	372	458	747	613	494	647	565	650	497
KD-158A	1780	445	353	317	359	236	250	198	146	403	296
KD-158A	1790	297	246	371	330	317	339	413	325	407	869
KD-158A	1800	450	402	346	346	330	356	321	250	251	174
KD-158A	1810	294	148	229	198	175	153	135	206	155	143
KD-158A	1820	114	99	169	165	189	159	238	244	314	381
KD-158A	1830	308	345	377	332	314	319	383	385	387	378
KD-158A	1840	308	372	467	446	488	364	372	244	455	494

KD-158A	1850	255	357	368	290	402	430	398	341	449	447
KD-158A	1860	446	526	351	570	508	471	414	324	284	197
KD-158A	1870	174	142	163	190	217	274	397	131	133	171
KD-158A	1880	219	74	316	300	261	208	223	203	262	290
KD-158A	1890	196	261	237	268	295	363	397	318	335	346
KD-158A	1900	334	317	359	370	309	338	284	427	345	324
KD-158A	1910	291	419	409	371	383	309	338	231	243	261
KD-158A	1920	284	252	204	269	247	264	292	262	313	269
KD-158A	1930	231	218	199	229	332	284	293	214	303	326
KD-158A	1940	358	244	516	224	247	143	202	305	276	512
KD-158A	1950	727	714	702	513	399	165	254	320	310	471
KD-158A	1960	343	253	341	333	437	500	354	567	519	456
KD-158A	1970	381	573	571	397	538	468	461	370	419	372
KD-158A	1980	468	572	588	354	440	534	554	405	549	776
KD-158A	1990	666	786	146	276	412	753	558	612	601	856
KD-158A	2000	270	296	381	392	156	202	352	114	75	110
KD-158A	2010	95	-9999								

KD158B	1656	648	739	1154	1220						
KD158B	1660	1166	1132	845	1166	1299	1688	1085	1242	1009	2025
KD158B	1670	2648	3097	2438	2542	2252	1895	2066	2199	1762	1382
KD158B	1680	1038	1530	1023	830	1073	964	1053	1052	912	948
KD158B	1690	969	1014	1131	1289	1086	1183	1273	1141	1014	1050
KD158B	1700	1168	953	934	1022	1188	1154	1234	1179	1421	1282
KD158B	1710	1556	1365	1286	1059	992	1093	1316	908	1135	1079
KD158B	1720	1393	1083	883	889	873	905	1269	711	1412	755
KD158B	1730	692	866	579	949	791	901	1136	990	1118	1059
KD158B	1740	1338	1222	1461	1405	1081	964	1296	946	913	719
KD158B	1750	590	724	605	776	607	701	550	456	414	270
KD158B	1760	406	403	392	383	498	544	536	582	451	469
KD158B	1770	507	522	568	808	581	457	745	592	808	655
KD158B	1780	629	582	543	618	756	687	644	559	663	625
KD158B	1790	556	563	638	597	591	503	548	248	281	368
KD158B	1800	307	396	468	348	671	534	421	393	249	418
KD158B	1810	333	333	282	267	286	231	381	289	287	255
KD158B	1820	224	370	244	274	175	241	326	608	453	323
KD158B	1830	375	392	413	569	559	531	463	650	629	596
KD158B	1840	504	512	521	721	500	584	535	607	718	500
KD158B	1850	475	572	406	716	672	514	539	516	691	530
KD158B	1860	713	400	475	638	634	705	446	678	334	342
KD158B	1870	448	421	505	536	433	431	238	291	302	367
KD158B	1880	180	517	403	412	381	306	320	313	471	288
KD158B	1890	314	315	391	396	514	575	554	647	675	384
KD158B	1900	463	487	444	464	712	941	541	519	452	355
KD158B	1910	524	501	451	391	275	203	279	350	316	324
KD158B	1920	360	359	212	299	351	459	408	407	383	306
KD158B	1930	309	388	385	403	325	470	354	349	289	339
KD158B	1940	234	183	240	322	221	366	434	416	708	631
KD158B	1950	646	625	613	468	582	323	362	435	852	649
KD158B	1960	530	544	557	706	986	779	750	583	831	477

```
KD158B  1970  602  740  687  209  464  547  828  998  515  770
KD158B  1980  735  879  642  875  379  375  572  721 1173 1073
KD158B  1990  886  441  718  472  744  523  579  784 1083 1183
KD158B  2000 1621  973  901  692 1244  775  967 1200 1098 1276
KD158B  2010 1131 -9999

KD175A  1618  623  537
KD175A  1620  580  676  704  866  859  903  840  784  688  540
KD175A  1630  706  696  664  571  554  750  673  519  464  551
KD175A  1640  547  568  376  334  474  802  589  377  451  543
KD175A  1650  551  523  560  544  564  407  561  561  735  654
KD175A  1660  546  532  588  662  767  784  518  702  987  883
KD175A  1670  710  858 1083 1554 1555 1876 1483 1351 1614 1702
KD175A  1680 1441 1437 1644 1117 1183 1366 1949 2297 1925 1750
KD175A  1690 1486 1600 1686 2292 1869 1571 1491 1239 1208 1075
KD175A  1700 1208  857 1292 1414 1183 1129 1235 1210  872 1026
KD175A  1710 1266 1086 1012 1205 1708 1486 1584 1636 1649 2049
KD175A  1720 1985 1996 1997 2111 1725 1821 1798 1783 1445 1697
KD175A  1730 1619 1344 1426 1478 1324 1897 1607 1703 1915  717
KD175A  1740 1234  960 1411 1340 1030 1011  951 1214 1124 1124
KD175A  1750 1438 1516 1521 1471 1297 1534 1448 1486 1477  994
KD175A  1760  991 1117 1116  960 1029 1308 1406 1517 1305 1380
KD175A  1770 1741 1826 1824 2110 1832 1477 1723 1556 1668 1722
KD175A  1780 1384 1185 1012 1317 1341 1263 1270  998 1082 1340
KD175A  1790 1121 1344 1629 1720 1563 1587 1387 1482 1563 1397
KD175A  1800 1318 1330 1177 1232 1359 1415 1269 1134  966 1166
KD175A  1810  895  996  870  912  998  867  950  919 1153 1074
KD175A  1820 1010 1025  953  689  726  930  791  772  840 1057
KD175A  1830  951  873  911  998 1026  902  915 1003  923 1153
KD175A  1840  781  857  744  887 1017 1158 1037  632  925  784
KD175A  1850  987 1114  822  848  920  949  738  667  798  754
KD175A  1860  791  773  741 1000  801  989  881  749  801  660
KD175A  1870  742  733  678  712  783  803  647  800  763  721
KD175A  1880  442  671  647  570  636  700  633  591  620  663
KD175A  1890  589  854  671  575  536  589  582  501  658  494
KD175A  1900  540  593  638  562  716  811  753  701  687  584
KD175A  1910  501  576  516  524  633  661  604  559  565  707
KD175A  1920  606  558  522  623  661  514  598  570  556  471
KD175A  1930  758  663  608  523  453  659  408  425  522  376
KD175A  1940  545  694  670  616  736  628  616  537  742  641
KD175A  1950  749  746  763  787  899  801  691  745 1201  865
KD175A  1960  928  909  643  813  761  856  877  876  781  848
KD175A  1970  945  811  653  591  590  549  759  843  797  674
KD175A  1980  932 1100  725  895  743  490  572  745  688  604
KD175A  1990  978  722  764  855 1027  748  730  531  691  726
KD175A  2000  945  824  740  719  708  835  737  608  711  795
KD175A  2010  744 -9999

KD175B2 1682 1250 1707 1483 1819 1522 1329 1612 1542
KD175B2 1690 1633 1895 1064 1498 1771 1606 1468 1752 1444 1140
```

KD175B2	1700	822	845	567	659	736	653	1008	1041	500	548
KD175B2	1710	643	735	839	1175	1434	1134	1255	1265	1391	1665
KD175B2	1720	1719	1726	2017	1792	1362	1388	1587	1447	1364	1481
KD175B2	1730	1476	1064	872	864	882	1165	1086	1503	1711	879
KD175B2	1740	909	1050	1004	823	858	836	812	907	1070	986
KD175B2	1750	1166	1158	1219	1265	1270	1526	1436	1463	1472	861
KD175B2	1760	1110	1232	1246	913	1112	1137	1432	1395	1321	1218
KD175B2	1770	1340	1216	1445	1804	1689	1506	1587	1444	1484	1433
KD175B2	1780	1286	1168	1114	1459	1651	1658	1932	1600	1872	2315
KD175B2	1790	2001	2490	2452	2860	2248	2120	2145	1895	1832	1718
KD175B2	1800	1628	1651	1457	1340	1742	1671	1385	1410	1243	1319
KD175B2	1810	1034	975	963	875	862	881	1110	1239	1243	1083
KD175B2	1820	1062	868	868	641	974	1038	902	826	960	994
KD175B2	1830	821	823	782	866	1100	1073	1027	1028	899	1195
KD175B2	1840	882	948	935	784	1019	1018	947	764	903	952
KD175B2	1850	1120	1196	892	937	983	1074	934	891	1057	945
KD175B2	1860	1119	1094	858	1113	986	1157	1075	986	1176	818
KD175B2	1870	1057	1046	978	1089	1042	904	841	991	1065	886
KD175B2	1880	534	775	841	809	889	971	814	878	890	1135
KD175B2	1890	938	1247	1128	1024	976	840	823	901	953	840
KD175B2	1900	869	883	830	729	916	1319	1247	1172	1134	1095
KD175B2	1910	897	866	780	882	985	1100	1199	996	989	985
KD175B2	1920	1054	882	748	769	810	675	912	809	836	800
KD175B2	1930	1006	881	870	845	796	806	681	785	890	839
KD175B2	1940	913	1079	1112	1058	1119	957	1027	1030	1192	867
KD175B2	1950	1177	1075	1172	1170	1158	1197	1009	1001	1435	1079
KD175B2	1960	1072	1039	885	892	915	1003	1265	1290	1157	1139
KD175B2	1970	1181	1196	894	880	750	880	965	1141	1258	1134
KD175B2	1980	1498	1844	1337	1547	1022	800	857	1078	859	720
KD175B2	1990	1130	850	851	845	956	692	697	626	741	775
KD175B2	2000	805	899	924	804	968	970	886	765	734	901
KD175B2	2010	900	-9999								

KD176A	1550	777	897	923	1150	1064	1350	861	1348	1109	1189
KD176A	1560	1187	1194	1197	1221	1605	1356	1853	1337	1087	1376
KD176A	1570	1338	1326	1551	1462	1638	1511	754	1039	1361	1219
KD176A	1580	1087	1057	1233	1466	870	1026	603	779	1153	1055
KD176A	1590	1218	1181	1162	954	911	1190	1428	1487	1284	1261
KD176A	1600	1163	1283	1100	1043	927	986	1061	1184	1050	843
KD176A	1610	843	1173	1259	998	1033	1016	1147	1143	873	786
KD176A	1620	609	943	979	816	795	853	789	877	673	692
KD176A	1630	854	693	1095	710	719	420	714	712	722	437
KD176A	1640	738	754	576	935	791	937	902	889	1031	500
KD176A	1650	577	986	849	722	953	787	1176	937	1073	1001
KD176A	1660	573	444	545	537	770	450	756	676	889	1005
KD176A	1670	925	777	763	859	959	970	755	699	923	1057
KD176A	1680	984	1003	1546	1181	1274	1327	1200	1561	1224	1661
KD176A	1690	1387	1237	1356	1363	1132	1129	1260	1265	1112	1023
KD176A	1700	1180	867	1031	1292	953	1415	1375	1367	857	913
KD176A	1710	1080	1157	985	1018	1258	990	1106	1150	1071	930

KD176A 1720 981 940 927 641 773 767 956 960 943 871
KD176A 1730 846 666 785 763 758 820 653 738 764 372
KD176A 1740 534 629 1105 945 815 804 864 911 809 813
KD176A 1750 1019 1092 997 899 749 845 833 876 735 600
KD176A 1760 723 765 786 670 804 817 1229 844 823 586
KD176A 1770 994 952 1021 1084 996 915 1045 1015 1071 962
KD176A 1780 1047 801 862 914 938 552 876 752 970 928
KD176A 1790 909 1048 1123 1044 1010 942 907 800 959 670
KD176A 1800 854 820 815 938 819 812 799 741 697 738
KD176A 1810 557 664 546 682 630 721 568 623 590 675
KD176A 1820 618 796 889 493 526 554 587 394 473 560
KD176A 1830 535 485 565 638 624 588 531 576 459 717
KD176A 1840 492 613 547 459 501 559 568 564 648 661
KD176A 1850 545 739 576 665 617 794 624 721 681 703
KD176A 1860 788 803 552 752 670 675 655 641 739 447
KD176A 1870 648 688 713 626 763 637 718 946 840 813
KD176A 1880 504 650 804 600 691 646 699 604 616 747
KD176A 1890 592 738 744 614 516 445 495 512 695 791
KD176A 1900 809 977 829 735 871 698 684 612 792 556
KD176A 1910 571 607 649 620 612 581 668 548 672 608
KD176A 1920 620 574 573 520 524 415 489 404 602 354
KD176A 1930 537 480 544 464 633 538 551 470 521 400
KD176A 1940 451 562 500 510 510 500 561 603 690 510
KD176A 1950 557 580 525 560 431 565 482 603 536 488
KD176A 1960 468 651 496 526 544 611 720 632 726 736
KD176A 1970 874 727 784 806 825 724 924 818 861 799
KD176A 1980 927 1021 763 838 795 570 651 825 795 781
KD176A 1990 1019 798 850 937 1062 970 1035 827 979 840
KD176A 2000 1056 1178 1058 784 997 930 938 894 969 1024
KD176A 2010 1158 -9999

KD176B 1694 1500 1320 1534 1395 1359 1423
KD176B 1700 1372 908 1050 1250 1353 1335 1380 1364 800 840
KD176B 1710 844 1034 1211 1241 1446 1207 1191 1243 1071 1502
KD176B 1720 1558 1583 2011 1667 1564 1492 1666 1815 1434 1450
KD176B 1730 1468 1294 1233 1311 1102 1286 1273 1532 1457 460
KD176B 1740 1055 1214 1577 1343 1273 1382 1445 1417 1652 1406
KD176B 1750 1669 1564 1539 1315 1049 1340 1112 1175 984 837
KD176B 1760 990 1269 1178 1134 1203 1316 1398 1282 948 926
KD176B 1770 1334 1316 1078 1379 1229 1001 1132 1451 1283 1198
KD176B 1780 1237 1096 1090 1155 1026 1043 1077 928 1158 1213
KD176B 1790 1005 1205 1300 1346 1225 1200 1069 1237 1224 956
KD176B 1800 1044 1187 884 1090 1184 1076 1090 1057 802 909
KD176B 1810 709 634 763 714 831 781 862 793 797 810
KD176B 1820 700 853 1033 470 521 790 730 572 566 903
KD176B 1830 599 736 618 749 647 830 698 862 784 1071
KD176B 1840 824 625 695 633 639 641 768 530 823 535
KD176B 1850 569 884 713 685 655 662 692 638 860 687
KD176B 1860 961 884 848 891 753 847 724 605 568 540
KD176B 1870 532 655 734 828 725 654 538 814 695 728

KD176B	1880	515	581	660	510	554	459	514	376	424	541
KD176B	1890	468	628	586	501	592	521	575	524	675	533
KD176B	1900	609	679	571	481	629	522	429	384	384	440
KD176B	1910	320	424	362	430	447	453	489	567	522	475
KD176B	1920	509	448	416	485	475	451	509	390	448	429
KD176B	1930	516	460	517	584	567	497	395	379	479	349
KD176B	1940	413	536	508	403	479	376	428	465	557	515
KD176B	1950	465	329	349	345	346	388	393	291	353	299
KD176B	1960	305	333	304	384	327	327	301	321	350	504
KD176B	1970	559	492	465	393	416	502	628	544	454	280
KD176B	1980	412	509	420	384	430	241	268	323	321	246
KD176B	1990	485	396	330	466	597	346	543	410	430	355
KD176B	2000	461	371	326	260	237	245	318	315	433	540
KD176B	2010	423	-9999								
KD-187A	1344	1846	1350	822	592	892	473				
KD-187A	1350	459	499	839	894	1071	1023	869	1120	1568	1805
KD-187A	1360	1572	1567	1646	1654	2091	1775	1192	1103	1362	966
KD-187A	1370	951	1100	618	477	493	418	315	469	266	307
KD-187A	1380	265	228	290	253	289	304	273	290	467	743
KD-187A	1390	910	594	566	538	509	624	910	867	1010	756
KD-187A	1400	918	817	628	873	788	874	1159	879	946	758
KD-187A	1410	887	714	713	719	718	665	725	712	737	821
KD-187A	1420	797	784	699	821	714	736	769	737	835	801
KD-187A	1430	944	713	976	971	1296	1643	1390	1729	1622	1385
KD-187A	1440	1473	1886	1618	1627	2237	1853	1530	1485	1551	1424
KD-187A	1450	1064	1038	1338	1114	1071	1013	1011	1072	982	1115
KD-187A	1460	1307	1111	917	721	494	591	792	763	823	925
KD-187A	1470	815	918	949	748	909	473	556	690	610	792
KD-187A	1480	763	671	995	760	569	721	765	668	607	713
KD-187A	1490	872	771	606	629	717	406	575	727	595	453
KD-187A	1500	571	561	598	527	756	570	646	621	786	653
KD-187A	1510	693	587	775	533	638	577	563	550	612	532
KD-187A	1520	808	565	671	544	723	694	1004	719	1107	835
KD-187A	1530	971	1070	741	514	589	584	854	676	680	626
KD-187A	1540	845	751	739	607	860	723	797	337	515	376
KD-187A	1550	492	456	436	570	678	640	633	632	678	628
KD-187A	1560	526	630	476	610	552	570	446	708	584	485
KD-187A	1570	425	597	577	658	513	703	639	401	576	575
KD-187A	1580	487	960	347	458	372	553	307	447	524	411
KD-187A	1590	429	463	416	382	398	439	449	492	431	525
KD-187A	1600	488	374	421	463	440	422	573	418	526	436
KD-187A	1610	403	331	496	205	363	243	375	302	445	242
KD-187A	1620	239	238	264	243	280	252	303	290	267	264
KD-187A	1630	215	255	279	240	263	139	220	254	271	243
KD-187A	1640	333	266	246	299	192	371	265	293	213	306
KD-187A	1650	197	272	171	215	246	304	317	348	250	273
KD-187A	1660	79	174	128	113	105	105	181	160	85	161
KD-187A	1670	80	118	129	124	225	138	170	123	176	193
KD-187A	1680	164	141	225	176	105	121	134	207	165	269

KD-187A	1690	233	204	265	300	266	249	313	223	229	182
KD-187A	1700	272	208	248	274	247	267	346	252	191	298
KD-187A	1710	304	368	365	351	294	310	309	289	330	356
KD-187A	1720	296	338	493	352	457	383	528	475	397	348
KD-187A	1730	239	346	186	395	275	376	528	437	380	326
KD-187A	1740	622	441	611	498	507	666	534	807	542	712
KD-187A	1750	525	592	362	287	128	129	190	143	116	146
KD-187A	1760	235	227	294	541	390	290	432	443	364	447
KD-187A	1770	662	793	475	543	360	408	267	300	417	387
KD-187A	1780	377	419	350	387	543	579	413	325	379	481
KD-187A	1790	630	626	1038	1076	652	679	676	456	713	810
KD-187A	1800	908	906	809	890	1053	1022	1032	833	922	982
KD-187A	1810	913	864	851	723	740	763	617	704	875	794
KD-187A	1820	831	569	824	475	599	636	779	581	581	659
KD-187A	1830	831	661	922	729	778	687	691	892	717	984
KD-187A	1840	588	498	586	725	686	765	746	515	648	580
KD-187A	1850	681	851	797	747	749	958	765	651	801	685
KD-187A	1860	728	818	684	944	843	836	815	567	485	534
KD-187A	1870	341	416	300	416	378	498	382	449	348	330
KD-187A	1880	174	281	350	357	267	304	300	240	335	557
KD-187A	1890	446	420	482	343	292	324	312	299	426	337
KD-187A	1900	466	429	358	378	407	350	322	272	303	329
KD-187A	1910	208	244	297	253	253	167	207	139	179	124
KD-187A	1920	166	162	158	185	191	153	188	180	248	233
KD-187A	1930	253	243	209	252	262	395	350	328	301	245
KD-187A	1940	217	261	314	261	266	238	236	279	328	354
KD-187A	1950	442	500	438	474	520	611	562	540	527	433
KD-187A	1960	476	447	456	537	571	587	683	703	598	792
KD-187A	1970	815	690	554	711	642	577	619	670	533	570
KD-187A	1980	657	704	509	558	695	570	523	729	741	539
KD-187A	1990	603	527	473	632	685	502	496	511	530	694
KD-187A	2000	714	729	799	565	382	553	491	432	574	1026
KD-187A	2010	793	-9999								

KD-187B	1364	986	1017	746	730	440	330				
KD-187B	1370	263	245	209	216	248	329	322	327	190	130
KD-187B	1380	210	124	114	143	144	167	225	551	450	346
KD-187B	1390	402	442	292	408	429	406	492	432	513	494
KD-187B	1400	499	570	537	571	785	588	566	489	628	639
KD-187B	1410	684	531	1059	893	818	644	544	774	795	539
KD-187B	1420	780	788	806	863	879	829	980	738	791	704
KD-187B	1430	1009	863	1005	1099	1015	1147	982	1019	963	960
KD-187B	1440	901	944	1327	1106	810	861	1124	1273	864	697
KD-187B	1450	697	595	647	589	535	607	700	696	562	405
KD-187B	1460	558	530	413	435	541	445	503	439	543	565
KD-187B	1470	393	337	325	273	372	567	556	541	663	419
KD-187B	1480	285	355	502	480	486	726	556	432	412	662
KD-187B	1490	631	675	660	773	472	542	637	631	299	580
KD-187B	1500	587	473	472	655	719	773	989	989	963	800
KD-187B	1510	994	750	665	716	789	707	669	705	656	840

KD-187B	1520	584	707	608	688	652	904	961	984	885	691
KD-187B	1530	953	632	610	669	671	1001	587	509	487	499
KD-187B	1540	644	474	656	749	876	749	492	494	727	513
KD-187B	1550	488	435	433	575	532	642	596	746	580	552
KD-187B	1560	565	499	489	537	547	357	631	625	615	562
KD-187B	1570	645	447	842	498	731	653	569	625	782	797
KD-187B	1580	634	397	372	526	373	464	277	334	452	486
KD-187B	1590	378	481	353	510	331	637	447	788	610	859
KD-187B	1600	525	782	574	729	609	592	698	802	737	605
KD-187B	1610	465	536	456	433	568	401	584	470	477	333
KD-187B	1620	297	438	542	391	343	342	477	409	314	302
KD-187B	1630	228	264	286	282	265	198	293	225	314	240
KD-187B	1640	360	218	238	282	188	280	274	287	356	379
KD-187B	1650	315	294	382	394	448	338	409	321	427	394
KD-187B	1660	267	200	285	195	209	201	277	194	281	287
KD-187B	1670	321	279	343	357	436	352	398	362	320	408
KD-187B	1680	293	305	265	287	181	312	189	308	307	347
KD-187B	1690	397	276	450	233	437	212	324	306	331	281
KD-187B	1700	401	309	405	356	402	328	382	333	269	343
KD-187B	1710	344	331	371	294	338	271	326	337	304	346
KD-187B	1720	377	339	415	241	451	341	385	389	483	478
KD-187B	1730	432	335	654	336	417	398	371	437	411	443
KD-187B	1740	660	410	326	255	342	423	311	552	378	519
KD-187B	1750	764	977	1071	927	778	740	865	543	544	445
KD-187B	1760	539	654	722	725	759	573	809	743	524	530
KD-187B	1770	769	895	650	1047	834	829	511	988	1026	908
KD-187B	1780	841	846	615	791	893	909	815	602	812	978
KD-187B	1790	854	1126	1088	1456	1253	1168	1331	657	923	879
KD-187B	1800	871	1364	859	930	1065	1034	848	917	816	945
KD-187B	1810	820	788	742	715	817	875	820	790	817	944
KD-187B	1820	732	560	743	642	585	692	1076	661	851	727
KD-187B	1830	1133	720	838	751	842	753	840	860	919	905
KD-187B	1840	917	689	874	980	1201	895	1122	615	906	485
KD-187B	1850	618	587	625	851	802	1007	882	894	1090	795
KD-187B	1860	876	872	682	905	957	1159	1079	986	845	754
KD-187B	1870	505	522	463	443	512	569	503	578	527	590
KD-187B	1880	310	403	569	496	526	479	431	246	465	599
KD-187B	1890	481	654	686	630	453	683	616	698	752	655
KD-187B	1900	871	879	809	947	1145	915	774	746	935	868
KD-187B	1910	712	704	797	748	641	579	759	643	748	872
KD-187B	1920	846	1153	812	924	841	888	814	701	814	748
KD-187B	1930	570	1502	1270	1290	1208	1177	971	1005	1441	838
KD-187B	1940	1290	1172	1218	1070	1149	1589	1397	1572	1664	1146
KD-187B	1950	1385	1188	1565	1300	1615	975	1026	937	1215	983
KD-187B	1960	955	1335	1077	1184	1142	1272	1429	1279	1517	1496
KD-187B	1970	1624	1355	1339	1315	1096	1205	1400	1557	1116	1355
KD-187B	1980	1390	1610	1425	1556	1592	1637	1860	2444	2250	1734
KD-187B	1990	1905	1333	1524	1931	2228	1770	1819	1716	2040	1984
KD-187B	2000	2595	2237	2254	1829	2064	2063	1848	2000	1962	2061
KD-187B	2010	2198	-9999								

KD188A 1867 756 1575 1031
KD188A 1870 832 549 454 288 265 235 236 215 226 139
KD188A 1880 173 487 525 251 311 426 341 326 299 377
KD188A 1890 293 404 126 226 493 338 383 365 535 564
KD188A 1900 646 531 421 338 688 454 610 400 645 618
KD188A 1910 515 618 740 811 1159 1029 916 1046 945 1081
KD188A 1920 1128 1204 1293 1551 1271 1198 1359 1396 2209 1765
KD188A 1930 2095 3107 3008 2526 2289 2337 2557 2132 2204 1994
KD188A 1940 1724 1540 1475 1406 1880 1662 1576 1389 1385 1176
KD188A 1950 1546 1452 1382 1375 1076 1168 1249 1039 1365 1807
KD188A 1960 1938 2146 1610 1583 1556 1932 1633 1552 1557 1787
KD188A 1970 2105 2418 2565 2491 1785 1415 1624 2073 1751 1372
KD188A 1980 1428 2011 1690 1771 1289 911 934 1045 1034 861
KD188A 1990 1447 943 1015 1033 1088 902 1117 1074 1004 922
KD188A 2000 1199 1219 1057 986 1029 914 993 1113 1041 1130
KD188A 2010 1057 -9999

KD188B 1767 561 399 518
KD188B 1770 703 883 885 1244 2164 1417 1158 1119 944 1071
KD188B 1780 1221 1062 1138 1028 1052 1019 921 1241 1464 1896
KD188B 1790 1405 1469 1158 1160 947 1020 1896 2058 1928 1559
KD188B 1800 1497 1244 812 875 824 872 722 641 963 884
KD188B 1810 672 672 644 703 810 759 768 752 813 868
KD188B 1820 992 447 745 652 537 678 639 539 725 1051
KD188B 1830 1085 889 1023 1164 1101 1350 1223 1148 864 1214
KD188B 1840 1308 1113 1091 1060 1434 1331 1277 833 1224 1250
KD188B 1850 1298 1208 1359 1187 1259 1403 1260 1147 1343 967
KD188B 1860 1259 1202 648 1018 478 713 938 1004 1204 1580
KD188B 1870 2244 1876 1333 1411 1671 1742 1566 1604 1688 1809
KD188B 1880 1518 2561 2408 2563 2694 2096 2143 1627 1403 1882
KD188B 1890 2066 2211 2596 2663 2212 1806 2099 1779 2073 1469
KD188B 1900 1667 1089 865 984 616 327 250 119 195 212
KD188B 1910 192 381 649 607 968 1127 1108 959 978 1129
KD188B 1920 1156 1207 1348 1749 1451 1329 1650 1718 2192 1134
KD188B 1930 1179 2144 1469 1348 1345 1418 1333 1087 1126 1119
KD188B 1940 1405 1753 1530 1467 1982 1684 1287 901 997 952
KD188B 1950 915 899 1153 1154 949 988 1273 1164 1268 950
KD188B 1960 1096 1149 970 1161 1260 1708 1389 1181 1222 1398
KD188B 1970 1719 1962 2027 2007 1388 1120 1361 1566 1203 1090
KD188B 1980 945 1523 1469 1565 1236 955 1150 1192 1156 1273
KD188B 1990 1786 1131 1179 1200 1276 945 1018 1036 1017 1032
KD188B 2000 1536 1526 1388 1286 1876 1900 1669 1602 1406 1616
KD188B 2010 2049 -9999

KD195A 1448 1079 1065
KD195A 1450 977 1135 1325 1636 1702 1368 1313 1158 1259 1353
KD195A 1460 1427 1091 1255 1063 1147 1117 1275 1659 1728 1599
KD195A 1470 1336 1233 1022 1256 878 729 970 719 821 797
KD195A 1480 744 829 712 589 579 680 603 488 574 730

KD195A	1490	766	585	707	695	525	462	707	849	588	899
KD195A	1500	803	766	645	911	936	976	1174	1181	922	972
KD195A	1510	710	753	719	726	763	731	793	628	824	960
KD195A	1520	902	914	721	587	767	878	809	897	1439	1393
KD195A	1530	1357	956	998	893	824	990	917	722	645	897
KD195A	1540	1125	1161	1045	1049	1170	1115	874	1008	984	802
KD195A	1550	871	1027	799	932	880	1015	841	1145	948	1057
KD195A	1560	1040	960	941	948	1046	1012	1286	966	985	715
KD195A	1570	1006	1054	1085	1121	1239	1091	658	758	742	678
KD195A	1580	745	696	491	655	483	503	494	456	496	503
KD195A	1590	487	550	431	484	446	527	587	714	757	716
KD195A	1600	655	655	554	627	475	596	884	889	814	577
KD195A	1610	580	599	561	534	547	611	716	599	536	663
KD195A	1620	580	602	668	612	671	545	580	502	509	627
KD195A	1630	530	492	649	592	574	448	465	425	486	501
KD195A	1640	552	388	409	468	448	500	641	531	514	655
KD195A	1650	796	770	769	580	674	740	797	634	672	620
KD195A	1660	496	600	510	454	680	601	745	721	708	751
KD195A	1670	721	650	595	656	732	647	565	574	577	569
KD195A	1680	465	590	618	455	433	530	486	668	486	552
KD195A	1690	760	772	788	775	660	786	598	659	470	477
KD195A	1700	530	448	517	484	396	457	497	447	540	559
KD195A	1710	523	491	479	564	534	467	516	503	508	572
KD195A	1720	591	603	709	435	480	453	532	594	505	541
KD195A	1730	499	568	620	611	492	506	502	498	559	405
KD195A	1740	524	368	412	415	412	392	351	466	380	444
KD195A	1750	562	466	455	385	335	372	516	420	445	409
KD195A	1760	411	478	468	504	487	497	653	520	495	486
KD195A	1770	544	557	425	616	480	547	547	469	504	386
KD195A	1780	551	411	344	480	510	560	590	479	517	642
KD195A	1790	485	589	672	689	743	695	722	713	840	728
KD195A	1800	886	847	751	801	1044	810	789	833	615	806
KD195A	1810	479	556	564	569	633	527	611	477	488	538
KD195A	1820	322	360	477	370	424	527	427	295	375	475
KD195A	1830	336	439	366	435	460	313	355	325	340	395
KD195A	1840	282	278	318	481	468	444	491	326	416	373
KD195A	1850	386	452	492	492	578	751	582	572	655	515
KD195A	1860	627	592	581	646	396	495	420	470	464	353
KD195A	1870	316	477	449	428	478	479	355	474	524	427
KD195A	1880	275	283	451	365	457	439	508	397	647	600
KD195A	1890	480	548	570	537	498	570	516	574	698	474
KD195A	1900	621	627	519	510	568	548	493	460	398	438
KD195A	1910	401	410	538	488	573	724	627	589	452	406
KD195A	1920	342	255	292	258	204	183	204	231	216	264
KD195A	1930	234	302	385	449	513	571	274	487	545	322
KD195A	1940	568	757	606	800	960	930	871	1239	1223	817
KD195A	1950	882	961	810	732	863	966	898	939	1132	820
KD195A	1960	896	1101	1175	1314	1262	1163	1356	1166	798	984
KD195A	1970	1370	944	1111	1186	948	1352	1581	1736	1448	1759
KD195A	1980	1565	1823	1238	1657	1898	1233	1594	2109	1427	1461

KD195A	1990	2181	1276	1987	2071	2107	1411	1507	1562	1911	1911
KD195A	2000	2083	1831	2017	1649	1769	2079	1846	2089	1870	1820
KD195A	2010	2020	-9999								

KD-195B	1430	2251	2138	1796	2037	2424	2088	2401	2476	2471	2030
KD-195B	1440	2254	2651	1788	2310	2108	2004	1873	1662	1439	1721
KD-195B	1450	1509	1726	2008	1515	1628	1653	1812	1483	1802	1838
KD-195B	1460	1507	989	1344	1266	959	1053	1178	1502	1623	1772
KD-195B	1470	1836	1710	1434	1633	1167	1133	1399	1021	998	1056
KD-195B	1480	1104	1261	744	917	920	1067	944	1141	897	940
KD-195B	1490	1136	851	934	900	526	562	800	797	586	884
KD-195B	1500	888	772	742	677	924	1090	1042	973	984	1030
KD-195B	1510	976	916	757	713	1016	940	921	1012	1313	1629
KD-195B	1520	1691	1523	1219	1019	1279	1338	1075	1229	1450	1402
KD-195B	1530	1445	866	1109	1054	954	1358	1175	980	789	1146
KD-195B	1540	1253	1354	1190	1317	1544	1202	856	1197	1077	756
KD-195B	1550	926	1206	1029	1238	1112	1034	918	1344	1287	1369
KD-195B	1560	1531	1229	996	1008	1128	1269	1453	1036	1063	952
KD-195B	1570	1167	1171	1228	1258	1134	984	569	698	591	550
KD-195B	1580	616	344	377	555	342	368	315	352	354	302
KD-195B	1590	330	389	358	305	333	424	583	679	802	736
KD-195B	1600	655	663	677	669	471	541	598	635	697	543
KD-195B	1610	547	561	472	530	507	525	661	628	536	510
KD-195B	1620	531	665	666	559	438	500	426	381	370	403
KD-195B	1630	348	334	422	477	341	341	374	393	482	387
KD-195B	1640	582	360	453	404	400	423	456	491	503	659
KD-195B	1650	768	885	785	548	642	659	869	633	622	585
KD-195B	1660	410	459	547	507	622	405	516	481	494	508
KD-195B	1670	576	496	450	525	552	424	390	479	513	480
KD-195B	1680	409	423	438	297	330	334	335	411	242	391
KD-195B	1690	337	345	380	342	307	351	337	297	294	300
KD-195B	1700	365	298	356	409	295	314	388	325	341	390
KD-195B	1710	399	402	363	279	327	252	304	328	290	312
KD-195B	1720	350	355	320	275	297	321	318	422	371	370
KD-195B	1730	371	266	340	278	288	339	390	357	432	254
KD-195B	1740	300	365	321	327	353	360	355	401	412	299
KD-195B	1750	512	381	341	291	268	236	329	334	327	303
KD-195B	1760	310	330	329	371	265	335	408	417	411	380
KD-195B	1770	495	518	450	560	450	407	412	606	606	474
KD-195B	1780	509	457	336	434	409	417	387	277	332	501
KD-195B	1790	322	390	383	440	425	356	357	364	369	311
KD-195B	1800	382	424	336	333	469	413	480	468	332	401
KD-195B	1810	269	276	262	266	294	212	260	268	244	268
KD-195B	1820	246	212	317	205	296	367	346	255	294	307
KD-195B	1830	207	265	320	381	415	251	301	410	415	463
KD-195B	1840	312	398	423	490	477	454	480	302	372	297
KD-195B	1850	258	451	378	396	446	593	467	316	385	270
KD-195B	1860	323	326	254	291	270	263	254	306	269	197
KD-195B	1870	220	288	260	282	303	232	247	377	397	251
KD-195B	1880	144	191	263	231	239	286	308	240	288	338

KD-195B	1890	267	257	336	306	237	300	260	295	388	227
KD-195B	1900	306	319	269	240	357	284	287	322	383	350
KD-195B	1910	324	323	322	388	453	547	393	278	205	149
KD-195B	1920	127	134	125	73	70	62	85	94	116	152
KD-195B	1930	100	114	100	145	189	276	222	249	281	191
KD-195B	1940	299	407	388	585	721	817	918	1189	993	791
KD-195B	1950	1094	914	912	826	1026	1200	978	1091	1516	893
KD-195B	1960	1077	1445	1041	1232	1269	1185	1524	1215	843	1144
KD-195B	1970	1264	771	978	1281	863	1036	1339	1434	1103	1096
KD-195B	1980	1128	1387	890	1005	1354	857	1043	1619	1160	1218
KD-195B	1990	1830	923	1466	1650	1804	949	1149	1326	1573	1399
KD-195B	2000	1651	1501	1660	1330	1576	2019	1577	1765	1477	1366
KD-195B	2010	1643	-9999								

APPENDIX B: Lichenometric Data

Landform Lichen Measurement Locations, Ages, and Maximum Diameters

Waypoint ID	Y (UTM Zone 10N)	X (UTM Zone 10N)	Estimated Landform Age (years)	Estimated Landform Year (AD)	Maximum Lichen Diameter (mm)
KCL-2	5182259.03	591486.55	114	1897	52
KCL-3	5182184.48	591423.02	206	1805	92
KCL-4/KL-45B	5182117.52	591390.60	195	1816	87
KCL-5	5181837.12	591246.22	142	1869	64
KCL-5C	5181789.70	591220.55	190	1821	85
KCL-6	5181570.36	591231.27	160	1851	72
KCL-7	5181341.95	591106.23	117	1894	53
KCL-9	5182262.35	591631.39	190	1821	85
KCL-10/KL-11B	5182225.73	591584.70	126	1885	57
KCL-11	5182159.03	591569.00	119	1892	54
KCL-12	5182113.92	591614.04	149	1862	67
KCL-13	5182076.06	591580.03	215	1796	96
KCL-13B	5182070.05	591579.59	222	1789	99
KCL-14	5181990.74	591538.96	263	1748	117
KCL-16	5182269.48	591719.92	87	1924	40
KCL-17	5182046.81	591673.78	167	1844	75
KCL-18B	5181500.47	591480.32	59	1952	28
KCL-19A	5181266.65	591183.35	62	1949	29
KCL-19B	5181279.27	591164.64	110	1901	50
KCL-22	5182095.35	591475.15	66	1945	31
KCL-22B	5182019.24	591447.60	82	1929	38
KCL-23	5181847.01	591421.44	78	1933	36
KCL-24	5181678.78	591365.98	62	1949	29
KCL-25	5181495.40	591308.22	57	1954	27
KCL-26	5181404.28	591273.11	55	1956	26
KCL-27	5181777.46	591371.73	208	1803	93
KCL-28	5182172.94	591526.72	147	1864	66
KCL-29	5182230.09	591505.92	103	1908	47
KCL-30	5182439.88	591655.02	91	1920	42
KCL-31	5181539.83	591495.83	108	1903	49
KCL-32	5181946.68	591652.78	277	1734	123
KL-33	5181981.41	591655.92	222	1789	99
KL-34	5182158.91	591604.80	222	1789	99
KL-35	5182168.66	591590.29	280	1731	124
KL-37	5182189.83	591628.00	110	1901	50
KL-37B	5182189.83	591628.00	105	1906	48
KL-37C	5182189.83	591628.00	117	1894	53
KL-42	5181365.65	590932.00	73	1938	34
KL-43	5181448.78	591161.27	144	1867	65
KL-44	5181510.73	591159.68	144	1867	65

Landform Lichen Measurement Locations, Ages, and Maximum Diameters

Waypoint ID	Y (UTM Zone 10N)	X (UTM Zone 10N)	Estimated Landform Age (years)	Estimated Landform Year (AD)	Maximum Lichen Diameter (mm)
KL-44C	5181736.65	591239.35	89	1922	41
KL-45A	5182071.50	591375.57	183	1828	82
KL-45B	5182095.70	591388.72	195	1816	87
KL-46	5182123.86	591263.13	101	1910	46
KL-47	5182118.70	591519.66	169	1842	76
KL-50	5181142.23	591063.30	151	1860	68
KL-51	5181175.67	591157.25	149	1862	67
KL-52	5182852.26	591772.99	89	1922	41
KL-52B	5182640.89	591760.96	59	1952	28
KL-53	5182640.89	591760.96	78	1933	36
KL-53B	5183415.00	592229.99	82	1929	38
KL-54	5183415.00	592229.99	96	1915	44
KL-56	5181647.02	591455.49	59	1952	28
KL-57	5181690.77	591409.01	144	1867	65
KL-58	5182014.30	591488.06	128	1883	58
KL-59	5182070.33	591517.75	174	1837	78
KL-60	5182327.77	591635.97	114	1897	52
KL-61	5182294.09	591613.58	183	1828	82
KL-62	5182227.76	591637.50	121	1890	55

Locations are in UTM Zone 10N NAD 1983
Age Estimates are calculated using growth curve equation of O'Neal and Schoenenberger, 2003
Dates are calculated by subtracting the age estimate from the measurement year (2011)

	Lichen Diameter in order of size (ranked 1 to 10)									
Waypoint ID	1	2	3	4	5	6	7	8	9	10
KCL-2	52	50	46	44	43	42	42	42	42	41
KCL-3	92	58	49	49	44	40	39	39	39	38
KCL-4/KL-45B	87	67	53	47	44	44	-	-	-	-
KCL-5	64	51	49	48	47	43	40	40	40	37
KCL-5C	85	62	57	39	-	-	-	-	-	-
KCL-6	72	70	60	50	46	44	43	35	-	-
KCL-7	53	45	42	39	39	38	37	37	33	31
KCL-9	74	72	58	54	52	49	48	47	40	-
KCL-10/KL-11B	57	56	54	54	52	50	50	44	41	-
KCL-11	54	53	52	50	47	41	40	38	38	33
KCL-12	67	63	60	57	56	51	50	49	45	35
KCL-13	96	73	57	57	55	47	-	-	-	-
KCL-13B	99	85	75	66	60	50	44	-	-	-
KCL-14	117	102	101	98	94	94	92	85	83	83
KCL-16	40	40	39	37	37	34	34	34	32	32
KCL-17	75	57	56	54	51	49	41	-	-	-
KCL-18B	28	28	27	26	26	25	25	22	20	19
KCL-19A	29	28	26	24	23	23	-	-	-	-
KCL-19B	50	45	41	40	36	35	35	34	33	33
KCL-22	31	31	31	28	28	28	24	22	22	22
KCL-22B	38	34	-	-	-	-	-	-	-	-
KCL-23	36	28	28	27	27	27	26	24	24	23
KCL-24	29	26	23	20	20	19	18	16	16	12
KCL-25	27	25	24	23	23	22	22	-	-	-
KCL-26	26	26	25	24	22	20	-	-	-	-
KCL-27	93	55	55	54	42	42	42	37	35	35
KCL-28	66	63	61	54	50	45	42	42	41	36
KCL-29	47	43	43	35	34	34	30	29	28	25
KCL-30	42	33	33	33	33	24	24	-	-	-
KCL-31	49	47	42	41	41	37	37	36	33	29
KCL-32	123	114	75	60	-	-	-	-	-	-
KL-33	75	73	70	65	63	60	58	-	-	-
KL-34	99	85	45	-	-	-	-	-	-	-
KL-35	150	124	113	85	55	-	-	-	-	-
KL-37	50	46	45	45	38	38	33	27	27	26
KL-37B	48	47	47	34	32	30	28	22	-	-
KL-37C	53	50	48	35	-	-	-	-	-	-
KL-42	34	24	-	-	-	-	-	-	-	-
KL-43	65	52	50	49	48	46	40	36	36	34
KL-44	41	39	38	38	36	34	33	32	29	28
KL-44C	41	39	38	38	36	34	33	32	29	28
KL-45A	82	66	57	55	54	50	46	44	41	35
KL-45B	87	67	53	47	44	44	-	-	-	-
KL-46	46	45	43	27	25	24	-	-	-	-
KL-47	76	71	69	62	62	59	55	-	-	-
KL-50	68	56	53	53	50	49	49	43	40	39
KL-51	67	63	52	37	34	32	28	-	-	-
KL-52	41	38	31	-	-	-	-	-	-	-
KL-52B	28	27	27	-	-	-	-	-	-	-
KL-53	36	29	28	27	27	26	24	24	19	16
KL-53B	38	37	35	35	34	30	28	-	-	-

Waypoint ID	Lichen Diameter in order of size (ranked 1 to 10) 1	2	3	4	5	6	7	8	9	10
KL-54	44	37	32	-	-	-	-	-	-	-
KL-56	28	27	25	18	-	-	-	-	-	-
KL-57	65	63	62	58	58	50	42	40	34	31
KL-58	58	57	49	48	43	42	-	-	-	-
KL-59	78	58	48	-	-	-	-	-	-	-
KL-60	52	51	50	48	45	41	40	35	34	29
KL-61	82	69	56	52	45	40	35	35	-	-
KL-62	55	53	50	47	46	46	45	44	43	43

Reported lichen diameters were measured along the axis coinciding with the largest diameter.

APPENDIX C: Radiocarbon Data

Geographic Locations of Radiocarbon Samples Analyzed for this Study

Location ID	Latitude**	Longitude**	Samples Analyzed At Location	Stratigraphic Column (in text)	Notes on Sample Type/Depth
12 KS 04A	46.769802	-121.824968	12-KS-04A	D	In-text description
12 KS 9A	46.761462	-121.833001	12-KS-09	E	In-text description
KRC 01*	46.747022	-121.84828	KRC-01	-	Sample KRC-1 collected from outermost rings of buried stump ~0.33m below forested terrace surface
KRC 04	46.790131	-121.798759	KRC-04A, KRC-04C	A	In-text description
KRC 05	46.787592	-121.798695	KRC-05B, KRC-05C	B	In-text description
KRC 06	46.774192	-121.812663	KRC-06A, KRC-06B, KRC-06C, KRC-06D, KRC-06E	C	In-text description
12-BF*	46.750942	-121.841377	12-BF	-	Sample 12-BF was collected from the outermost rings of a stump ~3 m below a terrace surface in a right cutbank of the main channel of Kautz Creek

* Samples not discussed in the main body of this thesis due to their young ages.

**Locations were marked with a handheld GPS with approximately 5 meters accuracy

Raw AMS laboratory results provided by Woods Hole Oceanographic Institute's National Ocean Sciences AMS Facility

Sample ID	Laboratory Receipt #	Date Reported	Type	Process*	Laboratory Accession #	F Modern	Fm Err	Age	Age Err	⊠13C	⊠14C
KRC-01	102722	2/7/2012	Plant/Wood	OC	OS-93055	0.96800	0.00390	260	30	-22.88	-39.07
KRC-04A	102723	2/7/2012	Plant/Wood	OC	OS-93056	0.92630	0.00300	615	25	-25.78	-80.52
KRC-04C	102724	2/7/2012	Plant/Wood	OC	OS-93057	0.95770	0.00310	345	25	-24.26	-49.32
KRC-05B	102725	2/7/2012	Charcoal	OC	OS-93058	0.96170	0.00300	315	25	-26.6	-45.35
KRC-05C	102726	2/7/2012	Plant/Wood	OC	OS-93059	0.95440	0.00330	375	25	-24.18	-52.62
KRC-06A	102727	2/7/2012	Plant/Wood	OC	OS-93060	0.88660	0.00310	965	30	-24.63	-119.95
KRC-06B	102728	2/7/2012	Plant/Wood	OC	OS-93061	0.97210	0.00320	225	25	-25.19	-35.04
KRC-06C	102729	2/7/2012	Plant/Wood	OC	OS-93062	0.92650	0.00300	615	25	-25.28	-80.34
KRC-06D	102730	2/7/2012	Plant/Wood	OC	OS-93063	0.87100	0.00280	1110	25	-23.52	-135.38
KRC-06E	102731	2/7/2012	Plant/Wood	OC	OS-93064	0.87450	0.00280	1080	25	-23.8	-131.93
12-BF	109100	10/5/2012	Plant/Wood	OC	OS-98408	0.97460	0.00310	205	25	-26.51	-
12-KS-09	109101	10/5/2012	Plant/Wood	OC	OS-98407	0.86880	0.00270	1130	25	-21.21	-
12-KS-04A	109102	10/5/2012	Plant/Wood	OC	OS-98406	0.87980	0.00280	1030	25	-23.5	-

* Organic Carbon